Department of Chemistry
Faculty of Science
University of Helsinki

Dissertationes Universitatis Helsingiensis 338/2024

Theoretical Insight on the Atmospheric Oxidation Reactions of Organic Nitrogen Compounds

Thomas Golin Almeida

Academic Dissertation

To be presented, with the permission of the Faculty of Science of the University of Helsinki, for public examination in Auditorium A111, Exactum, Kumpula, on the 17th of December, at 13 o'clock.

Helsinki 2024

Supervisor
Theo Kurtén, University of Helsinki, Finland

Pre-examiners
Gabriel da Silva, University of Melbourne, Australia
Stephen J. Klippenstein, Argonne National Laboratory, USA

Opponent
Matthew Stanley Johnson, University of Copenhagen, Denmark

Contact information
Thomas Golin Almeida
Department of Chemistry
University of Helsinki
A.I. Virtasen Aukio 1 (P.O. Box 55)
Helsinki 00014, Finland

Publisher: Helsingin yliopisto
Series: Dissertationes Universitatis Helsingiensis 338/2024

ISBN 978-952-84-0480-4 (print)
ISBN 978-952-84-0479-8 (online)
ISSN 2954-2898 (print)
ISSN 2954-2952 (online)
PunaMusta, Joensuu 2024

Abstract

From the thousands of different trace gases present in the Earth's atmosphere, nitrogen-containing organic compounds are among those whose oxidation chemistry is the least understood. Oxidation can quickly transform volatile compounds in the atmosphere into a variety of products, often possessing widely different properties, some of which can be not-so-volatile. Low-volatility vapors can in turn contribute to the formation of aerosol particles, key components of the planet's climate, by condensation. Other oxidation products, in particular the ones derived from organic nitrogen compounds, can be toxic. These atmospheric oxidation reactions can often proceed by complex mechanisms, where branched networks of reaction pathways connect the reactants to products via multiple reactive intermediates. This thesis employed theoretical methods to explore the oxidation mechanism of N-containing compounds, aiming to predict their fate and impact in the atmosphere. Quantum chemistry was first used to characterize the energetics of reaction pathways, based on which the speed and direction of oxidation was later predicted with theoretical reaction kinetics.

This thesis' work investigated the fate of the imine derivative of piperazine, an amine employed as a CO_2-scrub in carbon-capture technology, and imidazole, a nitrogen-containing aromatic compound found to be an important light-absorbing species in atmospheric aerosols. Beyond an assessment of the environmental and health impacts, by targeting these compounds this thesis aimed to explore the even-less-known atmospheric chemistry of imines and N-containing aromatics. Atmospheric oxidation of the imine is predicted to have a low yield of toxic compounds, such as nitrosamines, nitroamines, and an isocyanate. The latter is produced via a previously unreported reaction channel which, albeit minor for the investigated compound, can potentially be more competitive for other imines. Imidazole's fate upon oxidation, on the other hand, is dominated by the formation of a cyclic diimine and an acyclic amidine, with negligible yields of toxic products. This observation is due, in large part, to two new reaction pathways discovered in the work presented in this thesis: O_2-migration and 1,6 HO_2-elimination reactions. These reactions may be important in the oxidation of other N-containing aromatic and unsaturated compounds.

In addition, this thesis also investigated two critical reaction intermediates, namely alkyl and alkoxyl radicals, derived from the nitrate radical-initiated oxidation of monoterpenes, an abundant class of organic compounds in the atmosphere. Theoretical predictions show a divergent selectivity among different monoterpenes towards pathways branching-out from these intermediates, with a direct impact on the propensity to form aerosol particles. A pattern also emerged from this investigation, indicating that in general, oxidation of endocyclic-double-bond monoterpenes tend to yield less particles than exocyclic- counterparts.

Acknowledgements

I want to take this opportunity to acknowledge everyone who, in one way or another, contributed to make this thesis possible. First, I want to express my gratitude to my supervisor, Prof. Theo Kurtén, for the opportunity to work in his group and for introducing me to the fascinating field of atmospheric chemistry research. Thank you for your inspiring scientific mentorship, and for being always there to offer guidance throughout my PhD journey. I am also grateful to my co-supervisor, Prof. Ilkka Kilpeläinen, for the many insightful discussions, and for the opportunity to contribute to a research project in organic chemistry. Many thanks to the pre-examiners of this thesis, Dr. Stephen Klippenstein and Prof. Gabriel da Silva, who took time to carefully evaluate the work presented here and provide valuable feedback. I also thank Prof. Lauri Halonen and Prof. Matti Rissanen for their physical chemistry and atmospheric chemistry courses I was glad to have attended, and where I learned immensely.

I had a great time during my PhD, and that is largely because I had the privilege of working alongside great people. I want to say a huge thank you to past and present members of the Atmospheric Computational Chemistry Group as well as other great people from the fourth floor of the Deparment of Chemistry, Galib, Vili, Siddharth, Kajsa, Rashid, Christopher, Lauri, Robert, Federica, Benjamin, Nanna, Dominika, Emelda, Fraise, and Severi. I also thank other co-workers, from the University of Helsinki and beyond, with whom I was glad to have co-authored publications, Dr. Danielle Draper, Dr. Haiyan Li, Eva Gazagnaire, Prof. Mikael Ehn, and Prof. James Smith. Special thanks to Dr. Sommer Johansen, Dr. Judit Zádor, and Dr. Carles Martí, who hosted me during a month-long research visit to Sandia National Laboratories in Livermore, in addition to co-authoring one of this thesis' articles. I am thankful to the Department of Chemistry, the Doctoral Programme in Chemistry and Molecular Sciences (CHEMS), and the Research Council of Finland for funding, and to the CSC - IT center for science, for providing the computational infrastructure. On that note, thanks to Dr. Nino Runeberg, contact person at CSC who provided me with technical support countless times, and whom later I met during his sabbatical period visiting our research group.

I am thankful to my friends from outside of university for all the great times we had together during all these years. I certainly hope we will share many more of those moments in the future, regardless of which corner of the world each of us may find ourselves living in. Is we. I also thank my parents, who have always supported me despite the geographical distance, and no matter which path I decided to follow. Finally, I thank my partner, Ida. I have no words to express how grateful I am for your companionship, your kindness, and your unwavering support at all times.

List of Original Publications

This thesis is based on the following publications:

I **Golin Almeida, T.**; Kurtén, T. Atmospheric Oxidation of Imine Derivative of Piperazine Initiated by OH Radical. *ACS Earth and Space Chemistry* **2022** 6 (10), 2453-2464.

II Draper, D.; **Golin Almeida, T.**; Iyer, S.; Smith, J. N.; Kurtén, T.; Myllys, N. Unpacking the diversity of monoterpene oxidation pathways via nitrooxy-alkyl radical ring-opening reactions and nitrooxy-alkoxyl radical bond scissions. *Journal of Aerosol Science* **2024** 179, 106379.

III **Golin Almeida, T.**; Martí, C.; Kurtén, T.; Zádor, J.; Johansen, S. L. Theoretical analysis of the OH-initiated atmospheric oxidation reactions of imidazole. *Physical Chemistry Chemical Physics* **2024** 26, 23570-23587.

Other publications not included in the thesis:

IV Li, H.; **Golin Almeida, T.**; Luo, Y., Zhao, J.; Palm, B. B.; Daub, C. D.; Huang, W.; Mohr, C.; Krechmer, J. E.; Kurtén, T.; Ehn, M. Fragmentation inside proton-transfer-reaction-based mass spectrometers limits the detection of ROOR and ROOH peroxides. *Atmospheric Measurement Techniques* **2022** 15(6), 1811-1827.

V Hasan, G.; Salo, V.-T.; **Golin Almeida, T.**; Valiev, R.; Kurtén, T. Computational Investigation of Substituent Effects on the Alcohol + Carbonyl Channel of Peroxy Radical Self- and Cross-Reactions. *The Journal of Physical Chemistry A* **2023** 127 (7), 1686-1696.

VI Gazagnaire, E.; Helminen, J.; King, A. W.; **Golin Almeida, T.**; Kurtén, T.; Kilpeläinen, I. Bicyclic guanidine superbase carboxylate salts for cellulose dissolution. *RSC Advances* **2024** 14(17), 12119-12124.

VII Pichelstorfer, L.; Roldin, P.; Rissanen, M.; Hyttinen, N.; Garmash, O.; Xavier, C.; Zhou, P.; Clusius, P.; Foreback, B.; **Golin Almeida, T.**; Deng, C.; Baykara, M.; Kurtén, T.; Boy, M. Towards automated inclusion of autoxidation chemistry in models: from precursors to atmospheric implications. *Environmental Science: Atmospheres* **2024** 4, 879-896.

Author's contribution:

The author of this thesis was responsible for all of the theoretical work presented in Articles I, III, and VI, a majority of the theoretical work presented in Article IV, and half of the theoretical work presented in Article II. The author was responsible for writing the manuscripts for Articles I and III, and half of the manuscripts for Articles II and IV, with contributions from all co-authors. In Articles II and IV, the author shared joint first-authorship with Danielle Draper and Haiyan Li, respectively. Article IV was not included in this thesis because, as the type of chemical reactions investigated there differ significantly from the those investigated in the other three publications, its inclusion would complicate the overarching message that the author attempted to convey in the text.

List of Abbreviations

2,3-DHP 2,3-Dihydropyrazine

3,4-DHP 3,4-Dihydropyrazine

4H-4ol 4*H*-imidazol-4-ol

5-OH 5-Hydroxyimidazolyl radical

BO Born-Oppenheimer (approximation)

CC Coupled-cluster

CI Configuration interaction

DFT Density functional theory

FMF *N*,*N*'-diformylformamidine

HF Hartree-Fock

HOM Highly oxygenated molecule

HOMO Highest occupied molecular orbital

ILT Inverse Laplace transform

IVR Intramolecular vibrational energy redistribution

LCAO Linear combination of atomic orbitals

ME Master equation

MEP Minimum energy path

MO Molecular orbital

PES Potential energy surface

PSSA Pseudo-steady-state approximation

RHF Restricted Hartree-Fock

RRHO Rigid rotor-harmonic oscillator (approximation)

RRKM Rice-Ramsperger-Kassel-Marcus (theory)

SCF Self-consistent field

SOA Secondary organic aerosol

SOMO	Singly occupied molecular orbital
THP	1,2,3,6-Tetrahydropyrazine
TS	Transition state
TST	Transition state theory
UHF	Unrestricted Hartree-Fock
VOC	Volatile organic compound

Contents

Abstract iii
Acknowledgements iv
List of Original Publications v
List of Abbreviations vii

1 Introduction **1**

2 Atmospheric Oxidation Pathways **4**
2.1 Atmospheric Oxidants 4
2.2 Organic Radical Chain Initiation 5
2.3 General Reactivity Trends 7
2.4 Peroxyl Radicals 10
2.5 Alkoxyl Radicals 13
2.6 Alkyl Radicals 14

3 Theoretical Background **16**
3.1 Quantum Chemistry 16
3.1.1 The Mean-Field Approximation 18
3.1.2 Linear Combination of Atomic Orbitals 22
3.1.3 Electron Correlation – Coupled-Cluster Theory 24
3.1.4 Density Functional Theory 26
3.1.5 Nuclear Motion and the Potential Energy Surface 28
3.2 Statistical Thermodynamics 30
3.2.1 The Partition Function 31
3.2.2 Chemical Equilibrium 33
3.3 Reaction Kinetics 34
3.3.1 Transition State Theory 34

3.3.2 Quantum Tunnelling 37
3.3.3 Pressure Dependence and the Lindemann Mechanism . . . 38
3.3.4 Rice-Ramsperger-Kassel-Marcus Theory 40
3.3.5 Inverse Laplace Transform Method 43
3.3.6 Collisional Energy Transfer 45
3.3.7 The Chemical Master Equation 46

4 Results and Discussion **49**
4.1 Initial Oxidant Attack on a Cyclic Imine 49
4.2 Peroxyl Radical Reaction Pathways 51
4.2.1 1,2,3,6-Tetrahydropyrazine Derivatives 51
4.2.2 Imidazole Derivatives 53
4.3 Aminyl Radicals 57
4.4 Nitrooxy-alkyl and -alkoxyl Radical β-scissions 58
4.4.1 Nitrooxy-alkyl Radicals 58
4.4.2 Nitrooxy-alkoxyl Radicals 59

5 Conclusions and Future Outlook **61**

Appendix **63**
A1 Derivation of TST 63
A2 The Dissociation ILT Expression 65

References **85**

1. Introduction

Unique among the planetary atmospheres in the Solar System, Earth's gaseous envelope is suitable for the development and maintenance of complex life as we know it. The specific conditions and mechanisms that led to the emergence of life here are as-of-yet unknown, but general agreement has it that the atmosphere, and more specifically its chemical composition, must have been crucial in the process. [1–3] Central among the life-conducive characteristics of our atmosphere is the ability to provide, owing to the presence of the right amounts of heat-trapping greenhouse gases, surface temperature conditions that allow for the presence of liquid water oceans. [2, 4, 5] Around the time of the rise of the first organism, atmospheric chemical reactions may even have supplied the primordial oceans with critical organic compounds, [5–7] from which life built itself. Regardless of how exactly it emerged, life thrived and, in time, changed the atmosphere that made it possible. [1, 5, 8]

The present-day atmospheric composition is dominated, in terms of abundance, by four gases: 78% of molecular nitrogen (N_2), 21% of molecular oxygen (O_2), 1% of argon (Ar), and a variable concentration of water vapor (H_2O). [9] Present in lower concentrations, but not less important, are trace gases such as carbon dioxide (CO_2) and methane (CH_4), which alongside H_2O are the main gases responsible for the greenhouse effect, warming the planet's surface. Nearly all of the O_2 we breathe, however, appeared only with the rise of photosynthetic lifeforms early-on in Earth's history. [5] Making use of Sunlight and CO_2 as an abundant source of energy and carbon respectively, early microorganisms proliferated in the oceans and, over millions of years, injected copious amounts of O_2 into the atmosphere, in what is called the Great Oxidation Event. [10, 11] The uptake of CO_2 by these organisms meant also that the biosphere could regulate the planet's climate. [12] Later lifeforms took advantage of the now abundant, strongly oxidizing O_2 to power their metabolic machinery with more efficient oxidation of organic matter. [13, 14] Eventually, this allowed the rise of more complex lifeforms such as plants and animals, who in turn also had, and still have, a significant impact on the atmosphere.

Present in the atmosphere at even lower concentrations than CO_2 or CH_4

are a multitude of different complex volatile organic compounds (VOC). [15, 16] Monoterpenes ($C_{10}H_{16}$), for instance, are a class of hydrocarbons synthesized by terrestrial vegetation for various biological purposes, and emitted to the atmosphere in vast quantities. [17] In an oxidizing atmosphere, these VOCs can be short-lived, rapidly degraded by oxidation reactions to produce a variety of products, [18] some of which can be considerably less volatile than the parent compound. [19, 20] These low-volatility compounds can in turn contribute to the formation and growth of atmospheric aerosol particles. [21–23] Aerosols are solid, liquid, or mixed-phase particles suspended in air, a considerable portion of which originates in the atmosphere from condensing organic vapors, [23, 24] hence called secondary organic aerosol (SOA), and constitute another key component of the planet's climate. [25] Atmospheric aerosols have an overall cooling effect on climate, acting to increase planetary albedo, scattering a portion of incoming Solar radiation back to outer space both directly and by serving as seeds for the formation of clouds. [26, 27] Thus, the emission of VOCs represents another way in which life influences the climate. [28–30] However, not only plants and microorganisms can change the composition of the Earth's atmosphere, as humans too have done their share.

Other VOCs present in the atmosphere include nitrogen-containing compounds, such as amines. [31–33] Emission sources of amines include decomposition of organic matter, biogenic activity in the oceans, biomass burning, agricultural and industrial activities just to name a few. [31] While amines can also participate in aerosol particle formation, [34, 35] and do so effectively via clustering with sulfuric acid, [36] this thesis is concerned with their fate upon atmospheric oxidation. Particularly concerning is the potential of these oxidation reactions to produce toxic compounds, such as nitroamines and nitrosamines. [37–41] In an attempt to mitigate the effects of anthropogenic climate change, carbon-capture technologies were developed in recent years aiming to sequester CO_2 from the air, or from the flue gas of combustion systems. [42] Many such technologies employ amine solvents to act as CO_2 filters. [43, 44] During usage, production, or transport, large quantities of these amines may escape to the atmosphere, with a potentially detrimental impact on air quality. [45, 46]

The work presented in **Articles I** and **III** investigated the atmospheric fate of two cyclic nitrogen-containing compounds, namely 1,2,3,6-tetrahydropyrazine (THP) and imidazole, upon hydroxyl (OH) radical-initiated oxidation in the presence of O_2 and NO_x. The former is the major product of atmospheric photo-oxidation of piperazine, [47–49] an amine widely used as solvent for CO_2-sequestration in carbon-capture technology, [50] and the latter is an aromatic species found to be an important component of brown carbon, [51–54] (visible) light-absorbing compounds in atmospheric aerosol particles. [55–57] The work presented in **Article II** investigated the reactivity of nitrooxy-alkoxyl and nitrooxy-alkyl radicals, derived from the nitrate (NO_3) radical-initiated oxidation of different monoterpenes, towards β-scission reaction pathways. These reaction

intermediates are critical, as their reactivity can determine the overall yield of low-volatility products that may contribute to SOA formation and growth. [58–61]

Atmospheric oxidation reaction mechanisms are often complex, with branching reaction pathways, many of which proceed via multiple consecutive steps connecting extremely reactive intermediates. [18, 62] Thus, elucidation of such mechanisms is an arduous task to undertake with experiments, but which can often be successfully addressed with theoretical methods, at least to a certain extent. [63]

Articles I and **III** present exploratory reaction kinetics investigations – given a starting reactant, the available reaction pathways were searched for, drawing mostly from knowledge of which reactions are typically important in the oxidation mechanism of similar compounds, discussed in Chapter 2. In practice, reaction search entailed characterization of the energetics of each assumed reaction step, done with quantum chemistry methods. Later, theoretical reaction kinetics methods were employed to predict which of the available pathways are predominant, revealing the atmospheric fate of the investigated compounds upon oxidation. An overview of the theory applied to the work presented in this thesis is given in Chapter 3. Unexpected, and previously unreported, reaction pathways were also discovered in these mechanistic investigations, and Chapter 4 devotes some attention to their potential significance to the atmospheric chemistry of organic nitrogen in general. The research presented in **Article II** was not exploratory in nature, but involved instead a targeted investigation of structure-reactivity patterns for a series of reaction intermediates undergoing reactions of the same type.

The main objectives of this thesis are to:

- investigate the atmospheric fate of two important cyclic nitrogen-containing organic compounds upon oxidation, and assess the impact of their emissions on air quality.
- investigate how diverse the selectivity of different monoterpenes can be with respect to two critical branching points during NO_3-initiated oxidation, and the implications of this diversity to aerosol particle yields.
- explore the poorly-known chemistry of imines and heterocyclic aromatics in the Earth's atmosphere.
- expand our fundamental understanding of the structural features, such as substituent effects, which control the reactivity of organic nitrogen compounds towards different oxidation reaction pathways.

2. Atmospheric Oxidation Pathways

2.1 Atmospheric Oxidants

The Earth's atmosphere owes its oxidizing nature to the large abundance of O_2 in its bulk. However, molecular oxygen alone cannot be responsible for the oxidation of volatile organic compounds known to take place in the gas-phase. The direct reaction of O_2 with closed-shell organic species is forbidden by spin-selection rules, and hence it is too slow [64, 65] to efficiently initiate oxidative reaction chains under the lower temperature conditions found in the atmosphere (which is fortunate, as any organic matter in contact with air would otherwise be prone to spontaneous combustion). Atmospheric oxidation thus requires the participation of more reactive oxidizing agents, which are able to initiate (organic) radical chain reactions. On Earth, the most important of these oxidants are hydroxyl radical (OH), nitrate radical (NO_3) and ozone (O_3). [9]

In one way or another, the initial oxidants all are produced by photochemistry, so that atmospheric oxidation of organic compounds is ultimately driven by Solar radiation. In addition, the presence of NO_x (NO and NO_2) is critical because, as shall become clear throughout this chapter, these species are important catalysts involved in the formation and recycling of atmospheric oxidants. [9] The main source of ozone in the troposphere (the lowermost layer of the atmosphere) is photolysis of NO_2:

$$NO_2 \xrightarrow{h\nu} NO + O \tag{R2.1}$$

The oxygen atom produced this way can then react with a O_2 molecule, producing O_3:

$$O + O_2 \longrightarrow O_3 \tag{R2.2}$$

Ozone, in turn, is the precursor species for the other two oxidants, OH and NO_3 radicals. Photolysis of O_3 can produce O_2 and O in their electronic excited (singlet) states, with wavelengths of the Solar spectrum which are available in the troposphere:

$$O_3 \xrightarrow{h\nu} O(^1D) + O_2(^1\Delta_g) \tag{R2.3}$$

Unlike their electronic ground-state counterparts, excited $O(^1D)$ atoms are capable of reacting with H_2O to yield two OH radicals:

$$O(^1D) + H_2O \longrightarrow 2\,OH \tag{R2.4}$$

Finally, nitrate radicals can be produced from the reaction of O_3 with NO_2:

$$O_3 + NO_2 \longrightarrow O_2 + NO_3 \tag{R2.5}$$

Regarded as the main atmospheric oxidant, hydroxyl radical is able to initiate the oxidation of carbon monoxide, and most (if not all) organic compounds in the atmosphere. [62, 66] Due to this high reactivity, the lifetime of OH radical is short (0.01–1 s), [67] and the maintenance of a significant gas-phase concentration of this oxidant requires constant photochemical replenishment, which is possible only during the day. The average global day-time steady-state concentration of OH radical is about 10^6 molecules cm^{-3}, whereas nighttime concentrations can be as low as $\sim 10^4$ molecules cm^{-3}. [68, 69] Despite its photochemical source, ozone is less reactive than the OH radical, and significant gas-phase concentrations of this oxidant are possible also during the night. Nitrate radicals, on the other hand, are quickly lost via photolysis, [70]

$$NO_3 \xrightarrow{h\nu} NO + O_2 \tag{R2.6}$$

$$NO_3 \xrightarrow{h\nu} NO_2 + O \tag{R2.7}$$

so a significant concentration of this oxidant can only be reached in the nighttime atmosphere, or under severely polluted conditions (high $[O_3]$ and $[NO_x]$). [71]

2.2 Organic Radical Chain Initiation

Initial attack of an atmospheric oxidant on a complex organic compound may proceed via multiple reaction pathways. Often, several of these pathways can be competitive. The reaction of hydrocarbons with OH or NO_3 radicals, for instance, can proceed either via H-abstraction pathways,

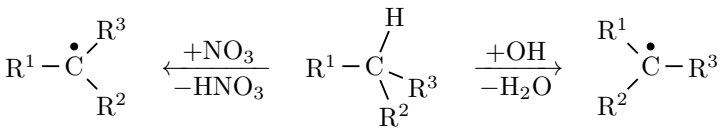

(R2.8)

or via electrophilic addition to a unsaturated C=C bond:

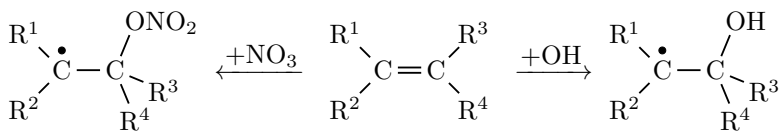

(R2.9)

However, whenever a C=C double-bond is available, addition channels tend to outcompete H-abstractions, [18, 62, 72] as is the case with alkenes. Nevertheless, the product of either of these types of reaction pathway is a C-centered (alkyl) radical, an open-shell species, which can then readily react with O_2, leading to the formation of a alkylperoxyl radical (RO_2):

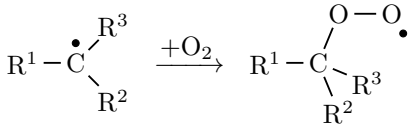

(R2.10)

Oxidation initiated by ozone (ozonolysis) proceeds via a different mechanism, [73] and requires the presence of a C=C double-bond in the organic substrate, but it may also eventually lead to the formation of C-centered radical products. [74] Since oxidation by ozone is not the main focus of this thesis, it shall not be discussed further here.

As for the oxidation of organic nitrogen compounds, if a primary or secondary amine functional group is present, initial attack by OH radicals may also proceed via H-abstraction from the nitrogen, [38, 75–78] producing a N-centered (aminyl) radical:

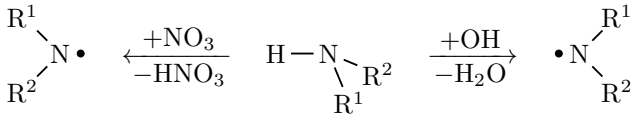

(R2.11)

Though less prone to do so than C-centered radicals, N-centered radicals can also react with O_2, [79–81] but ultimately leading to the formation of an imine plus hydroperoxyl radical (HO_2):

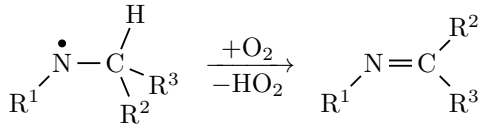

(R2.12)

Once formed in the atmosphere, imines can also undergo atmospheric oxidation. [82–86] Besides H-abstraction channels, initial attack by an OH radical on an imine can also proceed via addition to the C-terminus of the C=N double-bond:

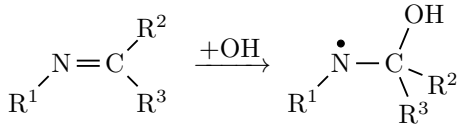

(R2.13)

Unlike with C=C analogues, OH-addition to an imine group tends to be slower than H-abstraction channels, albeit competitive. Initial attack on the N-terminus of C=N double-bonds have been observed to be negligible. [82, 86] The reactivity of a cyclic imine towards oxidation initiated by OH radicals was the central focus of **Article I**.

In general, O_2-addition to alkyl radicals involve large reaction rate coefficients ($k_{O_2} = \sim 10^{-12}$ cm^3 molecule^{-1} s^{-1}), which typically show a weak dependence on the identity of R substituent groups in the substrate. [87] Moreover, considering the sheer abundance of O_2 in the atmosphere, these O_2-addition reactions are extremely fast (with pseudo-first-order rate coefficients in the order of $\sim 10^7$ s^{-1}), outcompeting most other reaction channels. Save for a few exceptions, where the alkyl radical is prone to rapid rearrangement or dissociation reactions, it is usually assumed that reaction with O_2 is the sole fate of any alkyl radical formed in the atmospheric gas-phase. Some of these exceptional cases were investigated in **Articles II** and **III**, and are discussed in more detail in Section 2.6. On the other hand, N-centered radicals are much less reactive towards O_2 than C-centered radicals, [79, 81] with reaction rate coefficients ranging from 10^{-20} to 10^{-16} cm^3 molecule^{-1} s^{-1}. [80] At the lower end of this range of rate coefficients, other reaction channels can become competitive, most concerning of which being recombination with NO or NO_2 to yield a nitrosamine (R^1R^2NNO) or nitramine ($R^1R^2NNO_2$) respectively, [37, 88] known carcinogens:

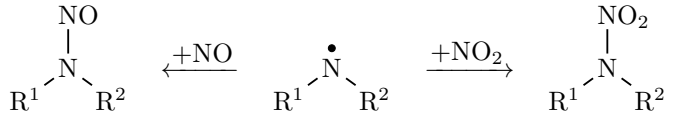

(R2.14)

The competing reaction pathways available to N-centered radicals was among the investigated topics in **Articles I** and **III**.

The fate of RO_2 radicals is less obvious still. These species are key reaction intermediates in atmospheric oxidation mechanisms, constituting branching points from which a multitude of different unimolecular or bimolecular reaction pathways may be available, [89, 90] oftentimes leading to products with widely different properties. The propagation (or termination) of atmospheric oxidative chain reactions by RO_2 chemistry shall be discussed in detail in Section 2.4. For now it suffices to say that the availability and, more importantly, the favorability of different unimolecular RO_2 reaction pathways is dictated by the identity of the R group, [89] and thus depend on which H-abstraction or addition pathway is preferentially followed upon initial attack by an oxidant. That being the case, it is worth exploring the general reactivity trends of atmospheric organic compounds towards reaction with OH or NO_3 radicals.

2.3 General Reactivity Trends

Considering the competition among reaction pathways of the same type, similar structural factors, such as the substitution pattern at the site of attack by an oxidant molecule, control the selectivity of both H-abstraction and addition reaction pathways. [91] For instance, reactions leading to the development of a radical center with a higher number of alkyl substituents are favored. Thus, H-abstraction from a tertiary carbon is more favorable than it is from a secondary

carbon, which in turn is more favorable than from a primary carbon. [92–94] Likewise, addition reaction pathways involving attack of the oxidant on the less substituted terminus of C=C double-bond (in asymmetric alkenes) are favored, as those lead to the development of the radical center on the most substituted carbon. The presence of heteroatoms in the organic substrate have a substantial impact on selectivity. Reactions proceeding via H-abstraction from an α-amino ($-NR^1R^2$), α-hydroxyl ($-OH$), α-alkoxyl ($-OR$) or α-oxo ($=O$) carbon are typically favored, [91] and tend to outcompete other channels.

The selectivity of OH or NO_3 radical attack can sometimes be rationalized in terms of the Bell-Evans-Polanyi relationship, that is, the more exothermic a reaction is, the faster it proceeds. [95] In essence, this means that the substituent effects which stabilize the products of a reaction (relative to the reactants) also work to stabilize the transition state (TS), at least to a certain extent. In the case of alkyl-substitution, reaction assistance is primarily due to hyperconjugation between the filled σ_{CH} orbitals on the substituents and the developing singly-occupied p_C orbital on the product's formal radical center (Figure 2.1a). [93, 94] In the TS of H-abstraction or addition reactions, the same hyperconjugative interaction would involve the empty antibonding orbitals of the partially broken bonds, σ^*_{CH} or π^*_{CC} respectively, as acceptor orbitals (Figure 2.1b and c).

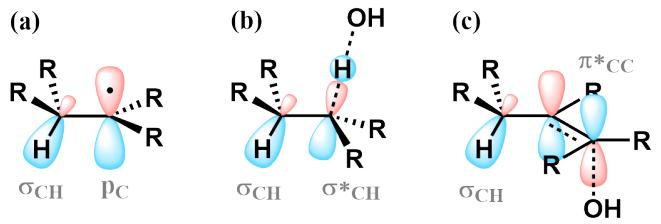

Figure 2.1: Stabilizing hyperconjugative interactions from alkyl substitution in the reaction of organic compounds with OH radical. Orbitals are not shown to scale.

In the case of α-amino, α-hydroxyl, and α-alkoxyl substitution, hyperconjugation has a somewhat greater stabilizing effect, involving a non-bonding lone-pair orbital on the heteroatom (n_N or n_O) as a donor. [96] Reaction assistance is even more pronounced in the case of allylic substitution, considering that resonance due to p-π conjugation has a greater stabilizing effect on a radical. In fact, H-abstraction from an allylic position is more favorable than from tertiary carbons, [92, 93] however, these pathways tend to be minor because the presence of a C=C double-bond in the substrate also allows for faster addition channels. [97–100]

That being said, the relative stability of the products of competing reactions can only partly explain selectivity trends in atmospheric oxidation mechanisms, and often it cannot explain them at all. This is not surprising, considering that exothermic channels in general have early transition states (i.e. their structure resemble more closely the reactants than the products), as per the Hammond postulate. [95] For instance, OH radical addition channels tend to be less exothermic

than competing allylic H-abstractions, despite being much faster. [97–101] OH and NO_3 radicals are relatively soft electrophiles (lower-energy SOMO), [102] and are thus more reactive towards softer nucleophiles (higher-energy HOMO). [93, 94, 103] Since π-bonds are in general softer than σ-bonds, it follows that C=C groups are better nucleophiles for attack of OH or NO_3 than C–H groups.

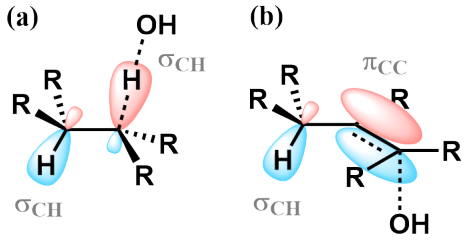

Figure 2.2: HOMO energy-raising hyperconjugative interactions from alkyl substitution in reaction of organic compounds with OH radical. Orbitals are not shown to scale.

Along this line of reasoning, substituents that raise the energy of the HOMO in an organic substrate via (hyper)conjugation (Figure 2.2) may increase their propensity to react with OH or NO_3 radicals. In other words, π-donating substituents can activate adjacent C–H or C=C bonds via interactions between filled orbitals, which have an overall destabilizing effect. [93, 94] For example, alkyl-substitution to the site of attack by an oxidant in a C=C double-bond (as opposed to the carbon developing the radical center) may also assist the reaction, making the π-bond softer via $\sigma_{CH} \rightarrow \pi_{CC}$ hyperconjugation. The atmospheric oxidation of limonene is an illustrative case of this phenomenon. [104] Limonene has two C=C double-bonds, one endocyclic and one exocyclic, both of which are able to accommodate the radical center in a tertiary carbon upon OH or NO_3 addition to the least-substituted carbon (Scheme 2.1). However, addition to the endocyclic double-bond, whose degree of substitution is higher overall, is favored. [104–106] The effect of π-donating substituents at the attack site appears to be secondary compared to the effect of substitution to the product's radical center, but it has a noticeable impact on the selectivity of addition channels.

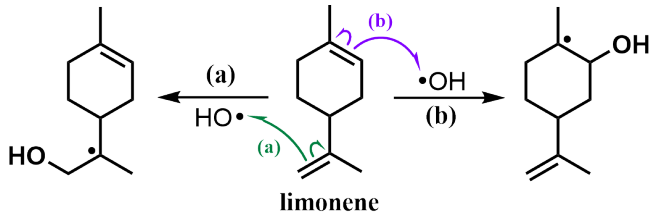

Scheme 2.1: Limonene reaction with OH radical via addition to exocyclic (a) or endocyclic (b) double-bond.

Much of the trends explored in this section also apply to the reactivity of intermediates formed further along oxidation mechanisms, with some notable caveats, and we shall return to them when necessary.

2.4 Peroxyl Radicals

Peroxyl radicals (RO_2) are critical reaction intermediates in atmospheric oxidation mechanisms, from which a myriad of unimolecular and bimolecular pathways may originate. [89, 90] The main unimolecular channels which are generally available to organic RO_2 are: 1) Intramolecular hydrogen shifts, where the peroxyl group (−OO) abstracts a hydrogen atom from another moiety, most often a carbon, producing a hydroperoxy-alkyl radical;

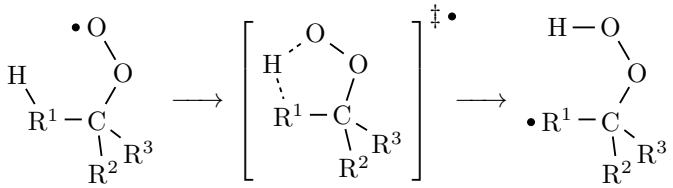

(R2.15)

2) Endo-cyclization reactions, [107] where the peroxyl group attacks a C=C double-bond instead, producing a (endo)cyclic alkylperoxy-alkyl radical;

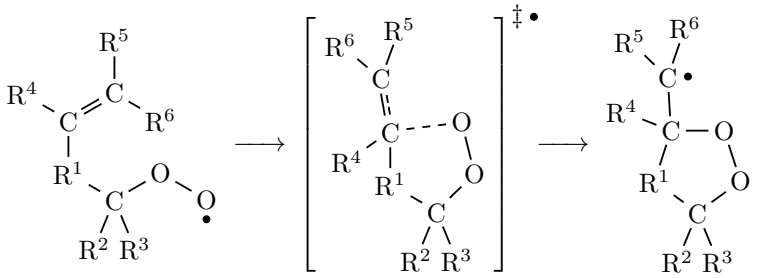

(R2.16)

3) And HO_2-elimination reactions, where a hydrogen abstraction from a β-peroxyl C, N, or O atom (1,4 H-shift) is concerted with C−O(O) bond cleavage, leading to loss of a HO_2 radical and producing a C=C, C=N, or C=O double-bond:

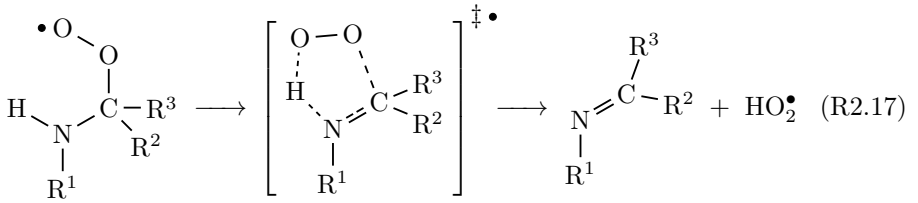

(R2.17)

In the first two pathways, a C-centered radical can be re-formed, allowing for the propagation of the organic radical chain upon addition of another O_2 molecule. The continuation of this process, via successive H-shift/endo-cyclization reactions followed by O_2-addition, is called autoxidation, and can potentially lead to the formation of highly-functionalized, low-volatility compounds, which in turn can contribute to the formation and growth of SOA particles. [19, 20, 108] The HO_2-elimination pathways, however, produce a closed-shell organic species and provoke an early termination of the oxidative chain.

Many relevant RO_2 bimolecular reaction pathways exist in the Earth's atmosphere, such as reaction with NO, NO_2, HO_2, or self- and cross-reactions with another $R'O_2$. [89] From these, perhaps the major pathway is reaction with NO, which proceeds predominantly with formation of a corresponding alkoxyl radical (RO) and NO_2:

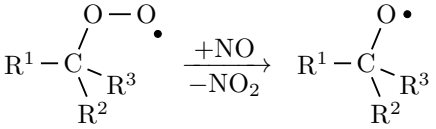

(R2.18)

Alkoxyl radicals comprise another important class of reaction intermediates in oxidation mechanisms, able to react via multiple different reaction pathways. [109] These intermediates and their role in atmospheric chemistry shall be discussed in more detail in the next section 2.5. Another major outcome of RO_2 + NO pathways is the regeneration of a NO_2 molecule, which can undergo photolysis to produce another O_3 molecule, which can also photolyse to produce another OH radical, which in turn may initiate the oxidation of another organic compound molecule. One may notice now where this is going: the NO_x species act as photocatalysts in atmospheric oxidation mechanisms. [9] It follows that, if both NO_x and VOCs are present in the air at elevated concentrations, exacerbated oxidation rates via NO_x cycling can eventually produce a high burden of ozone and fine aerosol particles (via condensable vapors), detrimental to air quality. At their worst, these conditions may create photochemical smog.

The availability of unimolecular pathways and the RO_2 selectivity towards them is highly dependent on the reactant's structure, [72, 110, 111] with rate coefficients that can span many orders of magnitude. Bimolecular pathways, on the other hand, tend to be near barrierless and are therefore always available as long as reaction partners can be found in the surrounding air, with second-order rate coefficients largely independent of the structure of the substrate. [112] Consequently, competition between RO_2 unimolecular and bimolecular pathways is ultimately driven by the unimolecular reactivity of the RO_2, as well as the concentration of bimolecular reaction partners. In pristine environments, for instance, NO_x concentrations can be as low as 1-10 ppt, allowing for unimolecular pathways to be competitive, whereas in polluted conditions, where NO_x concentrations can be as high as 1-10 ppb, RO_2 + NO reactions tend to outcompete them. With this in mind, it is worth briefly exploring the general reactivity trends of RO_2 towards unimolecular pathways.

H-shift and endo-cyclization pathways may be seen as unimolecular analogues of the initial H-abstraction and addition by OH or NO_3 radicals respectively, described in Section 2.2, but occuring with intramolecular electrophilic attack of the peroxyl group instead. Unsurprisingly, the effect of substituents at the site of attack by a peroxyl group is then largely the same as those controlling the reactivity of initial oxidation steps discussed in Section 2.3. However, because the intramolecular cases may require significant distortion of the substrate so that the reacting functional groups can meet, other structural factors can significantly

limit reactivity, as discussed next.

Alongside the substitution pattern at the H-donor, the span of the intramolecular attack (i.e. the size of organic backbone between the reacting groups) is perhaps the most important factor controlling the reactivity of H-shifts. [113] Reactions occurring over short spans, such as 1,3 or 1,4 H-shifts, are in general energetically unfavorable because the transition state of these reactions assume a four- or five-membered ring-like structure, which is destabilized by increased bond-angle strain and/or a sub-optimal overlap between the SOMO (on the –OO group) and the σ_{CH} orbital (on the attack site) required for the atom transfer to take place. Reactions occurring over long spans such as 1,7 or 1,8 H-shifts, on the other hand, albeit not involving overly strained TS structures, are generally unfavorable due to the entropic penalty involved in the loss of many internal rotors upon formation of a ring-like TS. It follows that, in general, 1,5 and 1,6 H-shifts have an optimal span from a combined energetic and entropic perspective, and are typically observed to be the most competitive among pathways of the same type. A similar trend can also be drawn for the reactivity of RO_2 towards endo-cyclization at different spans. [111]

That being said, the hindrance to reactivity towards these unimolecular pathways is compounded if the RO_2 is derived from a cyclic compound, such as monoterpenes. [111, 114] Here, the rigid carbon backbone can hinder, and sometimes completely prevent, the approach of the peroxyl group on potential attack sites due to the additional structural strain it introduces. Some pathways can even be rendered unavailable, like those involving attack on sites on the opposite side of a ring. Thus, cyclic RO_2 species are typically more stable with respect to unimolecular reaction channels, and their fate can be dominated by bimolecular reactions even under low NO_x conditions.

Lastly, HO_2-elimination reactions follow a somewhat different reactivity trend. In general, this pathway appears to be negligible in atmospheric oxidation mechanisms if it involves the formation of a C=C double-bond, [115] while it is a major pathway when it involves the formation of a C=N or C=O double-bond. [116–120] Moreover, since the C–O(O) interatomic distance is considerably lengthened in the TS, the extra strain imposed by rigid cyclic structures do not seem to hinder these reactions. [48, 49, 121, 122] HO_2-eliminations are particularly important in the atmospheric oxidation of primary and secondary amines, considering that an initial oxidant attack on these species tends to proceed preferentially via H-abstraction from a α-amino position, as discussed in Section 2.3. As a consequence, the major amine-derived RO_2 radicals tend to bear a β-peroxyl NH group granting access to a HO_2-elimination pathway, leading to an imine. The fact that imines consistently appear as major products of amine oxidation, can be explained by the favorability of this pathway, in combination with the reaction of N-centered radicals with O_2 (Section 2.2). **Articles I** and **III** explored the reaction pathways available to RO_2 derived from unsaturated cyclic N-containing compounds, where HO_2-eliminations take center place.

2.5 Alkoxyl Radicals

Compared to peroxyl radicals, alkoxyl radicals (RO) are typically much more reactive intermediates. Still, these species can react via multiple different unimolecular and bimolecular pathways. [109, 123, 124] The most important bimolecular reaction channel for RO radicals is perhaps H-abstraction from the α-oxyl carbon by O_2, producing a carbonyl plus HO_2:

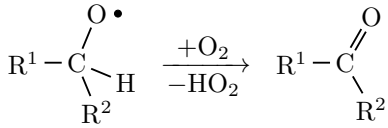

(R2.19)

Albeit not as fast as O_2-addition to alkyl radicals, these reactions still typically display large pseudo-first-order rate coefficient values $k_{O_2}[O_2] \sim 10^4\ s^{-1}$. [87, 109, 125] Needless to say, this pathway is not available for tertiary alkoxyl radicals, whose formation is favored over their secondary or primary counterparts during the oxidation of complex organic compounds (Section 2.2), such as monoterpenes, whenever possible. Moreover, as shall be discussed next, RO radical unimolecular pathways can be so fast, that reaction with O_2 can be outcompeted even when an abstractable hydrogen is available. [123, 126]

The main unimolecular pathways generally available to alkoxyl radicals are intramolecular H-shifts and β-scissions. [123, 127] The former are analogous to RO_2 H-shifts, and are subject to the same selectivity trends and structural constraints discussed in the previous section, [128] but involve intramolecular attack of an oxyl group instead, producing hydroxy-alkyl radicals:

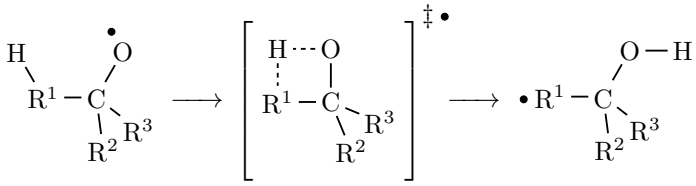

(R2.20)

β-Scission reactions, on the other hand, do not appear to suffer from the same constraints. These pathways involve the cleavage of a bond between the α-oxyl carbon and a β-oxyl atom (C_α–C_β), leading to the formation of a carbonyl and a C-centered radical:

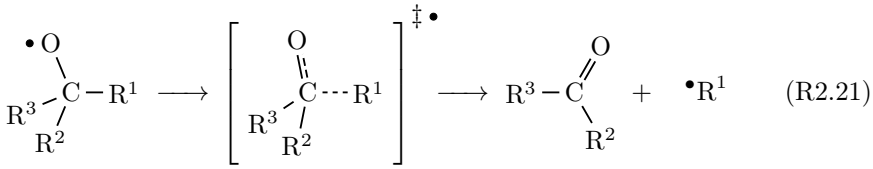

(R2.21)

Apart from a lengthening of the breaking C_α–C_β bond and a re-hybridization of the C_α and C_β atoms, this reaction does not require much more in terms of structural distortion in order to occur. Combined with the stabilizing effect from

formation of a C=O double-bond, this relative lack of constraint in the TS may explain why β-scission reactions are typically very competitive. In fact, β-scissions can be especially fast for cyclic alkoxyl radicals, as the TS can be further stabilized by release of ring-strain if cleavage occurs at an endocyclic bond, opening the cycle. That being said, selectivity towards these channels is strongly dependent on the identity of substituents to both the C_α atom developing the π-bond and the C_β atom developing the radical center. [126] The trends observed for the latter are similar to the ones discussed in Section 2.3.

The significance of RO β-scission pathways in the atmospheric oxidation of cyclic compounds becomes clearer considering that, as cyclic RO_2 tend to be relatively unreactive towards unimolecular channels, RO radicals may be their major products. Moreover, since RO H-shifts are as well unfavorable in a cyclic structure (perhaps even more than in RO_2, given that the attacking functional group is now one atom shorter), competition among β-scission pathways have a decisive role determining the overall fate and impact of oxidation. For instance, while β-scission reactions in acyclic compounds lead to fragmentation, producing lower-mass less-volatile products in the process, a cyclic RO molecule remains intact if cleavage occurs at an endocyclic bond, while undergoing ring-opening. Upon subsequent O_2-addition to the open-chain alkyl radical, the new RO_2 radical is no longer constrained by a rigid structure, and rapid H-shift and/or endo-cyclization pathways may now be open, potentially allowing for autoxidation.

Alkoxyl radical β-scissions were among the investigated reaction pathways in **Articles I**, **II** and **III**. In **Article II**, however, these pathways and how their selectivity can differ for several monoterpene-derived alkoxyl radicals, were the main focus of research.

2.6 Alkyl Radicals

The reaction of C-centered radicals with O_2 is so fast that, in most cases, it can be assumed with a high degree of certainty that peroxyl radical formation is their sole fate in the atmosphere. However, a few exceptions exist, where fast unimolecular isomerization or dissociation reaction channels are available and able to compete with O_2-addition. Two well known cases are the decomposition of α-hydroperoxyl- and α-nitrooxyl-alkyl radicals, [129, 130] unstable species whose spontaneous (typically barrierless) elimination of a OH radical or NO_2 leaves behind a (closed-shell) carbonyl compound:

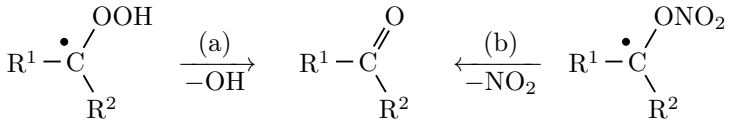

(R2.22)

In both of these cases, dissociation is expected to completely outcompete O_2-addition, leading to the termination of the organic oxidative chain. At the same

time, channels R2.22a and R2.22b regenerate OH radicals or NO_2, which can initiate the oxidation of another closed-shell organic species via reactions R2.1-R2.9.

As may be apparent from the substituent groups, these unstable alkyl radicals are not typically products of initial attack of OH or NO_3 on an organic substrate, but are more commonly produced during latter stages of oxidation mechanisms from RO_2 or RO chemistry. Since the formation of these intermediates is rapidly followed by termination of the oxidative chain (the organic product is a closed-shell species), it can limit the yield of low-volatility products from the oxidation of a given organic compound, and thus limit the contribution to the growth of secondary organic aerosols (SOA). [58] Moreover, in the case of α-nitrooxyl alkyl radicals, reaction channel R2.22b can also limit the production of closed-shell organonitrates ($RONO_2$), important atmospheric NO_x reservoir species. [9] **Article II** investigated how likely is the formation of these intermediates from alkoxyl radical β-scissions during the NO_3-initiated oxidation of five abundant monoterpenes.

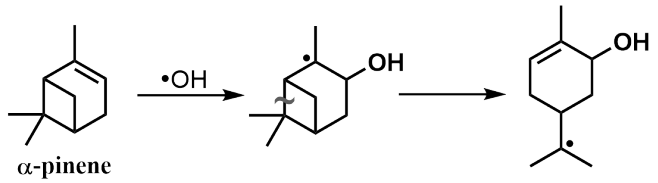

Scheme 2.2: Ring-opening rearrangement reaction following OH radical attack on α-pinene (top) and sabinene (bottom).

Another type of alkyl radical reaction which can be competitive with O_2-addition is the rearrangement by ring-opening. [61, 63, 131] In this rearrangement, opening of an adjacent cycloalkyl group (via $C_\alpha - C_\beta$ bond cleavage) produces a C=C double bond, and moves the radical center to the C_β atom. For the product of OH-addition to α-pinene, for instance, this pathway leads to opening of a four-membered secondary ring, producing another tertiary alkyl radical (Scheme 2.2), and is fast enough that about 50% of subsequent O_2-addition reactions actually occur with the ring-opened species. [61] Release of ring-strain contained in the four-membered ring translates into a bond-scission reaction energy barrier of 12.2 kcal mol^{-1}, which albeit low, is still not low enough to allow the reaction to compete with O_2-addition. However, a significant portion of vibrationally hot adduct molecules, produced immediately after the OH-addition step, may react via ring-opening before the excess energy from the preceding step can be dissipated into the surrounding gas via collisions, enhancing overall reaction rates. The non-thermal contribution to chemically activated reaction rates is discussed further in Section 3.3.3. **Article II** also explores the reactivity towards this pathway, as it becomes available to alkyl radicals derived from NO_3-addition to other monoterpenes.

3. Theoretical Background

3.1 Quantum Chemistry

The first step towards predicting the speed and direction of chemical change with *ab initio* methods (from first principles), is to characterize how the distribution of energy in a molecule changes as it undergoes a chemical reaction. The structure and behavior of chemical systems, such as atoms and molecules, is described by quantum mechanics. In quantum theory, particles are described as waves, by means of a wavefunction (Ψ). An immediate consequence of this description is that the intervals between energy levels that a quantum system is allowed to have are discrete, rather than continuous, as is observed with a classical system. This is especially evident if quantum particles are confined within a small space, such as electrons and atomic nuclei bound by electrostatic interactions in atoms and molecules.

The wavefunction contains all the information necessary to derive the properties of a quantum system, as well as how it evolves with time. Physical observables, such as the energy, can be extracted from the wavefunction of a system by employing operators associated with those observables. The operator associated with the total energy of a system, for instance, is the Hamiltonian operator ($\hat{H}$). Since the work presented in this thesis which relies on quantum chemistry is concerned only with the properties of ground-states, whose wavefunctions correspond to standing waves, the time-dependence of the system can be neglected. Thus, operating $\hat{H}$ on a wavefunction $\Psi(\mathbf{r})$, which depends only on the spatial positions $\mathbf{r}$ of each particle, yields the time-independent Schrödinger equation:

$$\hat{H}\Psi(\mathbf{r}) = E\Psi(\mathbf{r}) \tag{3.1}$$

Where E is the total energy of the system described by a wavefunction $\Psi(\mathbf{r})$. The Hamiltonian operator can be expanded in terms of a kinetic energy operator ($\hat{T}$) and a potential energy operator ($\hat{V}$):

$$\hat{H} = \hat{T} + \hat{V} = \frac{\hbar}{2m}\frac{\partial^2}{\partial \mathbf{r}^2} + V(\mathbf{r}) \tag{3.2}$$

Where $\hbar$ is the reduced Planck constant ($h/2\pi$) and m is the mass of the particle. The potential energy operator involves a multiplication by $V(\mathbf{r})$, which is the potential energy of the particle as a function of its position, and it is the "shape" of this function that determines much of the structure of bound quantum systems. For a molecule described by a wavefunction $\Psi(\mathbf{R}, \mathbf{r})$ dependent on the spatial positions of n electrons ($\mathbf{r} = \mathbf{r}_1, \mathbf{r}_2, \ldots, \mathbf{r}_n$) and m nuclei ($\mathbf{R} = \mathbf{R}_1, \mathbf{R}_2, \ldots, \mathbf{R}_m$), the kinetic and potential energy terms in the Hamiltonian may be further expanded as:

$$\hat{H} = \hat{T}_e + \hat{T}_N + \hat{V}_{ee} + \hat{V}_{NN} + \hat{V}_{eN} \tag{3.3}$$

Where $\hat{T}_e$ and $\hat{T}_N$ are the kinetic energy operators associated with the motion of electrons and nuclei respectively, $\hat{V}_{ee}$ and $\hat{V}_{NN}$ are the potential energy operators associated with inter-electronic and inter-nuclear repulsive Coulombic interactions respectively, and $\hat{V}_{eN}$ is the potential energy operator associated with electron-nuclear attractive Coulombic interactions. It quickly becomes apparent that, for molecules and multielectron atoms, the potential energy terms in the Hamiltonian are sums over many pair-wise interactions between moving particles.

$$\hat{V}(\mathbf{R}, \mathbf{r}) = \frac{1}{2}\sum_{i \neq j}^{n} \hat{V}_{ee}(\mathbf{r}_i, \mathbf{r}_j) + \frac{1}{2}\sum_{I \neq J}^{m} \hat{V}_{NN}(\mathbf{R}_I, \mathbf{R}_J) + \sum_{I=1}^{m}\sum_{i=1}^{n} \hat{V}_{eN}(\mathbf{r}_i, \mathbf{R}_I) \tag{3.4}$$

These electrostatic interactions are of similar magnitude, and therefore the motion of each electron and nucleus is coupled to that of all others. This is a many-body problem, which means that no analytical (exact) solution exists for the Schrödinger equation of any chemical system other than hydrogen-like atoms (one nucleus and one electron). Practical applications of quantum chemistry thus require a numerical approach, relying on a number of approximations to the Schrödinger equation, the most important of which are detailed next.

The first approximation to be discussed assumes that the coupling of the electronic motion with the nuclear motion is weak, and can be neglected. Since electrons are much less massive than atomic nuclei (by more than three orders of magnitude), they also move much faster. Thus, any perturbation in the potential caused by a (relative) displacement of nuclei, in a molecular vibration for instance, provokes an instantaneous response from the electrons, which change their overall spatial distribution to adjust to the new potential. In other words, the time-scale for the relaxation of the molecular electronic structure is much shorter than the time scale of nuclear motion. This is the basis of the Born-Oppenheimer approximation, whose application involves solving the molecular Schrödinger equation while the atomic nuclei are kept at fixed positions. It follows that the molecular wavefunction can be separated into an electronic term Ψ_e and a nuclear term Ψ_N:

$$\Psi = \Psi_e \Psi_N \tag{3.5}$$

Operating the molecular Hamiltonian (equation 3.3) on $\Psi_e\Psi_N$, while noticing that, since nuclei are static, the nuclear kinetic energy term ($\Psi_e\hat{T}_N\Psi_N$) is zero

and the inter-nuclear potential energy term ($\Psi_e \hat{V}_{NN} \Psi_N$) is a constant ($V_{NN}(\mathbf{R})$), the Schrödinger equation can be written in terms of electronic components.

$$\hat{H}_e \Psi_e(\mathbf{R}, \mathbf{r}) = (\hat{T}_e + \hat{V}_{ee} + \hat{V}_{eN}) \Psi_e(\mathbf{R}, \mathbf{r}) + V_{NN}(\mathbf{R}) \tag{3.6}$$

$$\hat{H}_e \Psi_e(\mathbf{R}, \mathbf{r}) = E_e(\mathbf{R}) \Psi_e(\mathbf{R}, \mathbf{r}) \tag{3.7}$$

Where $\hat{H}_e$ is the electronic Hamiltonian, and $E_e(\mathbf{R})$ is the electronic kinetic and potential energy plus the potential energy of inter-nuclear interactions (commonly referred to as just electronic energy), at a specific, fixed arrangement of nuclear positions ($\mathbf{R}$). Note that the Schrödinger equation within the BO approximation still depends on the positions of the nuclei $\mathbf{R}$, but it does so parametrically. Solution of equation 3.7 for a series of different nuclear arrangements (molecular geometries) yields a potential energy surface (PES). The PES may be thought of as a m-fold hyperdimensional potential energy landscape encountered by the molecule's nuclei as they move relative to one another, and the contribution that this motion has to the total energy can be later treated with statistical mechanics, as described in Section 3.2. For the purposes of predicting the rate of chemical reactions, only a few regions of the PES need to be characterized, as explored further in Sections 3.1.5 and 3.3.

Although the BO approximation alleviates some of the problems associated with the solution of a molecular Schrödinger equation, the challenge of describing inter-electronic interactions ($\hat{V}_{ee} \Psi_e$) still remains. The next assumption to be made, the mean-field approximation, attempts a neglect of electron-electron couplings, as shall be introduced in the next subsection in terms of the Hartree-Fock (HF) theory.

3.1.1 The Mean-Field Approximation

One of the earliest methods developed as an approximation to the Schrödinger equation for atoms and molecules originated from the Hartree-Fock (HF) theory. Although this theory (alone) is not sufficient to provide accurate energies, it serves as a basis for many other successful theories developed later on, which are widely employed nowadays to tackle problems in chemical kinetics. Moreover, many of the concepts discussed here are useful to understand theories which are technically not wavefunction-based, such as Density Functional Theory (DFT).

The starting point of HF theory is to assume that the *total* electronic wavefunction Ψ (we shall henceforth drop the subscript e for simplicity) of a n-electron molecule can be expanded as a product of n non-interacting one-electron wavefunctions ψ, called a Hartree product:

$$\Psi(\mathbf{r}) = \Psi(\mathbf{r}_1, \mathbf{r}_2, \ldots, \mathbf{r}_n) = \psi_1(\mathbf{r}_1)\psi_2(\mathbf{r}_2)\ldots\psi_n(\mathbf{r}_3) = \prod_{i=1}^{n} \psi_i(\mathbf{r}_i) \tag{3.8}$$

Each wavefunction $\psi_i(\mathbf{r}_i)$ is a function of the position in three-dimensional space (x_i, y_i, z_i in cartesian coordinates) as well as the spin state ($m_{s,i}$) of electron i.

Thus, ψ_i correspond to spin-orbitals, each containing a spatial (orbital) component $\varphi_i(x_i, y_i, z_i)$ and a spin $\sigma(m_{s,i})$ component:

$$\psi_i(\mathbf{r}_i) = \varphi_i(x_i, y_i, z_i)\sigma(m_{s,i}) \tag{3.9}$$

Spin is an intrinsic property of fundamental particles, whose description is absent from a non-relativistic treatment of quantum mechanics (such as that of the Schrödinger equation), and must be included here in an *ad hoc* manner. Electrons have a spin quantum number $s = 1/2$, so only two spin states are possible, $m_s = +1/2$ (α spin) or $m_s = -1/2$ (β spin). The inclusion of the spin dimension to the wavefunction introduces a constraint associated with the Pauli principle, which states that the total wavefunction must be antisymmetric with respect to the exchange of two identical fermions, particles with half-integer spin. In other words, since electrons are (identical) fermions, the total molecular wavefunction must change sign if two electrons exchange their occupied spin-orbitals:

$$\Psi(\mathbf{r}_1, \mathbf{r}_2, \ldots, \mathbf{r}_n) = -\Psi(\mathbf{r}_2, \mathbf{r}_1, \ldots, \mathbf{r}_n) \tag{3.10}$$

This may seem like a trivial issue (electrons are, after all, *identical* particles), but it has far-reaching implications for the structure of matter. A discussion on the nature of the Pauli principle would go beyond the scope of this thesis, but for now, it suffices to say that the fact that no more than two electrons can occupy the same orbital (or no more than one per spin-orbital) is an immediate consequence of the antisymmetry condition.

Returning to HF theory, one can realize that the Hartree product in equation 3.8 does not satisfy the antisymmetry condition. However, this condition can be accounted for if the total electronic wavefunction is instead expanded as an antisymmetrized linear combination of Hartree products. This expansion is often expressed in mathematical form as a determinant, called a Slater determinant:

$$\Psi(\mathbf{r}_1, \mathbf{r}_2, \ldots, \mathbf{r}_n) = \frac{1}{\sqrt{n!}} \begin{vmatrix} \psi_1(\mathbf{r}_1) & \psi_2(\mathbf{r}_1) & \cdots & \psi_n(\mathbf{r}_1) \\ \psi_1(\mathbf{r}_2) & \psi_2(\mathbf{r}_2) & \cdots & \psi_n(\mathbf{r}_2) \\ \vdots & \vdots & \ddots & \vdots \\ \psi_1(\mathbf{r}_n) & \psi_2(\mathbf{r}_n) & \cdots & \psi_n(\mathbf{r}_n) \end{vmatrix} \tag{3.11}$$

Where the $1/\sqrt{n!}$ factor is the normalization constant (expansion of a $n \times n$ determinant results in $n!$ terms). The columns in the Slater determinant correspond to different spin-orbitals, and the rows correspond to different electrons. If two rows exchange positions, the sign of Ψ is reversed, and if two rows are identical (corresponding to two electrons occupying the same spin-orbital), the wavefunction vanishes ($\Psi = 0$). The Pauli principle is thus satisfied.

Now, substituting the determinantal wavefunction Ψ into equation 3.7, multiplying both sides from the left by Ψ^* (complex conjugate of Ψ), and integrating

over all space, yields the expectation value for $E_e(\mathbf{R})$:

$$E_e(\mathbf{R}) = \frac{\int \Psi^*(\mathbf{r})\hat{H}\Psi(\mathbf{r})\mathrm{d}\mathbf{r}}{\int \Psi^*(\mathbf{r})\Psi(\mathbf{r})\mathrm{d}\mathbf{r}} + V_{NN}(\mathbf{R}) \tag{3.12}$$

If the spin-orbital components of Ψ are chosen to be an orthonormal set (orthogonal and normalized), such that:

$$\int \psi_i^*(\mathbf{r}_1)\psi_j(\mathbf{r}_1)\mathrm{d}\mathbf{r}_1 = \begin{cases} 1, & \text{if } i = j \quad \text{(normalized)} \\ 0, & \text{if } i \neq j \quad \text{(orthogonal)} \end{cases} \tag{3.13}$$

It follows that, the denominator in equation 3.12 is unity. Moreover, realizing that the electronic Hamiltonian has terms that depend on one-electron coordinates ($\mathbf{r}_i$) ($\hat{T}_e$ and $\hat{V}_{eN}$), and terms that depend on two-electron coordinates $\mathbf{r}_i, \mathbf{r}_j$ ($\hat{V}_{ee}$), and applying the Condon-Slater rules, [132] the non-zero terms in the numerator are:

$$\begin{aligned} \int \Psi^*(\mathbf{r})\hat{H}\Psi(\mathbf{r})\mathrm{d}\mathbf{r} \;=\; & \sum_{i=1}^{n} \int \psi_i^*(\mathbf{r}_1) \left[\hat{T}_e(\mathbf{r}_1) + \hat{V}_{eN}(\mathbf{R}, \mathbf{r}_1)\right] \psi_i(\mathbf{r}_1)\, \mathrm{d}\mathbf{r}_1 \\ & + \frac{1}{2}\sum_{i=1}^{n}\sum_{j=1}^{n} \iint \psi_i^*(\mathbf{r}_1)\psi_i(\mathbf{r}_1)\, \hat{V}_{ee}(\mathbf{r}_1, \mathbf{r}_2)\, \psi_j^*(\mathbf{r}_2)\psi_j(\mathbf{r}_2)\, \mathrm{d}\mathbf{r}_1\mathrm{d}\mathbf{r}_2 \\ & - \frac{1}{2}\sum_{i=1}^{n}\sum_{j=1}^{n} \iint \psi_i^*(\mathbf{r}_1)\psi_j(\mathbf{r}_1)\, \hat{V}_{ee}(\mathbf{r}_1, \mathbf{r}_2)\, \psi_j^*(\mathbf{r}_2)\psi_i(\mathbf{r}_2)\, \mathrm{d}\mathbf{r}_1\mathrm{d}\mathbf{r}_2 \end{aligned} \tag{3.14}$$

So that the expression for $E_e(\mathbf{R})$ becomes:

$$E_e(\mathbf{R}) = \sum_{i=1}^{n} h_i + \frac{1}{2}\sum_{i=1}^{n}\sum_{j=1}^{n}(J_{ij} - K_{ij}) + V_{NN}(\mathbf{R}) \tag{3.15}$$

The first term is a sum over one-electron integrals (h_i), which include the kinetic energy and potential energy due to the electrostatic field from all nuclei, that a single electron has in each spin-orbital. The two-electron integrals in the second term are called Coulomb integrals (J_{ij}), and correspond to the potential energy associated with the electrostatic interaction between the electronic charge densities of each spin-orbital pair ($\psi_i^*\psi_i$ and $\psi_j^*\psi_j$). The contribution of Coulomb integrals to the total energy is always positive (destabilizing), as the interactions are repulsive. The two-electron integrals in the third term are called exchange integrals (K_{ij}), whose contribution to the total electronic energy has no classical analogue, and arises from the use of an antisymmetrized wavefunction (note that the spin-orbital indices i and j are exchanged in the integral). The exchange energy is always negative and can be interpreted as a quantum mechanical correction to the electron-electron Coulombic potential. This correction is a consequence of spin correlation, in which the probability densities of two electrons with parallel spin vanish as the two come close to each other (a Fermi hole),

consequently decreasing their mutual Coulombic repulsion energy. The $^1/_2$ factor is applied to the double-sums to avoid double-counting of terms (J_{ij} and J_{ji}, or K_{ij} and K_{ji}). The J_{ii} term, which corresponds to the (unphysical) interaction of an electron with itself, is cancelled by the K_{ii} term ($J_{ii} = K_{ii}$).

Collecting the terms in equation 3.14, an operator that returns the electronic energy ϵ_i from each spin-orbital ψ_i can be created, called the Fock operator ($\hat{f}_i$):

$$\hat{f}_1\psi_i(\mathbf{r}_1) = \left[\hat{h}_1 + \sum_{j=1}^{n}\left(\hat{J}_j - \hat{K}_j\right)\right]\psi_i(\mathbf{r}_1) = \epsilon_i\psi_i(\mathbf{r}_1) \tag{3.16}$$

where $\hat{J}_j$ and $\hat{K}_j$ are the Coulomb and exchange operators respectively:

$$\hat{J}_j\psi_i(\mathbf{r}_1) = \left(\int \psi_j^*(\mathbf{r}_2)\ \hat{V}_{ee}(\mathbf{r}_1,\mathbf{r}_2)\ \psi_j(r_2)\ \mathrm{d}\mathbf{r}_2\right)\psi_i(\mathbf{r}_1) \tag{3.17}$$

$$\hat{K}_j\psi_i(\mathbf{r}_1) = \left(\int \psi_j^*(\mathbf{r}_2)\ \hat{V}_{ee}(\mathbf{r}_1,\mathbf{r}_2)\ \hat{P}_{12}\ \psi_j(\mathbf{r}_2)\ \mathrm{d}\mathbf{r}_2\right)\psi_i(\mathbf{r}_1) \tag{3.18}$$

and $\hat{P}_{12}$ is the permutation operator, swapping the indices of the spin-orbitals it acts on:

$$\hat{P}_{12}\psi_j(\mathbf{r}_2)\psi_i(\mathbf{r}_1) = \psi_i(\mathbf{r}_2)\psi_j(\mathbf{r}_1) \tag{3.19}$$

Replacing the Hamiltonian in equation 3.12 with Fock operators (one per spin-orbital), yields a set of equations corresponding to the HF approximation to the molecular Schrödinger equation.

An important consideration that becomes evident from the Fock operators is that, solution of equation 3.16 for each spin-orbital $\psi_i(\mathbf{r}_1)$ requires knowledge of the form of every other spin-orbital, which are, at this point, unknown. So, the HF equations have to be solved iteratively, starting from a set of guessed wavefunctions, and making use of the variational principle. Solution of the HF equations is repeated, updating the Fock operator each time a new set of eigenfunctions ψ_i is obtained, until the spin-orbital solutions are self-consistent (i.e. the resulting total energy does not change considerably compared to the last iteration). This iterative approach is referred to as the self-consistent field (SCF) method. The initial guess for molecular spin-orbitals is based on an expansion as a linear combination of atomic orbitals (LCAO), whose form is derived from the (exact) solution of the Schrödinger equation for hydrogen-like atoms. The LCAO expansion is briefly discussed in the context of basis sets in Section 3.1.2. The formalism implied here is referred to as an unrestricted HF approach (UHF), where the spatial function of spin-orbitals occupied by paired-electrons is allowed to be different. Alternatively, a restriction can be imposed on those spin-orbitals, such that their spatial functions are always the same, replacing singly-occupied spin-orbitals with doubly-occupied molecular orbitals, useful for calculations involving closed-shell systems. This formalism is hence referred to as restricted HF (RHF).

The expressions introduced so far are enough to understand the approximation introduced in Hartree-Fock theory to bypass the many-body problem, and what are its limitations. The particular form of the wavefunction introduced in Equation 3.8 effectively assumes that the total inter-electronic repulsion felt by each electron i is due to the *average* electrostatic field from all other electrons $j \neq i$, given by their probability densities $\psi_j^* \psi_j$. Thus, this assumption is sometimes called the mean-field approximation. In reality, electrons are not "smeared throughout" the spin-orbitals they occupy, but are rather point-like dimensionless particles, meaning that the interaction between any two electrons depends on their explicit, instantaneous distance from one another. The motion of electrons is therefore coupled, and cannot be completely separated. This coupling, called electronic correlation (not to be confused with spin correlation, which is already taken into account by the exchange energy), causes electrons to avoid each other in order to minimize their mutual Coulombic repulsion. Consequently, the form and energy of the spin-orbitals occupied by correlated-motion electrons would therefore be different from the mean-field HF solutions. By neglecting electron correlation, HF theory can recover about 99% of a molecule's exact electronic energy. However, since problems in chemistry, and particularly in reaction kinetics, are concerned with minute differences (relative energies) in large numbers (absolute energies), an assumption that fails to account for 1% of the total energy is not an acceptable compromise. Methods that expand upon HF theory in an attempt to account for electron correlation (post-HF methods) include the Møller-Plesset second-order perturbation theory (MP2), Configuration Interaction (CI), Coupled-Cluster (CC) theory, and Density Functional Theory (DFT). From these, CC and DFT were extensively employed in the work presented in this thesis, and both shall be briefly discussed in Sections 3.1.3 and 3.1.4.

3.1.2 Linear Combination of Atomic Orbitals

In the quantum chemistry methods described here, the molecular orbitals (MO) ψ_i are described as an expansion in terms of a set of basis functions (φ_μ), called a basis set, which correspond to atomic orbitals:

$$\psi_i = \sum_{\mu=1}^{N_b} c_{i\mu} \varphi_\mu \tag{3.20}$$

Where N_b is the number of basis functions in the set, and the $c_{i\mu}$ factors are expansion coefficients, giving the weight of the contribution of basis function φ_μ to molecular orbital ψ_i. As in molecular orbital theory, mixing of N_b basis functions yields the same number of molecular orbitals, half of which are occupied and the other half are unoccupied (also called virtual orbitals). As mentioned in the beginning of this chapter, the Schrödinger equation can be solved analytically for hydrogen-like atoms, systems containing one electron and one atomic nucleus. These exact solutions yield a set of wavefunctions corresponding to the well-known *s*-, *p*-, *d*-, and *f*-type atomic orbitals. Based on these solutions, the

simplest basis set can be constructed, whose functions are called Slater-type orbitals (STO).

$$\varphi_{n,l,m_l,\zeta}(r,\theta,\phi) = N \left(r^{n-1}e^{-\zeta r}\right) Y_l^{m_l}(\theta,\phi) \tag{3.21}$$

Where N is a normalization factor. The wavefunction is now given in spherical coordinates, where r, θ, and ϕ are the radial distance, polar angle, and azimuthal angle respectively. Each STO has a radial component, dependent on the principal quantum number n and a parameter ζ, as well as an angular component $Y_l^{m_l}(\theta,\phi)$, corresponding to spherical harmonics, dependent on the orbital angular momentum quantum numbers l and m_l. The orbital exponent parameter ζ (zeta) is related to the effective nuclear charge Z_{eff} felt by an electron in orbital φ when screening of the bare nuclear charge by other electrons is taken into account. The magnitute of ζ controls how fast the exponential radial function decays as r tends to infinity, so that a smaller ζ value yields a more diffuse function, while a larger ζ value yields a tighter function.

In practice, however, solving two-electron integrals of STO products can be an arduous task during electronic structure calculations. Thus, most basis sets employ Gaussian-type orbitals (GTO) instead, where the r-dependence in the exponential is replaced by an r^2-dependence, which greatly facilitates the solution of integrals.

$$\varphi_{n,l,m_l,\zeta}(r,\theta,\phi) = N \left(r^{2n-2-l}e^{-\zeta r^2}\right) Y_l^{m_l}(\theta,\phi) \tag{3.22}$$

On the other hand, a Gaussian function deviates from the true shape of an atomic orbital given by STOs, leading to a poorer description of the electronic structure. An improved description can be achieved if these basis functions are constructed as a linear combination of many different Gaussian functions, called primitive Gaussians, whose combined form better resembles that of an STO. The expansion of a GTO in terms of primitive functions is made so that the expansion coefficients are fixed parameters, and the resulting basis function is called a contracted Gaussian function. For instance, the STO-3G basis set is comprised of STOs approximated by contracted GTOs, each an expansion in terms of three primitive Gaussian functions.

The basis sets mentioned above include one basis function per core and valence atomic orbital (e.g. $1\,\mathrm{s}$, $2\,\mathrm{s}$, $2\,\mathrm{p}_x$, $2\,\mathrm{p}_x$, and $2\,\mathrm{p}_z$ functions for a carbon atom), corresponding to the minimum required for an electronic structure calculation. This is, however, not sufficient for an accurate description of a molecule's electronic structure, especially if different functional groups are present. An improved description can be achieved if atomic orbitals are expanded as a linear combination of two or more basis functions, each with a different value for the ζ parameter. The expansion coefficients for these basis functions are allowed to vary, so that a given type of atomic orbital can offer a greater contribution to a molecular orbital with its more diffuse components (e.g. a $p-$orbital in a π-bonding MO), while its tighter functions have a greater contribution to another molecular orbital (e.g. a

$p-$orbital in a σ-bonding MO). The addition of extra functions is often limited to valence orbitals, given that those are the ones involved in chemical bonding. Basis sets whose valence orbitals are described by more than one basis functions are called split-valence basis sets. Double-zeta (referring to the different ζ parameter values) basis sets have two basis functions per valence orbitals, triple-zeta basis sets have three, and so on.

In essence, the addition of extra basis functions to the overall expansion of MOs grants more flexibility to the mathematical description of a complex electronic structure. Any number of additional basis functions can in principle be added, however, if the basis set grows too large, the calculation may become too expensive to be feasible. Typically, basis functions with higher angular momentum quantum numbers, called polarization functions, are also added to the valence orbital expansion in order to improve the description of molecular orbitals corresponding to polarized bonds. For instance, a p-function can be added to a s-orbital expansion, or a d-function to a p-orbital expansion. Some systems, such as van der Waals complexes, also require an improved description of long-range interactions. For those, the basis set can be augmented with extra diffuse functions (small ζ), where the radial component of the wavefunction decays especially slowly as r increases. The double-zeta basis set 6-31+G*, [133–136] which was extensively used in the work presented in this thesis, is comprised of one GTO with six contracted primitives for each core-shell orbital, two GTOs (one of which being a contraction of three primitives) for each valence orbital, plus one polarization function (*) and one diffuse function (+) for each non-hydrogen valence orbital.

3.1.3 Electron Correlation – Coupled-Cluster Theory

Both the Configuration Interaction and Coupled-Cluster methods attempt a description of electron correlation by making use of a multi-Slater determinant wavefunction. The wavefunction is expanded by means of an excitation (cluster) operator $\hat{C}$.

$$\hat{C} = \hat{C}_1 + \hat{C}_2 + \cdots + \hat{C}_n \tag{3.23}$$

The effect that each $\hat{C}_i$ operator has when applied to a ground-state determinantal wavefunction is analogous to a i-fold electronic excitation, promoting i electrons from occupied MOs to unoccupied (virtual) MOs, producing a new Slater determinant for each possible excited electronic configuration. In Coupled-Cluster theory the $\hat{C}$ operator is applied in exponential form to a reference wavefunction Ψ_0, which is taken to be the HF Slater determinant:

$$\Psi_{CC} = e^{\hat{C}}\Psi_0 \tag{3.24}$$

Expanding the excitation operator, and taking the Taylor series of the exponential, yields a linear combination of the ground-state and excited-state Slater

determinants, each multiplied by a cluster amplitude (t_i^k, t_{ij}^{kl}, ...) factor giving the weight of each determinant in the mixed, total CC wavefunction Ψ_{CC}.

$$\Psi_{CC} = \Psi_0 + \hat{C}_1\Psi_0 + \left(\frac{\hat{C}_1^2}{2!} + \hat{C}_2\right)\Psi_0 + \cdots \tag{3.25}$$

$$\hat{C}_1\Psi_0 = \sum_{i,k} t_i^k \Psi_i^k \qquad \hat{C}_2\Psi_0 = \sum_{i,j,k,l} t_{ij}^{kl}\Psi_{ij}^{kl} \tag{3.26}$$

Where Ψ_i^k is a Slater determinant for the configuration where an electron is excited from the occupied MO ψ_i to the unoccupied (virtual) MO ψ_k, and t_i^k is the corresponding cluster amplitude.

The contribution of excited configurations to the overall electronic wavefunction Ψ_{CC} allows electrons to ever-so-slightly increase their mutual distance, given that unoccupied spin-orbitals have in general more nodal planes. Coupled-cluster thus accounts for electron correlation by allowing electrons to partially occupy those spin-orbitals. If the expansion is done up to the nth term, allowing for configurations where all electrons are excited to be included, then the exact electron correlation energy can be recovered from the CC wavefunction, for a given basis set. Application of CC theory with the complete expansion of the $\hat{C}$ operator, however, results in an intractable computational endeavor for all but the smallest of molecules (consider that the number of Slater determinants rises dramatically with the number of electrons in a molecule). In practice, most CC calculations truncate the $\hat{C}$ operator to a small number of terms. Methods such as CCS or CCSD, for instance, include only the Slater determinants corresponding to single-excitations ($\hat{C} = \hat{C}_1$) or only single- and double-excitations ($\hat{C} = \hat{C}_1 + \hat{C}_2$), respectively. The composite CCSD(T) method, which has become a "gold-standard" for quantum chemistry methods for its accuracy, includes a CC formalism for singly- and doubly-excited configurations, while the contribution from triple-excitations are included as a correction with fourth-order perturbation theory (hence the parenthesis "T").

In the work presented in this thesis, a explicitly-correlated variant of CCSD(T), namely CCSD(T)-F12, [137] was used to obtain electronic energies for reactants, transition states, and products. These methods add terms to the CC wavefunction expansion which depend on the explicit distance (r_{12}) between electron pairs, yielding an accelerated basis set convergence (to the limit of an infinite basis set) in comparison to a canonical CC approach. [138, 139] Since the method is computationally expensive, it was not used for more intensive tasks, such as molecular geometry optimizations or normal mode vibrational frequency calculations. For those purposes, the more cost-effective Density Functional Theory methods were used instead.

3.1.4 Density Functional Theory

Density Functional Theory follows a different approach to molecular electronic structure calculations. While methods such as HF and CC attempt to extract the properties of a system from the electronic wavefunction, DFT does so relying on the electron density function. Two theorems by Kohn and Hohenberg provide the theoretical basis for DFT. The existence theorem offers a proof that any ground-state electronic property of a chemical system, such as the energy, is uniquely determined by the corresponding electron density function $\rho(\mathbf{r})$. This means that there is a one-to-one relationship between the electron density and the ground-state energy, and knowing the former is in principle all one needs to derive the latter. The electronic energy is then expressed as a function of the electron density function, namely a density *functional* $E[\rho(\mathbf{r})]$.

Much like the molecular Hamiltonian under the BO approximation, the density functional can be expanded in terms of a electronic kinetic energy term (T_e), a electron-nuclear potential energy term (V_{eN}), and a electron-electron potential energy term (V_{ee}). The latter term includes a description for the (classical) electrostatic repulsion interactions, analogous to the HF Coulomb integrals, while corrections arising from exchange and correlation are given as a separate term (E_{XC}):

$$E[\rho(\mathbf{r})] = T_e[\rho(\mathbf{r})] + V_{eN}[\rho(\mathbf{r})] + V_{ee}[\rho(\mathbf{r})] + E_{XC}[\rho(\mathbf{r})] \tag{3.27}$$

Whereas an exact expression for the first three terms in equation 3.27 is known, the same cannot be said about the E_{XC} term. DFT methods therefore rely on approximations to the exchange-correlation functional.

Despite being initially developed as an orbital-free theory, Kohn and Sham later introduced one-electron wavefunctions to the DFT formulation. According to the Born interpretation of quantum mechanics, the probability density (ρ) of finding an electron in a given position is equal to the square of the electronic wavefunction (or more generally the product of the wavefunction and its complex conjugate). The electron density is then initially obtained from a set of guess molecular spin-orbitals as:

$$\rho(\mathbf{r}) = \Psi^*(\mathbf{r})\Psi(\mathbf{r}) = \sum_{i=1}^{n} \psi_i^*(\mathbf{r}_i)\psi_i(\mathbf{r}_i) \tag{3.28}$$

The second Hohenberg-Kohn theorem is the variational principle applied to DFT, stating that the true electron density of the system is the one that yields the lowest ground-state energy through the density functional $E[\rho(\mathbf{r})]$. Thus, like in HF theory, a set of DFT equations can be solved iteratively by minimizing the total energy with respect to MO expansion coefficients, until self-consistence.

The advantage of the DFT approach over wavefunction-based methods is that, while the wavefunction of a n-electron molecule is a $3n$-dimensional function, the corresponding electron density $\rho(\mathbf{r})$ is a function of three spatial dimensions

regardless of the number of electrons. In principle, due to the reduced dimensionality of the problem, DFT electronic structure calculations are feasible with much larger molecules than would be possible with wavefunction-based methods. However, since the true form of the exchange-correlation functional is not known, there is no clear systematic way in which DFT methods can be augmented to provide a more accurate description of electronic structures (such as including higher-order terms in the expansion of a CC excitation operator). Many different density functionals have been developed over the years, some being more widely employed than others, but no DFT method has yet been accepted as universally accurate. Next, a general overview of the different approximations to the exchange-correlation functional is briefly discussed.

Starting with the crudest, the local density approximation (LDA) is based on the exchange-correlation energy in a uniform electron gas model. [132] The molecule is placed on a three-dimensional grid and subdivided into small cubic cells, each with a locally uniform electron density. The contribution of each cell to the total exchange-correlation energy is then assumed to be proportional to its local electron density. An improved description can be achieved if, in addition to the local density, the exchange-correlation energy is taken to be proportional to the local gradient of the density $\nabla\rho(\mathbf{r})$ (first derivative with respect to position), as attempted by the generalized gradient approximation (GGA). One apparent shortfall of these approximations is the failure to accurately describe long-range interactions, due to the assumption that the exchange-correlation contributions to the total energy is a local effect. The exchange energy in particular, which is exact as treated by HF theory, can largely be non-local in nature.

In an attempt to mend this limitation, hybrid DFT methods were developed, where the description of exchange energy contains mixed contribution from HF and from a density functional. The B3LYP functional, [140, 141] which is perhaps the most widely used DFT method and was intensively used in the work presented here, is a hybrid GGA density functional employing the Becke 88 exchange functional [140] and the Lee-Yang-Parr correlation functional, [141] with a (global) 20% contribution of HF exchange. Other hybrid methods, taking notice that DFT fails at the description of exchange at long-ranges in particular, introduced range-separated density functionals. [139] The ωB97X functional is such an example, [142] where the contribution of HF to the total exchange increases with distance, up to 100% of the total exchange energy. Since HF does not account for electron correlation, a similar hybrid approach for the correlation energy component at long-range is not possible. Instead, empirical correction factors attempting to capture long-range correlation energy, required to properly describe dispersion interactions, have been developed from fits to experimental data. The work presented in this thesis also makes use of the ωB97X functional, in combination with empirical dispersion correction D2 developed by Grimme (2006). [143]

3.1.5 Nuclear Motion and the Potential Energy Surface

Having discussed how the molecular electronic structure can be treated with quantum chemistry, we now turn our attention to the contribution of nuclear motion to the total energy. As mentioned in the beginning of this chapter, solution of the electronic Schrödinger equation within the BO approximation for a set of different nuclear coordinates ($\mathbf{R}$) yields a molecular potential energy surface ($E_e(\mathbf{R})$). If the end goal is to model the kinetics of chemical reactions with statistical rate theories, then only a few critical points in the PES, or molecular geometries, may need to be characterized. These critical geometries correspond to the molecular structures of the reactant(s), transition state, and product(s) of the chemical reaction in question.

Each reactant or product is a stable species (in the sense that they can be, at least in principle, experimentally isolated), and thus has (at least) one associated minimum in the PES corresponding to an equilibrium molecular geometry $\mathbf{R}_0$. Minima are defined as points in the PES where the partial first-order derivatives of the potential energy $E_e(\mathbf{R})$ with respect to displacements in nuclear positions $\mathbf{R}$ are all zero, and the corresponding partial second-order derivatives are all positive. [132, 139, 144] So, any distortion made to the molecular geometry away from its equilibrium position is met with an opposing, restorative force, and the molecule is thus stable. Once the equilibrium geometry for a reactant is known, the contribution of nuclear motion to its total energy can be obtained. The energy associated with molecular vibrations in particular, is derived from the curvature of the PES at the minimum. [132, 139]

First, it is convenient to separate the nuclear degrees of freedom, and exclude for the moment, the six modes associated with the overall translational and rotational motion of the molecule as a whole. This can be done by transforming the nuclear Cartesian coordinates into a set of mass-weighted internal coordinates, taken to be mutually orthogonal with a linear combination. [139, 144] For a non-linear molecule composed of N atoms, this yields $3N-6$ vibrational normal coordinates, which shall be here denoted by $\mathbf{q} = q_1, q_2, ..., q_{3N-6}$. The three vibrational normal modes of water, for instance, correspond to a symmetric O–H stretch, an asymmetric O–H stretch, and a H–O–H bending motion. Two approximations are introduced here, namely the rigid rotor and the harmonic oscillator (RRHO) approximations, to assume the different modes of motion are separable. The first neglects coupling between rotational and vibrational modes by assuming no centrifugal distortion and coriolis effects in a rotating molecule, and the second neglects coupling among different vibrational modes.

It follows that the total nuclear wavefunction can be separated into terms for translational, rotational, and vibrational motion, the latter of which is a product of $3N-6$ one-dimensional harmonic oscillator wavefunctions:

$$\Psi_v(\mathbf{q}) = \prod_{i=1}^{3N-6} \psi_{v,i}(q_i) \tag{3.29}$$

Operating the Hamiltonian for a 1D quantum harmonic oscillator on each $\psi_{v,i}(q_i)$, and solving the set of Schrödinger equations, yields an expression for the total vibrational energy E_v of the molecule:

$$E_v = \sum_{i=1}^{3N-6} E_{v,i} \qquad E_{v,i} = \left(v + \frac{1}{2}\right) hc\tilde{\nu}_i \qquad v = 0, 1, 2, \ldots \tag{3.30}$$

where c is the speed of light in vacuum, v is the vibrational quantum number and $\tilde{\nu}_i$ is vibrational frequency (given in wavenumber units) of mode q_i. The harmonic vibrational frequency $\tilde{\nu}_i$ of each mode q_i can be calculated from the associated vibrational force constant $k_{f,i}$, which in turn is equal to the second-order derivative of the potential energy with respect to q_i, at the equilibrium position:

$$\tilde{\nu}_i = \frac{1}{2\pi c}\sqrt{\frac{k_{f,i}}{\mu}} \qquad k_{f,i} = \left(\frac{\partial^2 E_e}{\partial q_i^2}\right)_0 \tag{3.31}$$

Where μ is the effective mass (or reduced mass) of the vibrational mode, often containing weighted contributions from several nuclei. The functional groups most distorted by the vibrational mode in question have the greatest weight in μ. Although these modes were derived in the context of nuclear motion, electrons accompany the moving nuclei closely during a molecular vibration (as per the BO approximation). The effective mass then includes contributions from moving *atomic* masses instead of nuclear masses. [139]

Regarding transition states, a similar procedure can be followed, but with an important difference. For reactions with intrinsic energy barriers, the transition state is defined as the molecular geometry $\mathbf{q}^\ddagger$ corresponding to the maximum energy point in the minimum energy path (MEP) connecting the minima associated with the reactant(s) and product(s). The transition state geometry thus sits at a first-order saddle-point in the PES. A more general definition for transition states, encompassing those found in barrierless reactions, is presented in Section 3.3. Like minima, saddle-points are stationary points, meaning that the first derivative of the potential energy with respect to $\mathbf{q}^\ddagger$ are all zero. However, the second-order derivatives are positive with respect to all $\mathbf{q}^\ddagger$ modes, except the one associated with motion along the MEP, called the reaction coordinate $q_r^\ddagger$, for which it is negative. Due to this single negative curvature, transition states are not stable species, and exist only at the fleeting instant in time when the reactant molecule(s) rearrange their structures towards formation of the product(s).

At a minimum, the curvature of the potential energy along all q_i modes is positive, so that the associated vibrational frequencies are all real and positive. On the other hand, for a transition state, expression 3.31 yields an imaginary value for the vibrational frequency of the reaction coordinate $q_r^\ddagger$ (note the square-root of a negative force constant). The magnitude of this imaginary frequency $\tilde{\nu}_r^\ddagger$ gives a measure of the thickness of the reaction energy barrier, a parameter which is useful when estimating the effect of quantum tunnelling on reaction rates.

However, for the purposes of calculating the vibrational energy of a transition state, this mode must be excluded because it does not correspond to a real vibrational motion. Thus, for a non-linear N-atomic transition state, the sum in equation 3.30 is over $3N-7$ terms instead:

$$E_v^\ddagger = \sum_{i=1}^{3N-7} E_{v,i}^\ddagger \qquad E_{v,i}^\ddagger = \left(v + \frac{1}{2}\right) hc\tilde{\nu}_i^\ddagger \qquad v = 0, 1, 2, \ldots \tag{3.32}$$

Perhaps one could argue that, given that transition states are not stable, then not even the positive-curvature modes which are orthogonal to the reaction coordinate correspond to actual vibrations. However, even if that is the case, their description as vibrational modes can provide a measure of how wide the reaction path is at the saddle-point, that is, the looseness of the transition state.

Before we move on, one more inherently quantum effect needs to be discussed. If the v quantum number is zero for all vibrational modes, expressions 3.30 and 3.32 return the zero-point vibrational energy of a reactant ($E_{v=0}$) or a transition state ($E_{v=0}^\ddagger$) respectively. Since this is the lowest possible energy contained in molecular vibrations, present even at 0 K, the PES stationary points are often expressed in terms of zero-point energies E_0, or the sum of the electronic energy $E_e(\mathbf{q}_0)$ at the equilibrium geometry $\mathbf{q}_0$ and the zero-point vibrational energy $E_{v=0}$:

$$E_0 = E_e(\mathbf{q}_0) + E_{v=0} = E_e(\mathbf{q}_0) + \sum_{i=1}^{3N-6} \left(\frac{1}{2}\right) hc\tilde{\nu}_i \tag{3.33}$$

$$E_0^\ddagger = E_e^\ddagger(\mathbf{q}^\ddagger) + E_{v=0}^\ddagger = E_e^\ddagger(\mathbf{q}^\ddagger) + \sum_{i=1}^{3N-7} \left(\frac{1}{2}\right) hc\tilde{\nu}_i^\ddagger \tag{3.34}$$

Rotational and translational modes do not display a zero-point contribution to the total energy, because from their perspective, the potential is uniform everywhere and consequently their ground-state wavefunctions are allowed to have no curvature. The energy levels for these modes of motion are nevertheless quantized, but in much smaller intervals compared to vibrations. At higher temperatures, molecules may also be found in their excited vibrational (quantum numbers $v > 0$), rotational, and translational states. The *thermal* contribution to the total energy from these excited modes of motion at finite temperatures shall be discussed next.

3.2 Statistical Thermodynamics

At the temperatures typically found in the Earth's atmosphere, polyatomic molecules can be found in one of *many* combinations of excited translational, rotational, and vibrational states. Thus, we can no longer rely on the measure of energy for an individual molecule, and have to consider the average properties relating to the behavior of a large number of molecules. Statistical mechanics

provides a bridge between single-molecule properties, which can be calculated with quantum chemistry methods, and macroscopic (bulk) properties, such as equilibrium constants and rate coefficients of chemical reactions.

3.2.1 The Partition Function

Given a molecule with an internal energy of $E - E_0$, in how many ways can this energy be partitioned among available states? More often than not, the answer is *a lot*. This is a problem in combinatorics, which was addressed by the introduction of the Boltzmann distribution. [145] Consider a system of N molecules in thermal equilibrium. The Boltzmann distribution gives the fraction of molecules in the system (N_i/N) that can be found in a specific state with energy E_i, at the most probable combination (thermal) of how the total energy is partitioned among all states:

$$\frac{N_i}{N} = \frac{\exp(-E_i/k_B T)}{\sum_i \exp(-E_i/k_B T)} \tag{3.35}$$

Where k_B is the Boltzmann constant. The sum in the denominator corresponds to the molecular partition function $Q(T)$, a quantity that gives a measure of the number of thermally accessible states at a given temperature T.

$$Q(T) = \sum_i \exp\left(\frac{-E_i}{k_B T}\right) \tag{3.36}$$

The partition function is a critical quantity, because it contains all the the thermodynamic information of a system, much like the wavefunction contains all the quantum information. [145] Once $Q(T)$ is known, classical thermodynamic properties such as the internal energy U, enthalpy H, entropy S, and Gibbs free energy G can be derived. However, the rate theories discussed later in this thesis make explicit use of partition functions, and this section shall concentrate on these quantities instead.

The total molecular partition function $Q(T)$ is expressed as a product of electronic ($Q^e(T)$), vibrational ($Q^v(T)$), rotational ($Q^r(T)$), and translational ($Q^t(T)$) contributions:

$$Q(T) = Q^t(T)Q^r(T)Q^v(T)Q^e(T) \tag{3.37}$$

Next, one needs to know the available energy levels and their degeneracies for each of these components. Aside from rare cases, electronic excited-states are not significantly populated at typical atmospheric temperatures, so it is safe to assume that the electronic partition function is equal to the ground-state degeneracy, that is, its spin multiplicity g:

$$Q^e(T) = g, \qquad g = 1 \text{ (singlet)},\ 2 \text{ (doublet)},\ 3 \text{ (triplet)},\ \ldots \tag{3.38}$$

The remaining partition functions are calculated by summing Boltzmann-weighted energy levels, counted from the zero-point energy E_0. As seen in the previous section, the energy levels for vibrational degrees of freedom can be obtained from solution of the Schrödinger equation for a quantum harmonic oscillator. Replacing equation 3.30 into equation 3.36, yields an expression for the $Q^v(T)$ of a molecule with n_v vibrational modes:

$$Q^v(T) = \prod_{i=1}^{n_v} Q_i^v(T) = \prod_{i=1}^{n_v} \left[1 - \exp\left(\frac{-hc\tilde{\nu}_i}{k_B T}\right)\right]^{-1} \tag{3.39}$$

Errors associated with the calculation of partition functions as described here include, but are not limited to, anharmonicity effects and the inappropriate treatment of internal rotations as harmonic oscillators.

For rotational and translational degrees of freedom, energy levels can be derived from solution of the Schrödinger equation for a rigid rotor and for a particle in the box respectively. [132, 145] The latter also assumes the ideal gas approximation. Since the intervals between the energy levels of these modes of motion are small compared to the thermal energy at the considered temperatures, the distribution of states approaches the classical limit. So, the (discrete) sum in equation 3.36 is replaced by a (continuous) integral, yielding expressions for $Q^r(T)$ and $Q^v(T)$.

For the rotational contribution, an expression for non-linear and linear molecules can be derived:

$$Q^r(T) = \begin{cases} \dfrac{1}{\sigma}\left(\dfrac{k_B T}{hc\tilde{B}}\right) & \text{for a linear rotor} \\ \dfrac{1}{\sigma}\left(\dfrac{k_B T}{hc}\right)^{3/2}\left(\dfrac{\pi}{\tilde{A}\tilde{B}\tilde{C}}\right)^{1/2} & \text{for a non-linear rotor} \end{cases} \tag{3.40}$$

Where $\tilde{A}$, $\tilde{B}$, and $\tilde{C}$ are the rotational constants given in wavenumber units, which can be calculated from the molecule's principal moments of inertia. The latter can in turn be calculated from the equilibrium molecular geometry $\mathbf{q}_0$. The parameter σ is the rotational symmetry number, which corrects for the overcounting of rotational states in molecules containing rotational symmetry axes ($C_2, C_3, \dots$). This correction is another consequence of the Pauli principle, this time involving symmetry/antisymmetry conditions on the product of rotational and nuclear spin wavefunctions. A detailed discussion may be found elsewhere [132].

Finally, the translational partition function is expressed as:

$$Q^t(T) = \left(\frac{2\pi m k_B T}{h^2}\right)^{3/2} V \tag{3.41}$$

where m is the mass of the molecule, and V is the volume derived from the model of a quantum particle in a one-dimensional box, for the three translational degrees of freedom. In the gas-phase, this volume may be interpreted as the average volume occupied by the molecule. Using the ideal gas law, this volume is equal to $(k_B T/p)$, where p is the pressure. At 1 atm and 298 K, $V = 41$ nm^3

3.2.2 Chemical Equilibrium

Before moving on to reaction kinetics, it is useful to introduce the statistical treatment of chemical equilibrium, that is, in terms of partition functions.

Consider a reaction A $\rightleftarrows$ B. Isolated, each species has a thermal distribution of states given by equation 3.35, where the state energies $E_{\mathrm{A},i}$ and $E_{\mathrm{B},i}$ are taken to be relative to each species' zero-point energy, $E_{\mathrm{A},0}$ and $E_{\mathrm{B},0}$ respectively. At equilibrium, the states associated with species B are thermally accessible to species A, and vice-versa, so that the connected PES region associated with A and B may be seen as two merged potential energy wells with a common bottom (PES minimum), corresponding to the species with the lowest zero-point energy. Assuming, for instance, that B is the less stable species, so that the reaction zero-point energy ΔE_0 is positive, the Boltzmann distribution for the states of each species in the merged-well picture may then be expressed as: [145, 146]

$$\begin{aligned} \frac{N_{\mathrm{A},i}}{N} &= \frac{1}{Q(T)} \exp\left(\frac{-E_{\mathrm{A},i}}{k_B T}\right) \\ \frac{N_{\mathrm{B},i}}{N} &= \frac{1}{Q(T)} \exp\left(\frac{-(E_{\mathrm{B},i} + \Delta E_0)}{k_B T}\right) \end{aligned} \tag{3.42}$$

where N is the total number of molecules in the system ($N_{\mathrm{A}} + N_{\mathrm{B}}$) and $Q(T)$ is the total partition function of the merged system. The total number of A molecules N_{A} is the sum over the populations in each state associated with A. A similar expression can be derived for N_{B}, expanding each exponential into a term for $E_{\mathrm{B},i}$ and a term for ΔE_0, and taking the constant terms out of the sum:

$$\begin{aligned} N_{\mathrm{A}} &= \sum_{i=1} N_{\mathrm{A},i} = \frac{N}{Q(T)} \sum_{i=1} \exp\left(\frac{-E_{\mathrm{A},i}}{k_B T}\right) \\ N_{\mathrm{B}} &= \sum_{i=1} N_{\mathrm{B},i} = \frac{N}{Q(T)} \exp\left(\frac{-\Delta E_0}{k_B T}\right) \sum_{i=1} \exp\left(\frac{-E_{\mathrm{B},i}}{k_B T}\right) \end{aligned} \tag{3.43}$$

The thermodynamic equilibrium constant K for the reaction A $\rightleftarrows$ B can be expressed as the ratio of molar fractions χ_{B} and χ_{A} (assuming activity coefficients γ_{A} and γ_{B} are unity), which is equal to the ratio of the number of molecules N_{B} and N_{A}:

$$K = \frac{\chi_{\mathrm{B}}}{\chi_{\mathrm{A}}} = \frac{N_{\mathrm{B}}}{N_{\mathrm{A}}} \tag{3.44}$$

Substituting equation 3.43 into equation 3.44, while recognizing that the sums correspond to the partition functions of A and B ($Q_{\mathrm{A}}(T)$ and $Q_{\mathrm{B}}(T)$), and cancelling out terms, yields an expression for the equilibrium constant in terms of partition functions:

$$K = \frac{Q_{\mathrm{B}}(T)}{Q_{\mathrm{A}}(T)} \exp\left(\frac{-\Delta E_0}{k_B T}\right) \tag{3.45}$$

3.3 Reaction Kinetics

Equilibrium thermodynamics shows the direction of spontaneous chemical change, but tells nothing of the rate, or speed, at which this change takes place. For that purpose, chemical kinetics is necessary. Once the PES of a reaction pathway is known, given as the energetics of the critical stationary points, reactant(s) and transition state, the rate of the reaction can be predicted with theoretical reaction kinetics.

Before introducing the rate theories employed in this thesis, a note about the definition of transition state used here: The transition state is generally defined as a surface perpendicular to the reaction coordinate, which divides the PES region associated with the reactant(s) and the region associated with the product(s), hence also called the dividing surface, located so that the flux of molecules across it is at a minimum. [144] This surface is then the effective bottle-neck of the reactive flux. For reactions with significant intrinsic energy barriers, the dividing surface can be assumed to be located precisely at the saddle-point. The statistical rate theories employed in this thesis, namely Transition State Theory (TST) and Rice-Ramsperger-Kassel-Marcus (RRKM) theory, are formulated for this type of reactions and assume that this is always the case.

3.3.1 Transition State Theory

The simplest rate theory employed in this thesis, Transition State Theory (TST), can be used for predicting reaction rate coefficients at thermal equilibrium. [147, 148] Consider a unimolecular reaction going from reactant R to product P via transition state $TS^{\ddagger}$, with a rate coefficient $k(T)$:

$$\mathrm{R} \xrightarrow{\mathrm{TS}^{\ddagger}} \mathrm{P} \qquad \frac{\mathrm{d[P]}}{\mathrm{d}t} = k[\mathrm{R}] \tag{R3.46}$$

The starting point of TST is to assume that the transition state is in equilibrium with the reactant:

$$\mathrm{R} \underset{\longleftarrow}{\overset{\mathrm{K}^{\ddagger}}{\longrightarrow}} \mathrm{TS}^{\ddagger} \qquad K^{\ddagger} = \frac{[\mathrm{TS}^{\ddagger}]}{[\mathrm{R}]} \tag{R3.47}$$

It is important to note, however, that since the transition state is not a stable species, no such equilibrium exists in reality. The goal here is to derive an expression for the proportion of reactant molecules that, at any point in time, can be found in the vicinity of the PES saddle-point, which can be expressed mathematically as an equilibrium constant $K^{\ddagger}$. This brings us to the next assumption of TST, that upon reaching the transition state, a molecule *will* proceed further along the reaction coordinate towards the product side without returning (no-recrossing assumption):

$$\mathrm{TS}^{\ddagger} \xrightarrow{\mathrm{k}^{\ddagger}} \mathrm{P} \qquad \frac{\mathrm{d[P]}}{\mathrm{d}t} = k^{\ddagger}[\mathrm{TS}^{\ddagger}] \tag{R3.48}$$

Rate coefficient $k^\ddagger$ is for the rate at which the transition state falls apart. Combining the two assumptions, TST treats the reaction as a step-wise process involving a pre-equilibrium:

$$\mathrm{R} \underset{\longleftarrow}{\overset{\mathrm{K}^\ddagger}{\longrightarrow}} \mathrm{TS}^\ddagger \xrightarrow{\mathrm{k}^\ddagger} \mathrm{P} \qquad \frac{\mathrm{d[P]}}{\mathrm{d}t} = k^\ddagger K^\ddagger [\mathrm{R}] \tag{R3.49}$$

Where the $k^\ddagger K^\ddagger$ product is the rate coefficient k of the reaction.

Now, substituting the expression for equilibrium constant $K^\ddagger$ in terms of partition functions (equation 3.45), we obtain:

$$k(T) = k^\ddagger \frac{Q^\ddagger_{\mathrm{TS}}(T)}{Q_{\mathrm{R}}(T)} \exp\left(\frac{-\Delta^\ddagger E_0}{k_B T}\right) \tag{3.50}$$

The term in the exponential is the reaction energy barrier $\Delta^\ddagger E_0$, defined as the difference in zero-point energies between the transition state and reactant. The transition state partition function $Q^\ddagger_{\mathrm{TS}}(T)$ contains a component associated with the reaction coordinate $q^\ddagger_r$ that, as discussed in section 3.1.5, does not correspond to a real vibration. In the vicinity of the saddle-point $\delta q^\ddagger_r$, however, this mode resembles the translational motion of the groups in the molecule's reaction site.

The TST expression for reaction rate coefficients, called the Eyring equation, is then obtained from equation 3.50 by assuming that the motion along the reaction coordinate has an average translational velocity $v^\ddagger$ given by the Maxwell distribution, so that the flux over the saddle point is $k^\ddagger = v^\ddagger / \delta q^\ddagger_r$, and a corresponding one-dimensional translational partition function $Q^\ddagger_r$. Upon expansion of the $k^\ddagger Q^\ddagger_r$ product, shown in the Appendix, the only remaining factor is $k_B T/h$:

$$k(T) = \sigma\kappa \, \frac{k_B T}{h} \, \frac{\bar{Q}^\ddagger_{\mathrm{TS}}(T)}{Q_{\mathrm{R}}(T)} \exp\left(\frac{-\Delta^\ddagger E_0}{k_B T}\right) \tag{3.51}$$

Where $\bar{Q}^\ddagger_{\mathrm{TS}}(T)$ is the transition state partition function, *excluding* the component associated with the reaction coordinate.

The κ and σ factors, which are later added to the expression, correspond to transmission coefficient and the reaction path degeneracy, respectively. The transmission coefficient adds a correction to the rate coefficient arising from the effects of quantum tunnelling or reflection, and is briefly discussed in section 3.3.2. The reaction path degeneracy is a factor that accounts for the presence of more than one identical reaction pathways available to the same reactant. For example, if a carbon in the transition state is chiral, while the corresponding site in the reactant is not, then the reaction can occur via two distinct, but energetically identical TS enantiomers, making the pathway doubly-degenerate ($\sigma = 2$).

The Eyring equation for a bimolecular reaction rate coefficient $\mathrm{R}_1 + \mathrm{R}_2 \longrightarrow \mathrm{P}$ is obtained in much the same way as in the unimolecular case (equation 3.51). The single-reactant partition function $Q_{\mathrm{R}}(T)$ is replaced by a product of two

reactants' partition functions $Q_{\mathrm{R}_1}(T)Q_{\mathrm{R}_2}(T)$, and a new term corresponding to the gas-phase molar volume V_m° at standard pressure is included.

$$k(T) = \sigma\kappa \, \frac{k_B T}{h} \, \frac{\bar{Q}^\ddagger_{\mathrm{TS}}(T)}{Q_{\mathrm{R}_1}(T)Q_{\mathrm{R}_2}(T)} \exp\left(\frac{-\Delta^\ddagger E_0}{k_B T}\right)\left(\frac{RT}{p^\circ}\right) \tag{3.52}$$

The rate coefficient in Equation 3.52 has units of volume mol^{-1} s^{-1}, so, by replacing the ideal gas constant R by k_B, $k(T)$ has units of volume $\mathrm{molecule}^{-1}$ s^{-1}, convention among gas-phase kineticists. The origin of the molar volume term comes from the conversion of an equilibrium constant for gas-phase reactions, expressed in terms of partial pressures, to a constant in terms of concentrations. For the unimolecular case in equation R3.47, this was ignored because all of the V_m° terms cancel out (see Appendix).

At this point, some insight on the kinetics of chemical reactions can be gathered. The most important PES feature determining the rate of reactions is the energy profile along the reaction coordinate $q_r^\ddagger$, that is, the reaction energy barrier $\Delta^\ddagger E_0$, as seen from its exponential dependence in the Eyring equation. A difference of 1 kcal mol^{-1} in $\Delta^\ddagger E_0$, which is the general accuracy of state-of-the-art quantum chemistry methods applicable to the systems investigated in this thesis, translates into a factor of 5 difference in the rate coefficient. This is one reason why much of the effort involved in applications of theoretical kinetics is devoted to describing the electronic structure as accurately as possible.

Secondary, but still important, is the curvature of the PES along the modes perpendicular to the reaction coordinate, whose effect is captured by the partition functions of the stationary points. Lower-curvature real vibrational modes at the saddle-point, for instance, translate into looser transition states. The corresponding partition function is consequently larger, because low-frequency vibrations have more closely-spaced energy levels, and a reaction via a loose transition state is favored by entropy. The dependence of $k(T)$ on the ratio of partition functions, however, is linear and not exponential.

For association and dissociation reactions, on the other hand, entropy plays a much larger role. Consider that when two reactants meet in an association transition state, three translational and three rotational degrees of freedom are lost, and six vibrational modes with much larger intervals between energy levels, are created in their place. The entropic penalty (in terms of the Gibbs free energy barrier $\Delta^\ddagger G$) in association reactions is typically around 10 kcal mol^{-1} at 298 K and 1 atm, and is one reason why, in order to be competitive, most bimolecular reactions in the atmosphere have very low reaction energy barriers ($\Delta^\ddagger E_0 < 10$ kcal mol^{-1}).

Predicting absolute values for rate coefficients can be challenging, but often one is interested in the competition among parallel reaction pathways, and can rely on relative values being more accurate due to error-cancellation. Given a reactant with N_{path} available pathways, whose (pseudo-)first-order rate coefficients

$k_i(T)$ are known, the corresponding branching ratios $\alpha_i(T)$ can be calculated by a simple relationship:

$$\alpha_i(T) = \frac{k_i(T)}{\sum_{i=1}^{N_{\text{path}}} k_i(T)} \tag{3.53}$$

If the reactions are exergonic enough, so that back-reactions are not significant, then the branching ratios are exactly the yields ($\alpha_i(T) \times 100\%$) of the corresponding reaction products.

3.3.2 Quantum Tunnelling

Tunnelling is a well-known quantum phenomenon, [132] most often observed with light particles such as electrons, but which can potentially affect molecules undergoing chemical reactions too. [149, 150] The wavefunction of a particle confined in a potential energy well can penetrate ever-so-slightly the walls of the well and, if these walls are thin enough, pierce through the other side. This means that there is a small, but finite probability that the particle can be found outside the well, and therefore can tunnel through its potential energy barrier. In the context of chemical reactions, the functional groups participating in the motion along the reaction coordinate have a slight chance to pass through a reaction energy barrier, from the reactant side to the product side, without having enough kinetic energy to go over it.

The impact of tunnelling is most pronounced in reactions involving the movement of light atoms over thin energy barriers, such as H-shift reactions. [149, 150] Most chemical reactions have a transmission coefficient κ value of 1, meaning tunnelling has a negligible contribution, but H-shifts can have κ values spanning orders of magnitude, sometimes larger than 10^3. Rare, but still possible, are reactions with $\kappa < 1$, for which the coefficient actually accounts for quantum reflection. [151] Reflection may occur if the wavefunction has a larger kinetic energy than required to cross a barrier, creating a scattering pattern. [132] Reactions with very low (< 1 kcal mol^{-1}) and asymmetric energy barriers can display some quantum reflection, but with minimal impact in the rate coefficient. One such example was found during the work presented in **Article III**, where an especially low-barrier (0.9 kcal mol^{-1}) β-scission reaction (via TS8s) displayed a κ value of 0.96.

The coefficient κ can be calculated with the Eckart tunnelling correction. [151, 152] This method involves the solution of the Schrödinger equation for a wavefunction hitting a one-dimensional potential energy barrier, [132] whose shape is approximated from the magnitude of the transition state's imaginary frequency $\tilde{\nu}_r^{\ddagger}$ and the barrier height on both sides of the reaction coordinate. The TS's imaginary frequency contains a measure of the barrier width, but also of the mass of the moving atoms. Larger-magnitude frequencies are obtained from

higher-curvature saddle-points, characteristic of thinner barriers, and/or a lower reduced mass of moving groups (see Equation 3.31), [139] and consequently yield a greater contribution from tunnelling to reaction rate coefficients.

3.3.3 Pressure Dependence and the Lindemann Mechanism

The validity of TST holds if the distribution of reactant states follows a Boltzmann distribution. This means that inelastic (and unreactive) collisions with other gas-phase molecules are frequent enough to redistribute energy among species, and maintain the population of states in thermal equilibrium during the course of the reaction. To test the theory, picture for instance a hypothetical irreversible reaction where the reactant is initially at thermal equilibrium, but allowed to react in the complete absence of collisional energy transfer. The portion of molecules with enough kinetic energy to pass over the reaction energy barrier can do so and form products, but the remaining reactant molecules cannot, and the reaction will cease early. Without collisions, the high-energy tail of the Boltzmann distribution is chopped-off and does not grow back. This is a somewhat unrealistic scenario, but it tells us that, under low-enough pressures, the rate of activating collisions can be the limiting factor to the overall rate of unimolecular reactions, which is something TST cannot account for.

The first attempt to address this problem came from the Lindemann mechanism: [144, 148, 153]

$$\mathrm{R} + \mathrm{M} \underset{\mathrm{k_{-1}}}{\overset{\mathrm{k_1}}{\rightleftharpoons}} \mathrm{R}^* + \mathrm{M} \tag{R3.54}$$

$$\mathrm{R}^* \xrightarrow{\mathrm{k_2}} \mathrm{P} \tag{R3.55}$$

Here, M represents any gas-phase molecule in the air, such as N_2 and O_2, and their concentration [M] can be taken to be equal to the pressure as $[\mathrm{M}]RT = p$. Inelastic collisions with these bath-gas molecules can impart energy to the reactant (k_1), promoting it to the higher vibrationally excited states (R^*) required for a reaction (k_2) to occur. Collisions can also take energy away (k_{-1}), deactivating R^* back to its vibrational ground-state. Assuming the pseudo-steady-state approximation (PSSA) for the concentration of R^*, the rate of the reaction can be expressed as:

$$\frac{\mathrm{d[P]}}{\mathrm{d}t} = \frac{k_2 k_1 [\mathrm{M}]}{k_2 + k_{-1}[\mathrm{M}]}[\mathrm{R}] = k_{\mathrm{eff}}[\mathrm{R}] \tag{3.56}$$

At high-enough pressures, $k_{-1}[\mathrm{M}] \gg k_2$, and the denominator can be approximated as being equal to $k_{-1}[\mathrm{M}]$, so that the rate becomes independent of the pressure ([M] terms cancel-out), and thus effectively first-order in [R]:

$$\frac{\mathrm{d[P]}}{\mathrm{d}t} \approx \frac{k_2 k_1}{k_{-1}}[\mathrm{R}] = k_{\mathrm{eff}}^{\infty}[\mathrm{R}] \qquad \text{if } k_{-1}[\mathrm{M}] \gg k_2 \tag{3.57}$$

This is called the high-pressure limit, and it is the regime at which TST is applicable. The thermal rate coefficients obtained from the Eyring equation $k(T)$

are essentially high-pressure limit values k_{eff}^{∞}, although the theory takes this into account only implicitly with the thermal equilibrium assumption. At lower pressures, however, the rate can become second-order overall (in [R] and [M]) and consequently decrease with falling pressures, resulting in a much harder problem to solve. But, before describing how this is addressed in practice, another case of pressure-dependent rates shall be discussed.

Insofar as this thesis is concerned, the opposite of the scenario just described in reactions R3.54 and R3.55 is even more interesting, as it occurs often in atmospheric oxidation mechanisms. If a relatively low-barrier unimolecular reaction is preceded by an exothermic association reaction, then more frequent collisions with bath gas molecules can actually *decrease* the overall rate of the reaction. Consider the following mechanism:

$$\mathrm{A} + \mathrm{B} \xrightarrow{\mathrm{k_1}} \mathrm{C^*} \tag{R3.58}$$

$$\mathrm{C^*} \xrightarrow{\mathrm{k_2}} \mathrm{P} \tag{R3.59}$$

$$\mathrm{C^*} + \mathrm{M} \underset{\mathrm{k_{-3}}}{\overset{\mathrm{k_3}}{\rightleftharpoons}} \mathrm{C} + \mathrm{M} \tag{R3.60}$$

This time the species in consideration is a reaction intermediate C that is initially not in thermal equilibrium. Immediately after being formed from association of A and B, the intermediate retains all of the released reaction energy ΔE_0 in its vibrational modes, and the proportion of C molecules occupying higher-energy states is disproportionately large.

Once formed, a vibrationally hot C* molecule can either react to form products (P), or undergo deactivating collisions with bath-gas molecules and be stabilized to its vibrational ground-state C. At the high-pressure limit, the time-scale for thermalization, that is, the dissipation of excess vibrational energy into the surrounding gas via collisional energy tranfer, is much shorter than the time-scale of a chemical reaction, and the thermal equilibrium assumption of TST holds. However, some reactions can be far from the high-pressure limit regime even at atmospheric pressure, meaning that a significant portion of vibrationally hot molecules can react before thermalization. In these cases, the TST approach can severely underestimate overall rate coefficients.

This is particularly problematic in product distribution studies if, for example, a competing bimolecular reaction pathway is also available to the intermediate in question. Bimolecular reaction rates are much less sensititive to the vibrational state of reaction partners, and a delayed thermalization process that favors unimolecular pathways can lead to a dramatic shift in branching ratios. Reactions with submerged energy barriers (i.e. the energy barrier $\Delta^{\ddagger}E_0$ is lower than the preceeding reaction's energy ΔE_0) are especially prone to be at a non-equilibrium kinetics regime.

For these scenarios, where the reactant state populations deviate from a Boltzmann distribution, prediction of the overall reaction kinetics requires an energy-resolved, microcanonical approach. Instead of relying on thermal (canonical) properties such as the partition function to predict rate coefficients as a function of temperature ($k(T)$), microcanonical theories rely on the properties of a system at a constant internal energy E to predict energy-dependent rate coefficients $k(E)$. Many such rate theories have been developed over the last decades, however, this thesis focuses on the Rice-Ramsperger-Kassel-Marcus (RRKM) theory, [144, 154–156] which may be seen as the microcanonical counterpart of TST. Since both thermalization and chemical reactions can often occur at similar time-scales, an appropriate treatment of the overall reaction dynamics requires a description of collisional energy transfer in addition to energy-resolved reaction rates. These processes can be integrated in a chemical master equation, which shall be discussed in Section 3.3.7.

3.3.4 Rice-Ramsperger-Kassel-Marcus Theory

The aim now is to model the rate of a reaction not by a single, temperature-dependent rate coefficient $k(T)$, but by the summed contribution from several internal energy-dependent rate coefficients $k(E)$. In reality, a full microcanonical description of reaction rates would also involve conservation of angular momentum, so that the rate coefficient $k(E, J)$ is a function of both the total energy E and the total angular momentum J. [144] However, J-dependence is often neglected as it entails a much more complicated treatment of the reaction dynamics, particularly when it comes to the solution of chemical master equations, [157] as shall be seen in Section 3.3.7. Thus, the theory presented here is for E-dependent rate coefficients only. The formulation of RRKM theory for $k(E)$ is substantially more involved than that shown for TST, and a detailed and insightful discussion is given by Baer & Hase (1996) [144].

The starting point of RRKM theory is, just like for TST, to assume that the available energy states are populated statistically over the course of the reaction. [144] For a molecule at constant energy E, this means that the time-scale for intramolecular vibrational energy redistribution (IVR) is much shorter than the time-scale of the chemical reaction. For example, the energy of an exothermic association reaction, which initially is converted in its entirety into vibrational excitation of the newly formed bond(s), is assumed to be rapidly redistributed among all vibrational modes. Moreover, the internal energy of a molecule is assumed to flow freely among different modes, as long as the total energy E remains constant. It follows that the rate coefficient $k(E)$ must be proportional to the fraction of reactant molecules that, at any point in time, accumulates enough kinetic energy in the critical vibrational modes associated with the reaction coordinate, such that the transition state is reached. RRKM theory also assumes the no-recrossing condition, so that upon reaching the transition state, the system

will move on to form products without returning.

A quantity that provides a measure of the aforementioned proportion is the density of states $\rho(E)$, which is the total number of states accessible to a system at constant energy E, and may be interpreted as the microcanonical analogue of the partition function. [144] Similar to what is done in the formulation of TST, the mode associated with the reaction coordinate $q_r^\ddagger$ must be treated separately, such that the density of states at the saddle-point includes only states available to all other modes. Thus, the reaction rate coefficient for molecules with total energy E, whose motion along the reaction coordinate has a kinetic energy ϵ_r, can be expressed as:

$$k(E, \epsilon_r) = \frac{1}{h} \frac{\rho^\ddagger(E - \Delta^\ddagger E_0 - \epsilon_r)}{\rho(E)} \tag{3.61}$$

where $\rho(E)$ is the ro-vibrational density of states of the reactant at internal energy E, and $\rho^\ddagger(E - \Delta^\ddagger E_0 - \epsilon_r)$ is the the ro-vibrational density of states of the transition state at energy $E - \Delta^\ddagger E_0 - \epsilon_r$. The reaction energy barrier $\Delta^\ddagger E_0$ is subtracted from the total energy E because the states are counted from the zero-point of the transition state, and ϵ_r is subtracted because, as the reaction coordinate is excluded from the density of states evaluation, this energy is also not available to the other $q_i^\ddagger$ modes.

Equation 3.61 provides a rate coefficient $k(E, \epsilon_r)$ for molecules with a single specific value of ϵ_r. The minimum energy necessary for a reaction to occur is $E = \Delta^\ddagger E_0$, and under this condition a reactant molecule can trace only a single path (the MEP) to reach the transition state. At higher energies, however, the transition state may be reached via multiple paths, each corresponding to a different combination of how the $E - \Delta^\ddagger E_0$ energy is partitioned among the translational motion along the reaction coordinate ϵ_r and the other modes orthogonal to it. Thus, a summed contribution from all available paths is obtained by integrating $k(E, \epsilon_r)$ over all possible values of ϵ_r, from zero to $E - \Delta^\ddagger E_0$, yielding the RRKM expression for k(E):

$$k(E) = \frac{W^\ddagger(E - \Delta^\ddagger E_0)}{h\rho(E)} \tag{3.62}$$

Where the quantity in the numerator is now the sum of ro-vibrational states at the transition state $W^\ddagger(E - \Delta^\ddagger E_0)$, giving the number of states counted from the zero-point vibrational level up to the total energy E. Note that, since RRKM is a theory of unimolecular reactions, the translational degrees of freedom have been left-out because their contribution to the total energy do not change as the molecule evolves from reactant to transition state. The κ and σ factors are later also multiplied to the RRKM expression, to correct $k(E)$ for quantum tunnelling effects and reaction symmetry respectively. Here, the latter factor includes the rotational symmetry numbers of the reactant and TS (see Section 3.2.1) in addition to the path degeneracy (due to e.g. a chiral TS, as discussed in

Section 3.3.1), [158] because unlike for partition functions, the evaluation of sum and density of rotational states do not account for those.

The form of equation 3.62 provides some insight on the expected reactivity of non-thermal reactions of the type given in Equations R3.58-R3.60. Rate coefficients $k(E)$ increase with E because, with more energy to go around the different modes, there is an increased probability that, at any point in time, enough kinetic energy is allocated into the reaction coordinate, so that the transition state is reached. In other words, with increasing E, the sum of states at the transition state $W^{\ddagger}(E - \Delta^{\ddagger}E_0)$ grows faster than does the density of states of the system $\rho(E)$, and a greater number of paths across the dividing surface is available. Thus, the more exothermic is its preceding association reaction, the larger is the internal energy of a vibrationally hot intermediate, and the overall reaction rate is faster. The relationship of $k(E)$ with the size of the reactant molecule is less obvious, but perhaps just as important. In general, smaller vibrationally hot species tend to undergo faster non-thermal reactions than larger ones. Given the same E, larger molecules have more vibrational modes to redistribute the excess energy around, so that the probablity that enough of it is found in critical modes decreases. In terms of equation 3.62, the density of states $\rho(E)$ increases faster than does the sum of states $W^{\ddagger}(E - \Delta^{\ddagger}E_0)$ with larger molecule sizes.

Given a system with a distribution of internal energies, description of the overall reaction dynamics requires, in principle, evaluation of the density and sum of states for each E value in the distribution. In practice, this can be done by first discretizing the internal energy space into grains, each with a size of $E + \delta E$, and lumping together all states found within each grain's range. Next, the number of states in each grain can be obtained by a direct count method, such as that utilized by the Beyer-Swinehart algorithm, [144, 159, 160] assuming the RRHO approximation.

While partition functions are expanded as a product of its components, a joint density of states is instead calculated as a convolution. So, the ro-vibrational density of states $\rho(E)$ is expressed as:

$$\rho(E) = \rho_r(E) * \rho_v(E) = \int_0^E \rho_r(\tau)\rho_v(E - \tau)\mathrm{d}\tau \tag{3.63}$$

Where $\rho_r(E)$ and $\rho_v(E)$ are the rotational and vibrational densities of states respectively, and $*$ symbolizes a convolution. The integration variable τ has no physical meaning, but whose purpose is to provide all combinations of how the available energy is partitioned between the degrees of freedom. For instance, as the variable τ goes from 0 to E in the integration, it places more of the available internal energy into rotational modes. Similarly, the total $\rho_v(E)$ is itself a convolution of the densities of states of every vibrational mode.

3.3.5 Inverse Laplace Transform Method

The rate theories described previously in this thesis are not suitable to treat reactions which proceed without an intrinsic energy barrier, or whose saddle-point energetics are unknown. Radical recombinations, such as reaction of RO_2 with NO in the atmosphere, are essentially barrierless. The same is valid for the reverse of these channels, homolytic dissociation reactions. Albeit not chemical reactions, other barrierless processes relevant to the atmosphere include the association of (non-covalently bound) pre-reactive complexes and dissociation of post-reactive complexes. Other reactions, such as O_2-addition to alkyl radicals, may involve low-lying energy barriers with saddle-points whose electronic structures are challenging to characterize. In these cases, one alternative method for predicting microcanonical rate coefficients is the inverse Laplace transform (ILT) method. [161–164]

The canonical rate coefficient $k(T)$ of a reaction can be obtained from the microcanonical counterparts ($k(E)$) by averaging over the (Boltzmann) distribution of reactant internal energies found at a given temperature T: [144]

$$k(T) = \frac{1}{Q(T)} \int_0^\infty k(E)\rho(E) \exp\left(\frac{-E}{k_B T}\right) \mathrm{d}E \tag{3.64}$$

Next, one may recognize that the integral in equation 3.64 is the Laplace transform of the product $k(E)\rho(E)$, so that equation 3.64 can be rewritten as:

$$k(T)Q(T) = \mathscr{L}\{k(E)\rho(E)\} \tag{3.65}$$

Where the $\mathscr{L}$ operator symbolizes a Laplace transform. It follows that $k(E)\rho(E)$ can be obtained from the *inverse* Laplace transform ($\mathscr{L}^{-1}$) of $k(T)Q_R(T)$:

$$k(E)\rho(E) = \mathscr{L}^{-1}\{k(T)Q(T)\} \tag{3.66}$$

Laplace transforms are related to the more commonly known Fourier transforms. In simple terms, while a Fourier transform can extract the oscillation frequency of a sinusoidal function, performing a transformation from the time-domain to the frequency-domain, a Laplace transform can do the same with (decaying) exponential functions, such as those displayed by dampened oscillators. For the case considered here, the Laplace transform can extract a single value of a canonical property from an exponential distribution of values of a microcanonical property, in a transformation from the "energy-domain" to the "temperature-domain". This is useful because, if $k(T)$ values for a given reaction have been measured experimentally or calculated with variational TST, the corresponding $k(E)$ can be estimated. [164]

Consider an association/dissociation reaction of the type:

$$\mathrm{A} + \mathrm{B} \underset{\mathrm{k_d}}{\overset{\mathrm{k_a}}{\rightleftharpoons}} \mathrm{C} \tag{R3.67}$$

If the canonical rate coefficient for the association step ($k_a(T)$) is known for a range of different T, an Arrhenius expression may be derived:

$$k_a(T) = A\ \exp\left(\frac{-E_a}{k_B T}\right) \tag{3.68}$$

where A is the pre-exponential factor and E_a is the activation energy. The canonical rate coefficient for the dissociation step ($k_d(T)$) can be obtained from detailed balance:

$$k_d(T) = k_a(T)\ K(T) \tag{3.69}$$

where $K(T)$ is the equilibrium constant of reaction R3.67. Substituting equation 3.69 into equation 3.66 for $k_d(E)$:

$$k_d(E)\rho_{\mathrm{C}}(E) = \mathscr{L}^{-1}\{k_a(T)\ K(T)\ Q^{rv}_{\mathrm{C}}(T)\} \tag{3.70}$$

where $\rho_{\mathrm{C}}(E)$ is the ro-vibrational density of states at internal energy E and Q^{rv}_{C} is the canonical ro-vibrational partition function at temperature T, for the dissociating species C. Solution of equation 3.70 can be done by substituting the Arrhenius expression for $k_a(T)$, the equilibrium constant expression in terms of partition functions (Equation 3.45) for $K(T)$, rearranging the terms, and using the convolution theorem (detailed derivation given in the Appendix), yielding the ILT expression for microcanonical dissociation rate coefficients $k_d(E)$: [160, 164]

$$k_d(E)\rho_{\mathrm{C}}(E) = \begin{cases} \dfrac{2AC'}{\sqrt{\pi}}\ \dfrac{g_{\mathrm{A}}g_{\mathrm{B}}}{g_{\mathrm{C}}}\ \displaystyle\int_0^E \rho_{\mathrm{AB}}(E-\tau)\ (\tau - E')^{1/2}\ \mathrm{d}\tau, & \text{if } E \geq E' \\ 0, & \text{if } E < E' \end{cases}$$

$$E' = E_a + \Delta E_0\ ; \quad C' = \left(\frac{2\pi\mu}{h^2}\right)^{3/2} V \tag{3.71}$$

Where ΔE_0 is the zero-point energy of dissociation ($(E_{0,\mathrm{A}} + E_{0,\mathrm{B}}) - E_{0,\mathrm{C}}$), and $\rho_{\mathrm{AB}}(E)$ is the convolved ro-vibrational density of states of A and B at energy E. The constants collected in C' emerge from the ratio of translational partition functions ($Q^t(T)$) which appear upon expansion of $K(T)$ within the ILT, where μ is the reduced mass of the dissociation products ($m_{\mathrm{A}} + m_{\mathrm{B}}/m_{\mathrm{A}}m_{\mathrm{B}}$), and V is the volume (see Section 3.2.1). g_{A}, g_{B}, and g_{C} are the electronic ground-state degeneracies of species A, B, and C respectively, which are their electronic partition functions.

The $2/\sqrt{\pi}$ term and the $(\tau - E')^{1/2}$ term inside the integral derive from the inverse transform of the remaining term in the ratio of translational partition functions. The integral in equation 3.71 is a convolution much like equation 3.63. In this case, it convolves all combinations of how to distribute the internal energy E among the internal degrees of freedom of the dissociating fragments, represented by $\rho_{\mathrm{AB}}(E-\tau)$, and their relative translational motion as they move away from each other, represented by $(2C'/\sqrt{\pi})\sqrt{\tau - E'}$. The conditional in equation 3.71 derives from the transform of an exponential term ($e^{-E'/k_B T}$) and

has a simpler interpretation: the minimum energy E required for C to react is the dissociation energy ΔE_0 plus an activation energy E_a, so that if $E < E'$, the rate coefficient $k(E)$ is zero.

A corresponding ILT expression for microcanonical association rate coefficients $k_a(E)$ can be obtained in a similar procedure as seen above. However, using microscopic reversibility (detailed balance), [157] a $k_a(E)$ value can be obtained from the $k_d(E)$ rate coefficient of the corresponding reverse dissociation channel:

$$k_a(E)\frac{\rho_{\mathrm{AB}}(E)e^{-E/k_BT}}{Q_{\mathrm{AB}}(T)} = K(T)k_d(E)\frac{\rho_{\mathrm{C}}(E)e^{-E/k_BT}}{Q_{\mathrm{C}}(T)} \tag{3.72}$$

Where $Q_{\mathrm{AB}}(T)$ is the joint canonical ro-vibrational partition function of A and B.

3.3.6 Collisional Energy Transfer

After reviewing how energy-dependent rate coefficients can be predicted with RRKM theory or the ILT method, the last piece of the reaction dynamics puzzle to be discussed is the treatment of collisional energy transfer. The single-exponential-down model is perhaps the most widely employed model for this purpose. [165, 166] In this model, the rate coefficient of a deactivating inelastic transition is given as:

$$k_{\mathrm{CET}}(E, E') = \omega P(E, E') \tag{3.73}$$

Where $P(E, E')$ is the transition probability from energy E' to E, where $E' > E$, and ω is the total collision frequency, which is typically assumed to be energy-independent. The probability $P(E, E')$ is expressed as:

$$P(E, E') = \frac{1}{C_N(E')} \exp\left(\frac{-(E' - E)}{\langle \Delta E \rangle_d}\right) \tag{3.74}$$

Where the exponential-down parameter $\langle \Delta E \rangle_d$ is the average energy transferred in a deactivating collision (hence "down"), and $C_N(E')$ is a normalization constant. The probability of activating transitions are in turn calculated with detailed balance. The exponential dependence of the transition probability $P(E, E')$ on the energy difference $E' - E$ is based on the notion that strongly activating/deactivating collisions are far less likely than more elastic collisions. Thus, multiple collisions with bath-gas molecules may be necessary for efficient activation of a reactant in a thermal reaction, or for effective thermalization of a vibrationally hot intermediate.

The collision frequency ω is a function of the total concentration of gas-phase species ([M]) and the collisional cross-section, the latter of which can be estimated from the colliders' Lennard-Jones potential parameters ϵ_{LJ} and σ_{LJ}. [165]

3.3.7 The Chemical Master Equation

Consider two starting reactants A and B which, upon association, produce a reaction intermediate which is connected to several isomers and dissociation products via a complex network of reaction pathways. The time-evolution of the distribution of species in the reaction mechanism is given by a set of differential equations, each describing the rate of a chemical reaction or of a internal energy transition by collisional energy transfer. [157, 166–168] The assembled system of equations is called a chemical master equation (ME), where the time-evolution of the population $n_i(E)$ of species i at energy E is expressed as:

$$\begin{aligned}\frac{\mathrm{d}n_i(E)}{\mathrm{d}t} = &+ \int_{E_{0i}}^{\infty} \omega_i P_i(E,E') n_i(E')\ \mathrm{d}E' \ - \ \omega_i n_i(E) \\ &+ \sum_{j\neq i}^{M} k_{ji}(E) n_j(E) \ - \ \sum_{j\neq i}^{M} k_{ij}(E) n_i(E) \\ &+ K_i(T) k_{d,i}(E) \frac{\rho_i(E) e^{-E/k_B T}}{Q_i(T)} n_\mathrm{A} n_\mathrm{B} \ - \ k_{d,i}(E) n_i(E) \\ &- \sum_{p=1}^{N_p} k_{p,i}(E) n_i(E)\end{aligned} \tag{3.75}$$

The first and second terms in equation 3.75 are the collisional energy transfer terms: the first represents the population gain of species i at energy E due to transitions from all other energy levels E' of the same species, and the second represents the corresponding population loss due to transitions to all other levels E'. The third and fourth terms are isomerization terms, where M is the number of isomers in the mechanism: the former represents the population gain of species i at energy E from reaction of all other species j, at the same energy level, which are directly connected to it via isomerization channels, and the latter represents the corresponding population loss via the reverse reactions. The fifth and sixth terms are connections to the source, the starting reactants A and B: the former represents the population gain of species i at energy E from association of A and B (using microscopic reversibility, equation 3.72), and the latter represents the corresponding population loss due to re-dissociation to A and B. Finally, the seventh and last term is a sum of N_p sink terms, each representing the population loss of species i at energy E via an (assumed) irreversible reaction pathway such as an addition, exchange, or dissociation reaction. Due to the neglect of the angular momentum J dependence of rate coefficients, the master equation shown here is referred to as a one-dimensional ME (as opposed to a two-dimensional E, J-dependent one).

To complete the ME, two extra terms are added, [157] corresponding to the time-evolution of one of the starting reactants under pseudo-first-order conditions, so that the system of equations remain linear. Assuming that A is the deficient reactant ($n_\mathrm{B} \gg n_\mathrm{A}$), and that both starting reactants are at thermal

equilibrium:

$$\begin{aligned}\frac{\mathrm{d}n_{\mathrm{A}}}{\mathrm{d}t} = &- \int_{E_{0i}}^{\infty} K_i(T) k_{d,i}(E) n_{\mathrm{A}} n_{\mathrm{B}} \frac{\rho_i(E) e^{-E/k_B T}}{Q_i(T)} \,\mathrm{d}E \\ &+ \int_{E_{0i}}^{\infty} k_{d,i}(E) n_i(E) \,\mathrm{d}E\end{aligned} \tag{3.76}$$

Where the first term represents the population loss of A from association with B, and the second term represents the corresponding population gain from re-dissociation of adduct i at energy E. Combined, equations 3.75 and 3.76 may be expressed in matrix form:

$$\frac{\mathrm{d}}{\mathrm{d}t}\mathbf{n} = \mathbf{M}\mathbf{n} \tag{3.77}$$

where $\mathbf{n}$ is the population vector, containing the population density of each species at each evaluated energy level, and $\mathbf{M}$ is the collision-reaction transition matrix. Expansion of $\mathbf{M}$ and $\mathbf{n}$ can illustrate how the terms are arranged:

$$\frac{\mathrm{d}}{\mathrm{d}t}\begin{bmatrix} n_{\mathrm{A}} \\ \mathbf{n}_1 \\ \mathbf{n}_2 \\ \vdots \\ \mathbf{n}_M \end{bmatrix} = \begin{bmatrix} -k_{\mathrm{A}} & \mathbf{k}_{1\mathrm{A}} & \mathbf{k}_{2\mathrm{A}} & \cdots & \mathbf{k}_{M\mathrm{A}} \\ \mathbf{k}_{\mathrm{A}1} & \mathbf{M}_1 & \mathbf{K}_{21} & \cdots & \mathbf{K}_{M1} \\ \mathbf{k}_{\mathrm{A}2} & \mathbf{K}_{12} & \mathbf{M}_2 & \cdots & \mathbf{K}_{M2} \\ \vdots & \vdots & \vdots & \ddots & \vdots \\ \mathbf{k}_{\mathrm{A}M} & \mathbf{K}_{1M} & \mathbf{K}_{2M} & \cdots & \mathbf{M}_M \end{bmatrix} \begin{bmatrix} n_{\mathrm{A}} \\ \mathbf{n}_1 \\ \mathbf{n}_2 \\ \vdots \\ \mathbf{n}_M \end{bmatrix} \tag{3.78}$$

Each $\mathbf{n}_i$ is itself a vector containing the population density of species i at each evaluated energy level E. Similarly, $\mathbf{k}_{\mathrm{A}i}$ are column vectors containing the pseudo-first-order rate coefficients in the fifth term of equation 3.75 ($\mathrm{A} + \mathrm{B} \longrightarrow \mathrm{i}$) and $\mathbf{k}_{i\mathrm{A}}$ are row vectors containing the rate coefficients in the first term of equation 3.76 ($\mathrm{i} \longrightarrow \mathrm{A} + \mathrm{B}$)). The $-k_{\mathrm{A}}$ term is the total loss rate coefficient for the source species A, containing the second term in equation 3.76. If m is the number of evaluated energy levels, or grains, and assuming a hypothetical situation where all isomers i have the same PES well-depth for illustrative purposes, then the vectors may be expanded as: [168, 169]

$$\mathbf{n}_i = \begin{bmatrix} n_i^1 \\ n_i^2 \\ \vdots \\ n_i^m \end{bmatrix}, \; \mathbf{k}_{\mathrm{A}i} = \begin{bmatrix} k_{\mathrm{A}i}^1 \\ k_{\mathrm{A}i}^2 \\ \vdots \\ k_{\mathrm{A}i}^m \end{bmatrix}, \; \mathbf{k}_{i\mathrm{A}} = \begin{bmatrix} k_{i\mathrm{A}}^1 & k_{i\mathrm{A}}^2 & \cdots & k_{i\mathrm{A}}^m \end{bmatrix} \tag{3.79}$$

where the superscript $1, 2, \ldots, m$ represent energy grain indices $E_1, E_2, \ldots, E_m$.

The body of the $\mathbf{M}$ matrix is composed of diagonal $\mathbf{M}_i$ blocks and off-diagonal $\mathbf{K}_{ij}$ blocks. The $\mathbf{K}_{ij}$ block is the reaction matrix for isomerization of species i leading to species j at each energy level E, whose diagonal elements contain the

rate coefficients in the third term of equation 3.75, while off-diagonal elements are zero (reactions are at constant E). The $\mathbf{M}_i$ block is the collision matrix for species i, whose off-diagonal elements contain the rate coefficients in the first term of equation 3.75, and diagonal elements contain the *total* loss rate coefficient (second, fourth, sixth, and seventh terms) of each energy level or grain. Expanded, these matrices are expressed as:

$$\mathbf{M}_i = \begin{bmatrix} -k_i^1 & k_i^{21} & \cdots & k_i^{m1} \\ k_i^{12} & -k_i^2 & \cdots & k_i^{m2} \\ \vdots & \vdots & \ddots & \vdots \\ k_i^{1m} & k_i^{2m} & \cdots & -k_i^m \end{bmatrix}, \qquad \mathbf{K}_{ij} = \begin{bmatrix} k_{ij}^1 & 0 & \cdots & 0 \\ 0 & k_{ij}^2 & \cdots & 0 \\ \vdots & \vdots & \ddots & \vdots \\ 0 & 0 & \cdots & k_{ij}^m \end{bmatrix} \tag{3.80}$$

Naturally, the different isomers i in a real reaction mechanism would have different PES well-depths, so that low-lying energy levels may not be available to all species. Thus, energy level indices may be counted from top to bottom: $m, m-1, m-2, \ldots$, where m is the highest evaluated energy level, [168] typically chosen so that its population flux across the PES is not significant.

Once the chemical ME is assembled, equation 3.75 can be solved by matrix diagonalization techniques, which finds a matrix $\mathbf{U}$ that, upon multiplication, transforms the collision-reaction matrix $\mathbf{M}$ into a diagonal matrix $\mathbf{\Lambda}$: [160, 170]

$$\mathbf{U}^{-1}\mathbf{M}\mathbf{U} = \mathbf{\Lambda} \tag{3.81}$$

Each element in matrix $\mathbf{\Lambda}$ then may be seen as an effective first-order rate coefficient for the population flux in each evaluated energy grain of each species in the reaction mechanism. The population vector as a function of time $\mathbf{n}(t)$ may then be obtained from 3.75 as a first-order integrated rate law analogue, [170, 171] using the properties of matrix exponentials:

$$\mathbf{n}(t) = \mathbf{U}e^{\mathbf{\Lambda}t}\mathbf{U}^{-1}\ \mathbf{n}(0) \tag{3.82}$$

where $\mathbf{n}(0)$ is a vector containing initial population densities, at time $t = 0$. The population-time profile $n_i(t)$ for each species i in the reaction system can then be obtained by summing the population densities in all energy grains $n_i(E_j, t)$ corresponding to species i, in a series of time steps (t):

$$n_i(t) = \sum_{j=1}^{m} n_i(E_j, t) \tag{3.83}$$

4. Results and Discussion

4.1 Initial Oxidant Attack on a Cyclic Imine

The starting point of the explored mechanism in **Article I** was the attack of a OH radical on THP. Scheme 4.1 depicts the explored initial pathways and their corresponding branching percentages, including H-abstractions, from a C atom (pathways a, c, d, and e) or from the amine N atom (pathway b), and electrophilic addition to the C-terminus of the imine group (pathway g). Product yields were predicted with RRKM-ME calculations based on a PES obtained with two different DFT methods: ωB97X-D/aug-cc-pVTZ and M062X-GD3/aug-cc-pVTZ. [142, 143, 172–174] In both cases, more accurate electronic energies for each stationary point were obtained with a single-point RO-CCSD(T)-F12a/cc-pVDZ-F12 calculation. [137, 175] Differences in yields associated with the use of the two functionals are represented as uncertainty ranges in Scheme 4.1. DFT, CC and RRKM-ME calculations were done with Gaussian 16, [176] Molpro, [177–179], and the Master Equation Solver for Multi-Energy Well Reactions (MESMER) software, [160] respectively.

The theoretical predictions indicated that the fate of THP is dominated by the pathways involving abstraction of the axial hydrogen from one of the α-amino carbons (channels a and c in Scheme 4.1), with a combined yield of 59-84%. Attack of OH radical on α-amino positions have also been observed to be the major reaction pathways during the oxidation of other amines, [117–119] including cyclic ones, such as piperazine and piperidine. [48, 49, 121, 122] This finding further highlights how effective the $n_N \rightarrow \sigma^*_{CH}$ hyperconjugative interaction is at stabilizing H-abstraction transition states (Section 2.3). An imine group may in principle assist H-abstractions from adjacent positions in a similar manner via $\pi_{CN} \rightarrow \sigma^*_{CH}$ interactions, and one of the objectives of **Article I** was to ascertain how effective these are compared to α-amino substitution. The unsaturated cyclic structure of THP, however, complicated the comparison.

From the perspective of the Bell-Evans-Polanyi principle, H-abstraction from the α-N-imino position (pathway d) would be expected to be more competitive

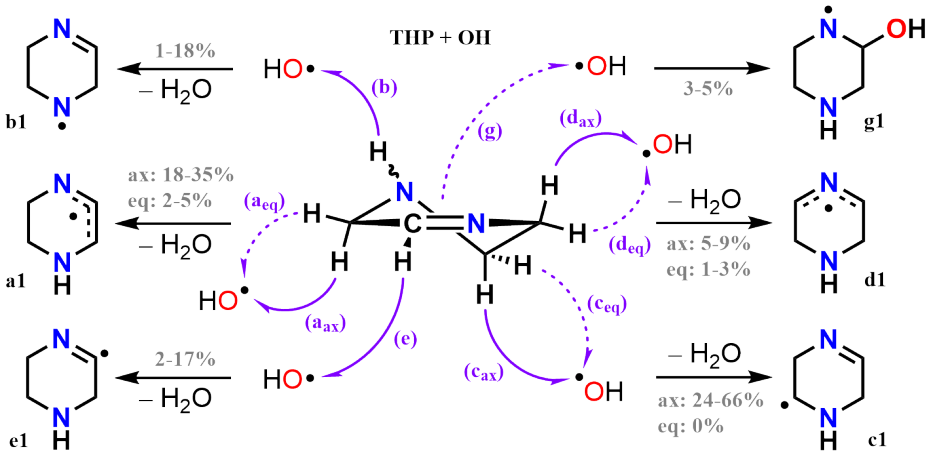

Scheme 4.1: Explored initial pathways for the reaction of THP with OH radicals. Product yields predicted with RRKM-ME calculations are shown in gray.

than pathway c, given that product d1 is 12.7 kcal mol^{-1} more stable than product c1. Moreover, H-abstraction from the position which is both α-C-imino and α-amino substituted (pathway a), whose product (a1) is even more stable than c1 (22.5 kcal mol^{-1}), is less competitive than pathway c considering the uncertainty ranges. Thus, $\pi_{CN} \rightarrow \sigma^*_{CH}$ hyperconjugation could in principle provide a stronger stabilizing effect on a H-abstraction TS. In THP, however, the endocyclic double-bond also constrains the orientation of C–H groups in adjacent carbons such that an antiperiplanar conformation, required for optimal reaction assistance (Section 2.3), cannot be achieved. One of the reasons why the equatorial C–H bonds in $-CH_2-$ moieties are the least labile is precisely due to a large deviation from such a conformation. At a β-position to the double-bond, the abstraction site in pathway c is less constrained, and thus hyperconjugative stabilization of the axial TS by the α-amino substituent is more pronounced.

Although minor, initial pathways b, d, e, and g are still competitive. From these, H-abstraction from the amine nitrogen (b) and OH-addition to the imine carbon (g) lead to formation of N-centered (aminyl) radicals, whose subsequent chemistry is of particular interest, owing to their potential to produce toxic nitroamines or nitrosamines via reaction with NO_x (Reaction R2.14). This potential is largely dependent on how fast are competing reactions, such as reaction with O_2, which were also investigated in this thesis, and discussed further in

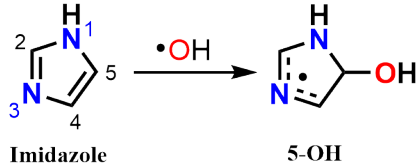

Scheme 4.2: Attack of OH radical on imidazole via addition to position C5.

Section 4.3. As revealed in **Article I**, abstraction of the aldiminic hydrogen via pathway e leads, upon subsequent reaction with O_2, to the formation of an isocyanate, another potentially toxic compound. [180]

Article III did not investigate the initial steps of imidazole's OH-initiated oxidation, but rather relied on previously published work, [181–185] indicating that attack of the oxidant proceeds preferentially via addition to position C5, producing the 5-hydroxyimidazolyl radical (5-OH). The starting point of **Article III** was then the exploration of imidazole's first-generation RO_2 reaction pathways, available upon O_2-addition to 5-OH. These pathways shall be discussed in the next section, alongside the ones explored for the THP-derived RO_2 radicals.

4.2 Peroxyl Radical Reaction Pathways

The product yields and rate coefficients presented in this section were predicted with RRKM-ME and TST calculations respectively, based on PESs obtained at the RO-CCSD(T)-F12a/cc-pVDZ-F12 // ωB97X-D/aug-cc-pVTZ level of theory.

4.2.1 1,2,3,6-Tetrahydropyrazine Derivatives

Article I explored the reactivity of first-generation peroxyl radicals derived from O_2-addition to alkyl radicals a1, c1, d1, and e1, produced from THP's OH-initiated oxidation. The first thing to consider here is the PES well-depth corresponding to these RO_2, that is, how negative is the reaction energy ΔE_0 of the O_2-addition step that produces them. Species a1 and d1 are stabilized by resonance, which is lost upon O_2-addition, meaning that their respective RO_2 derivatives, a2 and d2, correspond to shallower wells ($\Delta E_0 = -14.8$ and -21.9 kcal mol^{-1} respectively). [186] The RO_2 derived from species c1 and e1, on the other hand, correspond to deeper wells, with calculated ΔE_0 values similar to those observed for RO_2 derived from saturated heterocycles such as piperazine, piperidine and pyrrolidine ($-34 \sim -38$ kcal mol^{-1}). [48, 121, 122] This is important because larger ΔE_0 values may drive subsequent unimolecular reactions at non-thermal rates, while smaller ΔE_0 values may let re-dissociation reactions be significant, as seen later in the case of imidazole.

The major first-generation RO_2 products from THP oxidation, a2 and c2, are β-amino peroxyl radicals, and thus both have access to rapid imine-forming HO_2-elimination pathways, producing 2,3-dihydropyrazine (2,3-DHP) and 3,4-dihydropyrazine (3,4-DHP) respectively. This pathway is so fast for a2 and c2, that it outcompetes $RO_2 + NO$ reactions even at high NO_x conditions (5 ppb), with 98% and 94% yields respectively. For c2, the impact of excess vibrational energy is significant, as the reaction energy barrier is $\Delta^{\ddagger}E_0 = 17.2$ kcal mol^{-1} for HO_2-elimination, with a corresponding thermal rate coefficient value of only 6 s^{-1}. Product yields obtained from test RRKM-ME calculations starting from a

thermalized c2 species are remarkably different. At 5 ppb of NO, HO_2-elimination has a yield of 35%, while RO_2 + NO reactions become the major channel, with 44% yield. A 1,5 H-shift pathway (involving abstraction from the other α-amino carbon) also becomes significant if excess energy is neglected, with 39% and 22% yield at 5 ppt and 5 ppb of NO respectively. A similar observation was previously reported for RO_2 derived from dimethylamine (DMA) and diethylamine (DEA), [118] where an analogous 1,5 H-shift is outcompeted by HO_2-elimination despite involving slightly lower energy barriers ($\sim 0.3 - 1$ kcal mol^{-1}). While back-reactions may be significant for isomerization channels, such as H-shifts, HO_2-elimination is essentially an irreversible dissociation reaction pathway, and may therefore be disproportionately favored by a vibrationally hot system prior to thermalization. Species a2 is produced with less excess vibrational energy, but the energy barrier for HO_2-elimination is also lower (14.4 kcal mol^{-1}), presumably because it leads to a conjugated diimine, unlike with c2.

The minor first-generation RO_2 products from THP, d2 and e2, do not have access to imine-forming HO_2-elimination pathways, and are therefore less reactive with respect to unimolecular channels. For d2, a 1,5 H-shift producing a N-centered radical is the fastest, with an energy barrier of 16.8 kcal mol^{-1}, but also endothermic ($\Delta E_0 = 5.6$ kcal mol^{-1}). Subsequent reaction steps available to this N-centered radical are not as fast, and the fate of d2 is dominated by RO_2 + NO reactions, leading to the corresponding alkoxyl radical. The C-imino peroxyl radical e2 is even less reactive. The only unimolecular pathway available to this species is a slow 1,4 H-shift, and RRKM-ME calculations predicted that only bimolecular pathways are competitive, even under low [NO_x] conditions. Exploration of the fate of the e2-derived alkoxyl radical resulted in one of key findings of **Article I**.

The ring-opening β-scission pathway available to THP's C-imino alkoxyl radical derivative is very fast, with an energy barrier of only 2.8 kcal mol^{-1}, and leads to the formation of an isocyanate functional group (RN=C=O). The significance of this channel stems from the fact that it is the sole fate of an initial oxidant attack on the aldiminic hydrogen. The peroxyl group in the subsequently formed RO_2 is bonded to a sp^2 carbon, and its orientation is thus constrained to the plane of the C=N moiety, largely hindered from reaching potential intramolecular attack sites. This is likely also true for analogous RO_2 derived from any other cyclic aldimine, such as the major photo-oxidation product of piperidine, [121] or from the (*Z*)-isomer of any acyclic Schiff base aldimine (RN=CHR′):

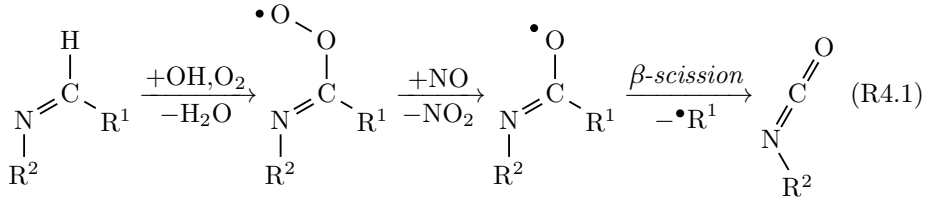

(R4.1)

The imine derivative of piperidine, in particular, may be especially prone to

produce isocyanates via this channel given that, since no competing α-amino abstraction site is available, attack of OH radical on the aldiminic hydrogen may have much larger yields. For acyclic Schiff base aldimines, the significance of this channel may depend on how likely formation of the (*Z*)-isomers are, and how fast are N-inversion reactions leading to the respective (*E*)-isomers (both in the parent imine and in RO_2 derivatives):

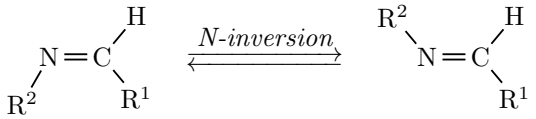

(R4.2)

Unlike (*Z*)-isomer-derived RO_2, the (*E*)-isomer counterparts may have access to fast H-shift pathways, possibly outcompeting reaction with NO and, consequently, the isocyanate-forming channel.

4.2.2 Imidazole Derivatives

Article III explored the reactivity of first- and second-generation peroxyl radicals produced during imidazole's atmospheric oxidation initiated by OH radical addition to position C5. Like the THP-derived alkyl radicals a1 and d1, the imidazole-OH adduct 5-OH is resonance-stabilized, meaning that the subsequently formed RO_2 products correspond to relatively shallow wells. Moreover, O_2-addition to 5-OH may occur at two different positions (either C2 or C4), and from two different directions (either *syn* or *anti* to the hydroxyl group), so that one of four different RO_2 isomers may be initially formed (Scheme 4.3): C2-*syn* (2s-RO_2), C2-*anti* (2a-RO_2), C4-*syn* (4s-RO_2), and C4-*anti* (4a-RO_2). The 4s- and 4a-RO_2 isomers are slightly more stable ($\Delta E_0 = -20.4$ and -20.7 kcal mol^{-1} respectively) than their 2-RO_2 counterparts ($\Delta E_0 = -17.9$ and -16.7 kcal mol^{-1} respectively) because some of the resonance is maintained in the amidine group upon addition to position C4.

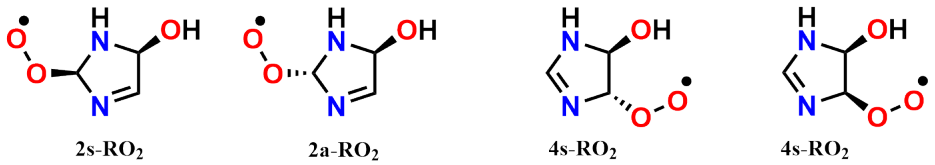

Scheme 4.3: First-generation RO_2 products from imidazole oxidation initiated by OH radical addition to position C5.

In **Article III**, the PES was explored using KinBot, [122, 187, 188] an automated gas-phase reaction search and kinetics code. Species 2s-RO_2 and 2a-RO_2 are β-amino peroxyl radicals and each has access to an imine-forming HO_2-elimination pathway, both leading to the same diimine, 4H-imidazol-4-ol (4H-4ol). Compared to the THP-derived analogues a2 and c2, however, the imidazole derivatives are not as reactive. HO_2-elimination energy barriers are slightly

higher for 2s-RO_2 and 2a-RO_2 ($\Delta^{\ddagger}E_0$ = 19.2 and 17.6 kcal mol^{-1} respectively), and are close-to but not-quite submerged under the entrance level, so that non-thermal reactions are not so significant. The 4s-RO_2 and 4a-RO_2 isomers may react via different pathways. While 4a-RO_2 may react via HO_2-elimination, this time involving H-abstraction from a carbon, 4s-RO_2 has instead access to a 1,5 H-shift from the hydroxyl group. Neither of these pathways, however, involve submerged energy barriers (24.3 and 20.5 kcal mol^{-1} respectively). Furthermore, two additional reaction channels were found: A low-barrier ($\Delta^{\ddagger}E_0$ = 11.9 and 14.0 kcal mol^{-1}) reaction pathway connecting each 2-RO_2 species to their respective, more stable 4-RO_2 isomers. These pathways are fast (k(298 K) = 2×10^4 and 2×10^5 s^{-1}), and involve the attack of the peroxyl group on the imine's C-terminus concerted with scission of the C–O(O) bond, exchanging the positions of the two functional groups:

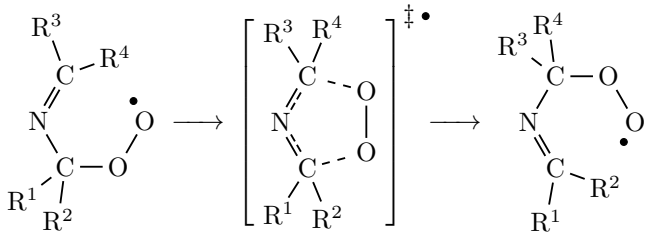

(R4.3)

Due to these O_2-migration reaction pathways, an equilibrium between the *anti*- and *syn*-isomer pairs is achieved after $\sim$ 1 μs, with two consequences. First, δ-amino peroxyl radicals 4s-RO_2 and 4a-RO_2 gain prompt access to reaction pathways available to their respective 2-RO_2 isomers, and vice-versa. Second, the effective HO_2-elimination energy barrier encountered by the merged-well 4-RO_2 $\rightleftarrows$ 2-RO_2 system is higher, 21.7 and 21.6 kcal mol^{-1} for the *syn* and *anti* pair respectively. That being said, since the RO_2 wells are shallow and the energy barriers to exit unimolecular channels are not submerged, re-dissociation reactions to yield 5-OH + O_2 become significant. Thus, after $\sim$ 1 s, right about the time-scale of unimolecular and bimolecular reactions, an equilibrium among all four RO_2 isomers is approached. The discovery of O_2-migration reaction pathways was one of the key findings of **Article III**, and their significance becomes clearer once their effect on imidazole's second-generation RO_2 reactivity is considered.

For the first-generation RO_2, the established (or approached) equilibrium means that competition among exit reaction pathways is largely controlled by their barrier heights taken relative to the common entrance level. Thus, the lowest-barrier pathway overall, and most competitive unimolecular channel, is the 1,5 H-shift accessible from the 4s-RO_2 isomer, leading to a hydroperoxyl-alkoxyl radical. This pathway is endothermic (ΔE_0 = +15.2 kcal mol^{-1}), but the alkoxyl radical produced can react further via rapid ring-opening β-scission ($\Delta^{\ddagger}E_0$ = 0.9 kcal mol^{-1}), followed by α-OOH alkyl radical decomposition (see Section 2.6), leading to the closed-shell *N*,*N*'-diformylformamidine (FMF). A very

similar reaction channel was previously reported to be available in the oxidation of monoethanolamine (MEA), [119] but leading to decomposition of the acyclic reactant into three fragments: formamide, formaldehyde, and OH radical. That being said, unimolecular channels producing 4H-4ol and FMF are the main loss terms for imidazole's first-generation RO_2 only under low NO_x conditions ([NO] = 10 ppt), and are outcompeted by $RO_2 + NO$ reactions at more polluted environments ([NO] = 0.1-1 ppb), where the major products are the alkoxyl radicals 4a-RO and 4s-RO derived from the more stable 4-RO_2 isomers.

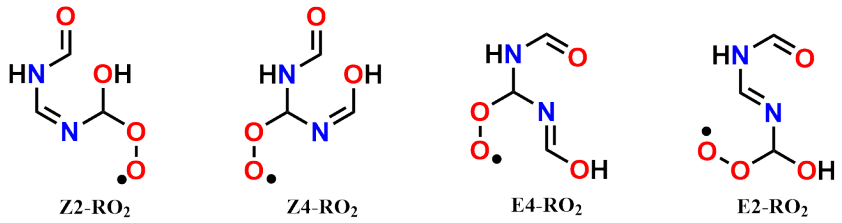

Scheme 4.4: Second-generation RO_2 products from imidazole oxidation initiated by OH radical addition to position C5.

Many interesting reaction pathways and intermediates were found exploring the mechanism of decomposition of the alkoxyl radical 4-RO diastereomers, but for the sake of brevity, it suffices to say that their fate ($> 95\%$) is dominated by ring-opening β-scission, both leading to the same highly-conjugated, completely planar alkyl radical, held in an eight-membered ring-like conformation by an intramolecular H-bond. Similarly, the explored oxidation mechanism following O_2-addition to this exotic alkyl radical is complex, including four possible second-generation RO_2 radical intermediates (Scheme 4.4), but pathways inevitably converge to the production of FMF via carbonyl-forming HO_2-elimination, with $\sim 100\%$ yield. As discussed next, the appearance of a single product is due to the availability of a fast O_2-migration pathway, and a new type of HO_2-elimination reaction uncovered in **Article III**.

The possible second-generation RO_2 are shown in Scheme 4.4. Imine-forming HO_2-elimination pathways are available for the two α-amino peroxyl radicals, Z4-RO_2 and E4-RO_2, and carbonyl-forming HO_2-elimination pathways are available for the two α-hydroxyl peroxyl radicals, Z2-RO_2 and E2-RO_2. While the energy barriers associated with the first two are relatively high (21.0 and 23.8 kcal mol^{-1} respectively), the last two involve very low barriers (8.9 and 8.8 kcal mol^{-1} respectively), as is typical of HO_2-eliminations with carbonyl group formation. Moreover, one extra HO_2-elimination pathway was found for each of the (Z)-isomers, involving a hydrogen transfer with a 1,6 span instead of the more typical 1,4 span shown in Reaction R2.17. In this reaction, the peroxyl group attacks a δ-position alongside cleavage of the C−O(O) σ-bond and the $N_\beta{=}C_\gamma$ π-bond,

creating a conjugated diimine or N-imino carbonyl:

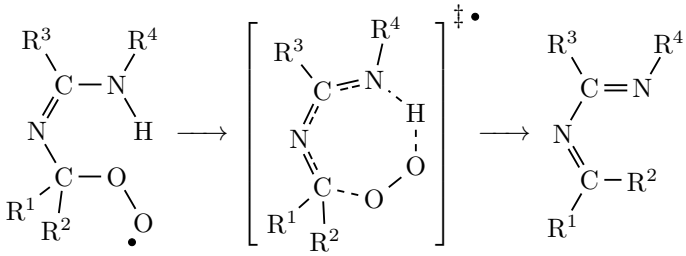

(R4.4)

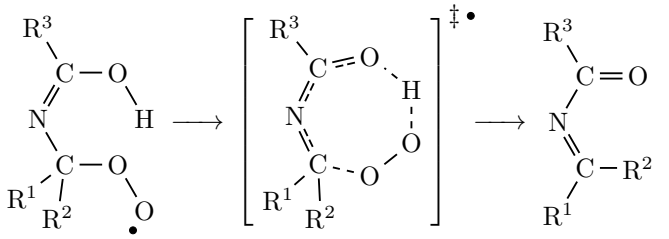

(R4.5)

With this new pathway, which is available only to (*Z*)-isomers, Z4-RO_2 can also undergo rapid carbonyl-forming HO_2-elimination leading to FMF, with a reaction energy barrier of 10.4 kcal mol^{-1}. Albeit not competitive, species Z2-RO_2 also gains access to a imine-forming HO_2-elimination. It is important to note, however, that this channel has a lower barrier (18.0 kcal mol^{-1}) than the analogous shorter-span pathways available to Z4-RO_2 and E4-RO_2, highlighting the potential significance of 1,6 HO_2-elimination pathways in general. Finally, four O_2-migration channels were also found, two connecting Z4-RO_2 to Z2-RO_2 and E2-RO_2, and two connecting E4-RO_2 to E2-RO_2 and Z2-RO_2, with forward and reverse energy barriers ranging from 9.5 to 18.2 kcal mol^{-1}. These pathways are inconsequential to the most reactive species, Z2-RO_2, E2-RO_2, and Z4-RO_2, however, the one connecting the more stable E4-RO_2 to E2-RO_2 is critical, as it is especially fast, and grants the former prompt access to the latter's rapid HO_2-elimination pathway, yielding FMF.

The new reaction pathways reported in **Article III**, O_2-migrations and 1,6 HO_2-eliminations, could be important also during the atmospheric oxidation of other N-containing aromatics, such as oxazole, pyrazine, and pyridine, or more broadly, unsaturated organic nitrogen compounds in general. In fact, a O_2-migration pathway was originally found during preparation of **Article I**, for the THP-derived RO_2 species d2. However, since for d2 this reaction leads just to an inversion of optical symmetry, the finding was not included in the publication. The transition state structure of some of these pathways is shown in Scheme 4.5. So far, it is unclear whether these pathways are available only to α-N-imino RO_2 species, or if the presence of a β-γ unsaturation is enough. If the latter is true, then these pathways could potentially open-up new channels in the atmospheric oxidation of homocyclic aromatics too.

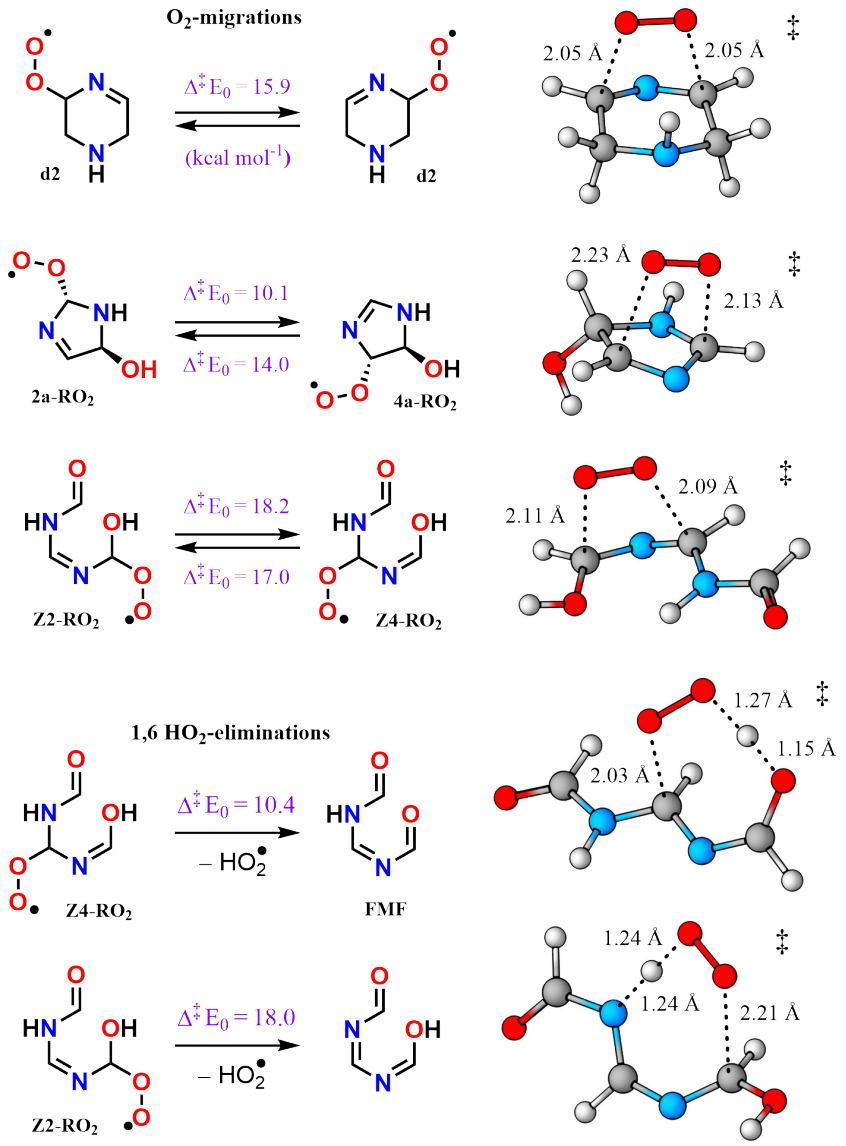

Scheme 4.5: Structure of three O_2-migration and two 1,6 HO_2-elimination transition states found in **Article I** and **III**. Color scheme: red = O, blue = N, gray = C, white = H.

4.3 Aminyl Radicals

Article I also explored the reactivity of the N-centered radicals produced from minor channels of OH-initiated oxidation of THP, b1 and g1, in order to ascertain the imine's potential to produce nitroamines and nitrosamines via Reaction R2.14. The calculated predictions indicate that, overall, the yield of these carcinogenic compounds is minor but non-negligible. Considering the uncertainties associated with calculated reaction energy barriers, estimates give a maximum

yield of 7% and 11% for nitrosamines and nitroamines respectively, from THP + OH under high NO_x conditions (10 ppt). The major sink term for b1 is reaction with O_2 (Reaction R2.12), leading to the diimines 2,3-DHP or 3,4-DHP via a step-wise O_2-addition/HO_2-elimination mechanism. For the product of initial OH-addition to the imine double-bond g1, however, the only competitive pathway is an aminyl radical β-scission reaction, forming an imidic acid functional group and a C-centered radical. This β-scission has a low energy barrier (14 kcal mol^{-1}), and is considerably submerged below the entrance level (THP + OH) by about 18 kcal mol^{-1}. It is possible that other substituted imines may share the same fate upon OH-addition to the double-bond, especially cyclic ones:

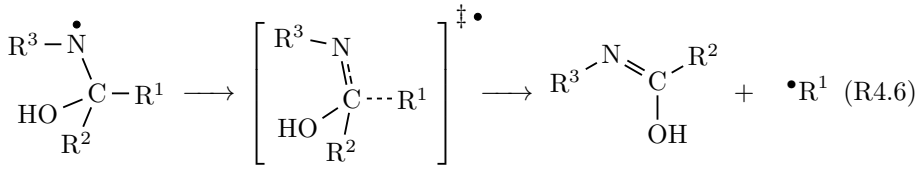

(R4.6)

4.4 Nitrooxy-alkyl and -alkoxyl Radical β-scissions

The reaction energetics presented in this section were obtained with the same DFT methods described previously, but electronic energies were calculated at the RO-DLPNO-CCSD(T)-F12a/cc-pVTZ-F12 level instead, [175, 189–191] using Orca 4.2.1. [192, 193]

4.4.1 Nitrooxy-alkyl Radicals

As discussed in Section 2.6, a special case of potentially competitive alkyl radical unimolecular pathway is that involving a ring-opening rearrangement via β-scission, available to α-cycloalkyl substituted alkyl radicals. One of the targets of **Article II** was to investigate how reactive are the NO_3-adducts of a series of bicyclic monoterpenes, namely nitrooxy-alkyl radicals, towards this ring-opening β-scission pathway. The studied systems were products of NO_3-addition to the least-substituted terminus of C=C double-bonds (see Section 2.3), in monoterpenes bearing three-membered (sabinene and α-thujene), four-membered (β-pinene), and five-membered (camphene) secondary rings (Scheme 4.6). These reactions are important because they lead to the formation of a less rigid RO_2 species, whose unimolecular channels may be more competitive. Moreover, the recreated C=C double-bond may enhance reactivity by opening-up endo-cyclization pathways and allylic H-abstraction sites.

Calculation results revealed that, except for camphene, alkyl radical ring-opening β-scission is competitive for every studied monoterpene. Reactivity is, however, strongly dependent on the size of the opened ring – the greater strain relief experienced by opening of a smaller ring is translated into a lower-energy transition state, relative to the reactant. Thus, β-scission outcompetes O_2-addition

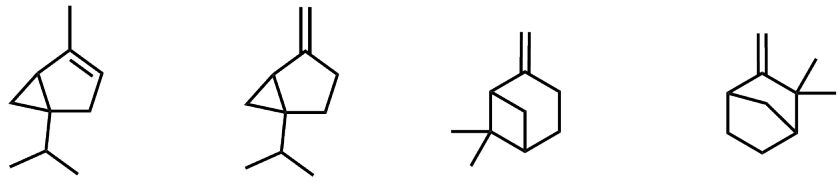

Scheme 4.6: Monoterpenes investigated in **Article II**.

for sabinene (86%), while it is a minor channel for β-pinene (10%), and negligible for camphene. That being said, release of ring-strain alone cannot account for diverging reactivities among monoterpenes. The two possible diastereomers of the α-thujene derivative display a significantly lower reactivity towards ring-opening than sabinene (11-31%), despite also having a three-membered secondary ring and a very similar structure overall. Here, the fact that the competitiveness is remarkably different also between the (*R*)- and (*S*)-isomers (11% and 31% respectively) provided a hint on which stereoelectronic effects are behind the differing reactivity.

Hyperconjugative interaction between the singly-occupied p_C orbital and the empty σ^*_{CO} can stabilize both the reactant and the transition state of a $R^{\bullet}ONO$ β-scission, but requires the C−O bond to be perpendicular to the radical center's nodal plane. This interaction is stronger for the sabinene derivative and its connected TS because, since the α-ONO_2 carbon is exocyclic, the CH_2ONO_2 group may rotate about the $C_\alpha - C_\beta$ bond so that stabilizing interactions are optimized. In the α-thujene derivative isomers, however, the α-ONO_2 carbon is endocyclic, and a conformation that optimizes the $p_C \rightarrow \sigma^*_{CO}$ interaction is either hindered, or far from present, such as in the TS for β-scission in the (*R*)-isomer.

The energy barriers for these reactions are low (9.6-13.0 kcal mol^{-1}), but not low enough to explain the high yields. Comparison between the product yields obtained with RRKM-ME calculations, which include treatment of the preceding NO_3-addition step, and the values obtained from thermal rate coefficients estimated with TST, reveals the overwhelming impact of non-equilibrium kinetics. Branching ratios from thermal rate coefficients predict that ring-opening β-scission is competitive only for the sabinene-derived nitrooxy-alkyl radical, and with a much diminished yield of 12%.

4.4.2 Nitrooxy-alkoxyl Radicals

The second target of **Article II** was to investigate which C−C bond is preferentially cleaved via β-scission in nitrooxy-alkoxyl radical derivatives of five monoterpenes, including the ones mentioned in the previous subsection, plus the monocyclic limonene (Scheme 2.1). If an endocyclic bond is broken, the newly formed open-chain alkyl radical is prone to further propagation of the organic radical chain (Section 2.5) upon O_2-addition (Scheme 4.7). However, β-scission

leading to an α-ONO_2 alkyl radical is followed by spontaneous NO_2-elimination (Section 2.6), terminating oxidation early. A previous study [58] revealed that the NO_2-loss channel is preferentially followed for the nitrooxy-alkoxyl radical derived from α-pinene, whereas an alternative β-scission pathway is more competitive for Δ-carene, which can explain the disparate experimentally observed SOA yields from NO_3-initiated oxidation of these two monoterpenes. [60, 194]

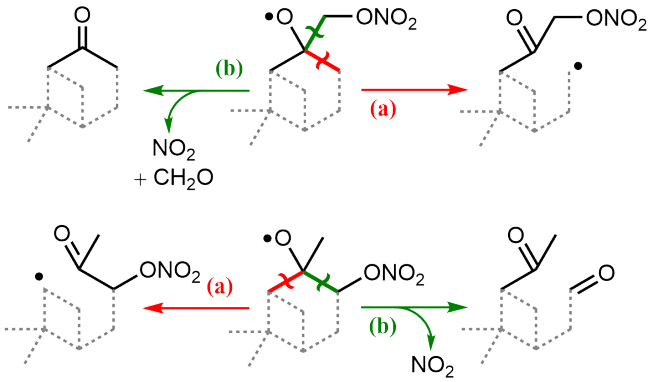

Scheme 4.7: Competing β-scission reactions in nitrooxy-alkoxyl radicals derived from exocyclic-double-bond monoterpenes (top), and endocyclic-double-bond monoterpenes (bottom).

Predictions presented in **Article II** reported a similarly diverse fate for the five investigated monoterpenes, revealing a structural pattern controlling the selectivity of β-scission pathways. Nitrooxy-alkoxyl radical derivatives of endocyclic-double-bond monoterpenes (limonene, α-thujene, and α-pinene [58]) react preferentially via the NO_2-loss channel, while those derived from exocyclic-double-bond monoterpenes (sabinene, β-pinene, camphene, and Δ-carene [58]) do not. Here again, the exocyclic or endocyclic position of α-ONO_2 carbon is critical. The transition state of NO_2-loss channels for the endocyclic cases is stabilized by release of ring-strain and by α-ONO_2 substitution to the new developing radical center, whereas only the latter of these effects stabilizes the TS for exocyclic cases. Reaction assistance by ring-strain relief is, however, considerably more effective, and exocyclic-nitrate species react preferentially via a ring-opening β-scission pathway, even if it leads to a primary alkyl radical.

A notable exception was observed for the β-pinene-derived systems. More interesting still, the two diastereomers of this monoterpene's nitrooxy-alkoxyl radical derivatives react preferentially via different β-scission pathways. While 85% of the (*R*)-isomer reacts via the NO_2-loss channel, 87% of the (*S*)-isomer reacts via the ring-opening β-scission leading to a primary alkyl radical. A tentative explanation for this observation put forth in **Article II** invokes steric effects: In the NO_2-loss channel TS, the CH_2ONO_2 leaving group experiences a greater steric repulsion in the (*S*)-isomer (due to one of the methyl groups), than it does in the (*R*)-isomer. This was an unexpected finding of **Article II**, since stereoisomers typically display similar selectivity towards this type of reactions.

5. Conclusions and Future Outlook

The first of the research objectives posed in the introduction to this thesis was to investigate the fate of two cyclic nitrogen-containing organic compounds, namely THP and imidazole, upon oxidation in the atmospheric gas-phase. The theoretical calculations presented in **Articles I** and **III** predict that the atmospheric fate of both compounds is dominated by reaction channels provoking an early termination of the oxidative chain, largely due to the ubiquity of fast HO_2-elimination pathways in their oxidation mechanism. For THP, the major OH-initiated oxidation products are the (closed-shell) cyclic diimines 2,3-DHP and 3,4-DHP, while for imidazole, the cyclic diimine 4H-4ol and the acyclic amidine FMF are the major products (and overwhelmingly so). Still, calculations predict a small but non-negligible yield of nitrosamines, nitroamines, and a potentially toxic isocyanate from THP's oxidation.

The theoretical predictions presented in **Article I** have some backing in the form of previously reported smog-chamber experiments studying piperazine's photo-oxidation. [49, 195] For instance, those experiments report the detection of oxidation products which may correspond to the DHP isomers and the imine derived from O_2-addition/HO_2-elimination reaction with the isocyanate. In the case of imidazole, however, no such experiments have been reported yet, so the predictions in **Article III** lack experimental backing. A particularly important question to be addressed in future works is perhaps the fate of FMF, imidazole's major photo-oxidation product, since an isocyanate can potentially be formed from its oxidation as well, as speculated in **Article III**.

Another main objective of this thesis was to explore the not well-known atmospheric chemistry of imines and N-containing aromatics (by means of THP and imidazole as surrogates). Perhaps the most important findings in this context were the uncovered reaction channels: O_2-migration (Reaction R4.3), 1,6 HO_2-elimination (R4.4 and R4.5), isocyanate-forming alkoxyl radical β-scission (R4.2), and hydroxy-aminyl radical β-scission (R4.6). From these, the last two do not involve novel types of reaction pathways, but the work presented in this thesis revealed their significance. It remains to be seen, however, if these reaction channels prove to be important in the atmospheric oxidation of other organic ni-

trogen compounds. Future research may also benefit from a quantitative analysis of how competitive the gas-phase oxidation of imines is against reactive uptake by aqueous aerosol particles, where they may undergo hydrolysis.

As for the work done on the NO_3-initiated oxidation of monoterpenes, this thesis had the goal to investigate the reactivity of alkyl radical intermediates and the selectivity of alkoxyl radical intermediates towards β-scission pathways. Theoretical predictions indicated that, in general, the oxidation mechanism of endocyclic- and exocyclic-double-bond monoterpenes diverges after formation of alkoxyl radicals. Endocyclic monoterpenes tend to react via the NO_2-loss channel, leading to an early oxidative chain termination, whereas exocyclic monoterpenes react preferentially via an alternative channel allowing for further propagation. The work presented in **Article II** also predicts that a ring-opening β-scission in nitrooxy-alkyl radicals can be competitive with (or even outcompete) O_2-addition, especially if it involves opening of a strained three-membered ring. The fact that the NO_3-initiated oxidation of limonene, an endocyclic-double-bond monoterpene, is observed to be have high SOA yields in experiments, can be explained by the attack of a second oxidant molecule on the remaining C=C double-bond on the NO_2-loss product.

Finally, this thesis also attempts to provide insight on the explored reaction mechanisms from a more fundamental physical (organic) chemistry perspective. Quantum chemistry is particularly well suited for this purpose, given that a detailed analysis and comparison of different reaction pathways' energetics can, alongside visual inspection of molecular geometries, provide critical information on the structural factors controlling reactivity, such as stereoelectronic and steric effects. So, with such a powerful tool in hand, a theoretical kineticist can not only predict which outcomes are the most likely for a certain chemical reaction, but also seek to understand *why* some pathways are faster than others. This information is valuable from a more practical perspective if one considers that it can be used to, for example, guide the design of new compounds which are less harmful to health and environment.

Appendix

A1 Derivation of TST

The derivation for TST shown here is partly reproduced from Pilling & Seakins (1995) [148]. Consider a reaction of the type:

$$\mathrm{A} + \mathrm{B} \overset{\mathrm{TS}^{\ddagger}}{\longleftrightarrow} \mathrm{C} \tag{RA1}$$

The thermodynamic equilibrium constant K for this reaction may be expressed in terms of partial pressures p_{A}, p_{B}, and p_{C}: [146]

$$K = \frac{(p_{\mathrm{C}}/p^{\circ})}{(p_{\mathrm{A}}/p^{\circ})(p_{\mathrm{B}}/p^{\circ})} \tag{A2}$$

where p° is the standard pressure (1 bar). Using the ideal gas law, the equilibrium constant may be expressed in terms of molar concentrations instead:

$$p_{\mathrm{A}} = [\mathrm{A}]RT \qquad p_{\mathrm{B}} = [\mathrm{B}]RT \qquad p_{\mathrm{C}} = [\mathrm{C}]RT \tag{A3}$$

$$K = \frac{([\mathrm{C}]RT/p^{\circ})}{([\mathrm{A}]RT/p^{\circ})([\mathrm{B}]RT/p^{\circ})} \tag{A4}$$

cancelling-out terms in the numerator and denominator:

$$K = \frac{[\mathrm{C}]}{[\mathrm{A}][\mathrm{B}]}\left(\frac{p^{\circ}}{RT}\right) \tag{A5}$$

As seen in Section 3.3.1, TST assumes a pre-equilibrium between the transition state and the reactants $\mathrm{A} + \mathrm{B}$. The constant $K^{\ddagger}$ for this assumed equilibrium may then be expressed as:

$$K^{\ddagger} = \frac{[\mathrm{TS}^{\ddagger}]}{[\mathrm{A}][\mathrm{B}]}\left(\frac{p^{\circ}}{RT}\right) \tag{A6}$$

The rate of the reaction is given as:

$$\frac{\mathrm{d}[\mathrm{C}]}{\mathrm{d}t} = k^{\ddagger}[\mathrm{TS}^{\ddagger}] \tag{A7}$$

Now, substituting Equation A6 into Equation A7,

$$\frac{\mathrm{d[C]}}{\mathrm{d}t} = k^{\ddagger}K^{\ddagger}\mathrm{[A][B]}\left(\frac{RT}{p^{\circ}}\right) \tag{A8}$$

yields a rate coefficient for the forward (bimolecular) reaction:

$$k(T) = k^{\ddagger}K^{\ddagger}\left(\frac{RT}{p^{\circ}}\right) \tag{A9}$$

Next, the constant $K^{\ddagger}$ may be expanded in terms of partition functions (3.45):

$$k(T) = k^{\ddagger}\frac{Q^{\ddagger}_{\mathrm{TS}}(T)}{Q_{\mathrm{A}}(T)Q_{\mathrm{B}}(T)}\exp\left(\frac{-\Delta^{\ddagger}E_0}{k_BT}\right)\left(\frac{RT}{p^{\circ}}\right) \tag{A10}$$

Separating the partition function associated with motion along the reaction coordinate $Q^{\ddagger}_r$ from all other components $\bar{Q}^{\ddagger}_{\mathrm{TS}}(T)$:

$$k(T) = k^{\ddagger}Q^{\ddagger}_r(T)\frac{\bar{Q}^{\ddagger}_{\mathrm{TS}}(T)}{Q_{\mathrm{R}}(T)}\exp\left(\frac{-\Delta^{\ddagger}E_0}{k_BT}\right)\left(\frac{RT}{p^{\circ}}\right) \tag{A11}$$

The $k^{\ddagger}$ rate coefficient corresponds the flux of molecules passing through the vicinity of the saddle-point $\delta q^{\ddagger}_r$, and can be approximated as the velocity of the reaction mode $v^{\ddagger}$ at $\delta q^{\ddagger}_r$:

$$k^{\ddagger} = \frac{v^{\ddagger}}{\delta q^{\ddagger}_r} \tag{A12}$$

Taking $v^{\ddagger}$ to be the average velocity in one-dimension given by the Maxwell distribution,

$$k^{\ddagger} = \left(\frac{k_BT}{2\pi\mu^{\ddagger}}\right)^{1/2}\frac{1}{\delta q^{\ddagger}_r} \tag{A13}$$

and assuming a one-dimensional translational partition function for $Q^{\ddagger}_r$,

$$Q^{\ddagger}_r = \left(\frac{2\pi\mu^{\ddagger}k_BT}{h^2}\right)^{1/2}\delta q^{\ddagger}_r \tag{A14}$$

most terms in the $k^{\ddagger}Q^{\ddagger}_r(T)$ product cancel-out:

$$k^{\ddagger}Q^{\ddagger}_r = \left(\frac{k_BT}{2\pi\mu^{\ddagger}}\right)^{1/2}\frac{1}{\delta q^{\ddagger}_r}\left(\frac{2\pi\mu^{\ddagger}k_BT}{h^2}\right)^{1/2}\delta q^{\ddagger}_r = \frac{k_BT}{h} \tag{A15}$$

Finally, substituting into Equation A11 yields the Eyring equation for the forward reaction (Equation 3.52):

$$k(T) = \kappa\,\frac{k_BT}{h}\,\frac{\bar{Q}^{\ddagger}_{\mathrm{TS}}(T)}{Q_{\mathrm{A}}(T)Q_{\mathrm{B}}(T)}\exp\left(\frac{-\Delta^{\ddagger}E_0}{k_BT}\right)\left(\frac{RT}{p^{\circ}}\right)$$

For unimolecular reactions, all of the RT/p° terms in Equation A4 cancel-out, so that the Eyring equation reduces to the one shown in Equation 3.51.

A2 The Dissociation ILT Expression

The forward (association) $k_a(T)$ and reverse (dissociation) $k_d(T)$ reaction rate coefficients are related to the equilibrium constant $K(T)$ by detailed balance:

$$k_d(T) = k_a(T)\ K(T) \tag{A16}$$

Replacing the expression for $K(T)$, given in equation 3.45:

$$k_d(T) = k_a(T)\ \left(\frac{Q_{\mathrm{A}}(T)Q_{\mathrm{B}}(T)}{Q_{\mathrm{C}}(T)}\right)\ \exp\left(\frac{-\Delta E_0}{k_B T}\right) \tag{A17}$$

where $Q_{\mathrm{A}}(T)$, $Q_{\mathrm{B}}(T)$, and $Q_{\mathrm{C}}(T)$ are the *total* canonical partition function of A, B, and C respectively, and ΔE_0 is the zero-point energy of dissociation. Replacing into the ILT expression for the dissociation reaction (equation 3.70):

$$k_d(E)\rho_{\mathrm{C}}(E) = \mathscr{L}^{-1}\{k_d(T)Q_{\mathrm{C}}^{rv}(T)\} \tag{A18}$$

$$k_d(E)\rho_{\mathrm{C}}(E) = \mathscr{L}^{-1}\left\{k_a(T)\ \left(\frac{Q_{\mathrm{A}}(T)Q_{\mathrm{B}}(T)}{Q_{\mathrm{C}}(T)}\right)\ \exp\left(\frac{-\Delta E_0}{k_B T}\right)\ Q_{\mathrm{C}}^{rv}(T)\right\} \tag{A19}$$

If experimental data for the rate coefficient of the association reaction is available, then we can replace the Arrhenius expression:

$$k_a(T) = A\ \exp\left(\frac{-E_a}{k_B T}\right) \tag{A20}$$

into the ILT expression:

$$k_d(E)\rho_{\mathrm{C}}(E) = \mathscr{L}^{-1}\left\{A\ \exp\left(\frac{-E_a}{k_B T}\right)\ \frac{Q_{\mathrm{A}}(T)Q_{\mathrm{B}}(T)}{Q_{\mathrm{C}}(T)}\ \exp\left(\frac{-\Delta E_0}{k_B T}\right)\ Q_{\mathrm{C}}^{rv}(T)\right\} \tag{A21}$$

and rearranging:

$$k_d(E)\rho_{\mathrm{C}}(E) = A\ \mathscr{L}^{-1}\left\{Q_{\mathrm{C}}^{rv}(T)\frac{Q_{\mathrm{A}}(T)Q_{\mathrm{B}}(T)}{Q_{\mathrm{C}}(T)}\exp\left(\frac{-E_a - \Delta E_0}{k_B T}\right)\right\} \tag{A22}$$

Now, expanding the total partition functions in terms of their components, the ro-vibrational partition function of C cancel-out, and the remaining terms are:

$$Q_{\mathrm{C}}^{rv}(T)\frac{Q_{\mathrm{A}}(T)Q_{\mathrm{B}}(T)}{Q_{\mathrm{C}}(T)} = Q_{\mathrm{A}}^{rv}(T)Q_{\mathrm{B}}^{rv}(T)\frac{Q_{\mathrm{A}}^{t}(T)Q_{\mathrm{B}}^{t}(T)}{Q_{\mathrm{C}}^{t}(T)}\frac{Q_{\mathrm{A}}^{e}(T)Q_{\mathrm{B}}^{e}(T)}{Q_{\mathrm{C}}^{e}(T)} \tag{A23}$$

Simplifying, and taking the electronic partition functions to be equal to the ground-state degeneracies g_{A}, g_{B}, and g_{C}:

$$Q_{\mathrm{C}}^{rv}(T)\frac{Q_{\mathrm{AB}}(T)}{Q_{\mathrm{C}}(T)} = Q_{\mathrm{AB}}^{rv}(T)\frac{Q_{\mathrm{A}}^{t}(T)Q_{\mathrm{B}}^{t}(T)}{Q_{\mathrm{C}}^{t}(T)}\left(\frac{g_{\mathrm{A}}g_{\mathrm{B}}}{g_{\mathrm{C}}}\right) \tag{A24}$$

Where the $Q_{\mathrm{A}}(T)Q_{\mathrm{B}}(T)$ terms are expressed as joint partition functions of A and B ($Q_{\mathrm{AB}}(T)$). Substituting the expression for the translational partition functions $Q^t(T)$ (equation 3.41):

$$Q^t(T) = \left(\frac{2\pi m k_B T}{h^2}\right)^{3/2} V \tag{A25}$$

where m is the molecular mass and V is the volume. Cancelling-out terms and simplifying:

$$Q_{\mathrm{C}}^{rv}(T)\frac{Q_{\mathrm{AB}}(T)}{Q_{\mathrm{C}}(T)} = Q_{\mathrm{AB}}^{rv}(T)\left(\frac{2\pi k_B T m_{\mathrm{A}} m_{\mathrm{B}}}{h^2 m_{\mathrm{C}}}\right)^{3/2} V\left(\frac{g_{\mathrm{A}} g_{\mathrm{B}}}{g_{\mathrm{C}}}\right) \tag{A26}$$

$$Q_{\mathrm{C}}^{rv}(T)\frac{Q_{\mathrm{AB}}(T)}{Q_{\mathrm{C}}(T)} = Q_{\mathrm{AB}}^{rv}(T)\left(\frac{2\pi\mu}{h^2}\right)^{3/2} (k_B T)^{3/2} V\left(\frac{g_{\mathrm{A}} g_{\mathrm{B}}}{g_{\mathrm{C}}}\right) \tag{A27}$$

where μ is the reduced mass of the dissociating fragments A and B, recognizing that $m_{\mathrm{C}} = m_{\mathrm{A}} + m_{\mathrm{B}}$. Substituting back into the ILT expression, and taking the constant terms out of the transform:

$$k_d(E)\rho_{\mathrm{C}}(E) = AC'\left(\frac{g_{\mathrm{A}} g_{\mathrm{B}}}{g_{\mathrm{C}}}\right)\mathscr{L}^{-1}\left\{(k_B T)^{3/2} Q_{\mathrm{AB}}^{rv}(T)\exp\left(\frac{-E_a - \Delta E_0}{k_B T}\right)\right\} \tag{A28}$$

where the constants derived from the ratio of translational partition functions are collected in C':

$$C' = \left(\frac{2\pi\mu}{h^2}\right)^{3/2} V \tag{A29}$$

Now, using the convolution theorem for Laplace transforms:

$$\mathscr{L}^{-1}\{f(x)g(x)\} = \mathscr{L}^{-1}\{f(x)\} * \mathscr{L}^{-1}\{g(x)\} \tag{A30}$$

where the $*$ symbol signifies a convolution. For functions which cannot be zero, the truncated convolution is:

$$(f * g)(x) = \int_0^x f(\tau)g(x-\tau)\ \mathrm{d}\tau \tag{A31}$$

Next, one may take the ILT for individual terms in equation A30, using the thermodynamic $\beta = (k_B T)^{-1}$ for convenience. For a partition function, the ILT is simply the corresponding density of states: [144]

$$\mathscr{L}^{-1}\{Q_{\mathrm{AB}}^{rv}(\beta)\} = \rho_{\mathrm{AB}}(E) \tag{A32}$$

Fortunately, one may rely on Laplace transform tables to obtain the ILT of the remaining terms:

$$\mathscr{L}^{-1}\left\{(y)^{-3/2}\right\} = \frac{2}{\sqrt{\pi}}\ x^{1/2} \tag{A33}$$

$$\mathscr{L}^{-1}\{f(y)\exp(-ay)\} = f(x-a)\ u(x-a) \tag{A34}$$

where $u(x-a)$ is a Heaviside step function, which is unity if $x \geq a$ and zero if $x < a$. Substituting the ILT expression for the first and last terms:

$$\mathscr{L}^{-1}\left\{(\beta)^{-3/2}\exp(-\beta E')\right\} = \frac{2}{\sqrt{\pi}}\ (E-E')^{1/2}\ u(E-E') \tag{A35}$$

where $E' = E_a + \Delta E_0$ for conciseness. Now, taking the convolution of equation A32 and equation A35:

$$\begin{aligned} &\mathscr{L}^{-1}\left\{Q^{rv}_{\mathrm{AB}}(\beta)\right\} * \mathscr{L}^{-1}\left\{(\beta)^{-3/2}\exp\left(-\beta E'\right)\right\} = \\ &\frac{2}{\sqrt{\pi}}\int_0^E \rho(E-\tau)\ (\tau - E')^{1/2}\ u(\tau - E')\ \mathrm{d}\tau \end{aligned} \tag{A36}$$

Substituting into the expression for $k_d(E)\rho_R(E)$, and replacing the Heaviside step function $u(\tau - E')$ by a conditional, yields the ILT expression for a micro-canonical dissociation rate coefficient $k_d(E)$ (equation 3.71):

$$k_d(E)\rho_{\mathrm{C}}(E) = \begin{cases} \dfrac{2AC'}{\sqrt{\pi}}\ \dfrac{g_{\mathrm{A}}g_{\mathrm{B}}}{g_{\mathrm{C}}}\ \displaystyle\int_0^E \rho_{\mathrm{AB}}(E-\tau)\ (\tau - E')^{1/2}\ \mathrm{d}\tau, & \text{if } E \geq E' \\ 0, & \text{if } E < E' \end{cases}$$

$$E' = E_a + \Delta E_0\ ; \quad C' = \left(\frac{2\pi\mu}{h^2}\right)^{3/2} V$$

References

(1) Fitz, D.; Reiner, H.; Rode, B. M. Chemical evolution toward the origin of life. *Pure and Applied Chemistry* **2007**, *79*, 2101–2117.

(2) Lammer, H.; Selsis, F.; Chassefière, E.; Breuer, D.; Grießmeier, J.-M.; Kulikov, Y. N.; Erkaev, N. V.; Khodachenko, M. L.; Biernat, H. K.; Leblanc, F., et al. Geophysical and atmospheric evolution of habitable planets. *Astrobiology* **2010**, *10*, 45–68.

(3) Eschenmoser, A. The search for the chemistry of life's origin. *Tetrahedron* **2007**, *63*, 12821–12844.

(4) Kasting, J. F. Earth's early atmosphere. *Science* **1993**, *259*, 920–926.

(5) Kasting, J. F.; Catling, D. Evolution of a habitable planet. *Annual Review of Astronomy and Astrophysics* **2003**, *41*, 429–463.

(6) Trainer, M. G. Atmospheric prebiotic chemistry and organic hazes. *Current Organic Chemistry* **2013**, *17*, 1710–1723.

(7) Bada, J. L. New insights into prebiotic chemistry from Stanley Miller's spark discharge experiments. *Chemical Society Reviews* **2013**, *42*, 2186–2196.

(8) Grenfell, J. L.; Rauer, H.; Selsis, F.; Kaltenegger, L.; Beichman, C.; Danchi, W.; Eiroa, C.; Fridlund, M.; Henning, T.; Herbst, T., et al. Co-evolution of atmospheres, life, and climate. *Astrobiology* **2010**, *10*, 77–88.

(9) Wayne, R. P., *Chemistry of Atmospheres*, 3rd ed.; Oxford University Press: 1985.

(10) Lyons, T. W.; Reinhard, C. T.; Planavsky, N. J. The rise of oxygen in Earth's early ocean and atmosphere. *Nature* **2014**, *506*, 307–315.

(11) Buick, R. When did oxygenic photosynthesis evolve? *Philosophical Transactions of the Royal Society B: Biological Sciences* **2008**, *363*, 2731–2743.

(12) Schlesinger, W. H.; Bernhardt, E. S., *Biogeochemistry: An Analysis of Global Change*, 3rd ed.; Academic Press: 2013.

(13) Sperling, E. A.; Frieder, C. A.; Raman, A. V.; Girguis, P. R.; Levin, L. A.; Knoll, A. H. Oxygen, ecology, and the Cambrian radiation of animals. *Proceedings of the National Academy of Sciences* **2013**, *110*, 13446–13451.

(14) Catling, D. C.; Glein, C. R.; Zahnle, K. J.; McKay, C. P. Why O_2 is required by complex life on habitable planets and the concept of planetary "oxygenation time". *Astrobiology* **2005**, *5*, 415–438.

(15) Sindelarova, K.; Granier, C.; Bouarar, I.; Guenther, A.; Tilmes, S.; Stavrakou, T.; Müller, J.-F.; Kuhn, U.; Stefani, P.; Knorr, W. Global data set of biogenic VOC emissions calculated by the MEGAN model over the last 30 years. *Atmospheric Chemistry and Physics* **2014**, *14*, 9317–9341.

(16) Guenther, A.; Hewitt, C. N.; Erickson, D.; Fall, R.; Geron, C.; Graedel, T.; Harley, P.; Klinger, L.; Lerdau, M.; McKay, W., et al. A global model of natural volatile organic compound emissions. *Journal of Geophysical Research: Atmospheres* **1995**, *100*, 8873–8892.

(17) Laothawornkitkul, J.; Taylor, J. E.; Paul, N. D.; Hewitt, C. N. Biogenic volatile organic compounds in the Earth system. *New Phytologist* **2009**, *183*, 27–51.

(18) Atkinson, R.; Arey, J. Atmospheric degradation of volatile organic compounds. *Chemical Reviews* **2003**, *103*, 4605–4638.

(19) Ehn, M.; Thornton, J. A.; Kleist, E.; Sipilä, M.; Junninen, H.; Pullinen, I.; Springer, M.; Rubach, F.; Tillmann, R.; Lee, B., et al. A large source of low-volatility secondary organic aerosol. *Nature* **2014**, *506*, 476–479.

(20) Bianchi, F.; Kurtén, T.; Riva, M.; Mohr, C.; Rissanen, M. P.; Roldin, P.; Berndt, T.; Crounse, J. D.; Wennberg, P. O.; Mentel, T. F., et al. Highly oxygenated organic molecules (HOM) from gas-phase autoxidation involving peroxy radicals: A key contributor to atmospheric aerosol. *Chemical Reviews* **2019**, *119*, 3472–3509.

(21) Tröstl, J.; Chuang, W. K.; Gordon, H.; Heinritzi, M.; Yan, C.; Molteni, U.; Ahlm, L.; Frege, C.; Bianchi, F.; Wagner, R., et al. The role of low-volatility organic compounds in initial particle growth in the atmosphere. *Nature* **2016**, *533*, 527–531.

(22) Riipinen, I.; Pierce, J.; Yli-Juuti, T.; Nieminen, T.; Häkkinen, S.; Ehn, M.; Junninen, H.; Lehtipalo, K.; Petäjä, T.; Slowik, J., et al. Organic condensation: a vital link connecting aerosol formation to cloud condensation nuclei (CCN) concentrations. *Atmospheric Chemistry and Physics* **2011**, *11*, 3865–3878.

(23) Hallquist, M.; Wenger, J. C.; Baltensperger, U.; Rudich, Y.; Simpson, D.; Claeys, M.; Dommen, J.; Donahue, N.; George, C.; Goldstein, A., et al. The formation, properties and impact of secondary organic aerosol: current and emerging issues. *Atmospheric Chemistry and Physics* **2009**, *9*, 5155–5236.

(24) Zhang, H.; Yee, L. D.; Lee, B. H.; Curtis, M. P.; Worton, D. R.; Isaacman-VanWertz, G.; Offenberg, J. H.; Lewandowski, M.; Kleindienst, T. E.; Beaver, M. R., et al. Monoterpenes are the largest source of summertime organic aerosol in the southeastern United States. *Proceedings of the National Academy of Sciences* **2018**, *115*, 2038–2043.

(25) IPCC, *Climate Change 2021: The Physical Science Basis. Contribution of Working Group I to the Sixth Assessment Report of the Intergovernmental Panel on Climate Change*; Cambridge University Press: Cambridge, United Kingdom and New York, NY, USA, 2021; Vol. In Press.

(26) Rosenfeld, D.; Andreae, M. O.; Asmi, A.; Chin, M.; de Leeuw, G.; Donovan, D. P.; Kahn, R.; Kinne, S.; Kivekäs, N.; Kulmala, M., et al. Global observations of aerosol-cloud-precipitation-climate interactions. *Reviews of Geophysics* **2014**, *52*, 750–808.

(27) Ramanathan, V.; Crutzen, P. J.; Kiehl, J.; Rosenfeld, D. Aerosols, Climate, and the Hydrological Cycle. *Science* **2001**, *294*, 2119–2124.

(28) Kulmala, M.; Suni, T.; Lehtinen, K.; Dal Maso, M.; Boy, M.; Reissell, A.; Rannik, Ü.; Aalto, P.; Keronen, P.; Hakola, H., et al. A new feedback mechanism linking forests, aerosols, and climate. *Atmospheric Chemistry and Physics* **2004**, *4*, 557–562.

(29) Sporre, M. K.; Blichner, S. M.; Karset, I. H.; Makkonen, R.; Berntsen, T. K. BVOC–aerosol–climate feedbacks investigated using NorESM. *Atmospheric Chemistry and Physics* **2019**, *19*, 4763–4782.

(30) Paasonen, P.; Asmi, A.; Petäjä, T.; Kajos, M. K.; Äijälä, M.; Junninen, H.; Holst, T.; Abbatt, J. P.; Arneth, A.; Birmili, W., et al. Warming-induced increase in aerosol number concentration likely to moderate climate change. *Nature Geoscience* **2013**, *6*, 438–442.

(31) Ge, X.; Wexler, A. S.; Clegg, S. L. Atmospheric amines–Part I. A review. *Atmospheric Environment* **2011**, *45*, 524–546.

(32) Cape, J.; Cornell, S.; Jickells, T.; Nemitz, E. Organic nitrogen in the atmosphere—Where does it come from? A review of sources and methods. *Atmospheric Research* **2011**, *102*, 30–48.

(33) Jickells, T.; Baker, A.; Cape, J.; Cornell, S.; Nemitz, E. The cycling of organic nitrogen through the atmosphere. *Philosophical Transactions of the Royal Society B: Biological Sciences* **2013**, *368*, 20130115.

(34) Murphy, S.; Sorooshian, A.; Kroll, J.; Ng, N.; Chhabra, P.; Tong, C.; Surratt, J.; Knipping, E.; Flagan, R.; Seinfeld, J. Secondary aerosol formation from atmospheric reactions of aliphatic amines. *Atmospheric Chemistry and Physics* **2007**, *7*, 2313–2337.

(35) Smith, J. N.; Barsanti, K. C.; Friedli, H. R.; Ehn, M.; Kulmala, M.; Collins, D. R.; Scheckman, J. H.; Williams, B. J.; McMurry, P. H. Observations of aminium salts in atmospheric nanoparticles and possible climatic implications. *Proceedings of the National Academy of Sciences* **2010**, *107*, 6634–6639.

(36) Kurtén, T.; Loukonen, V.; Vehkamäki, H.; Kulmala, M. Amines are likely to enhance neutral and ion-induced sulfuric acid-water nucleation in the atmosphere more effectively than ammonia. *Atmospheric Chemistry and Physics* **2008**, *8*, 4095–4103.

(37) Pitts Jr, J. N.; Grosjean, D.; Van Cauwenberghe, K.; Schmid, J. P.; Fitz, D. R. Photooxidation of aliphatic amines under simulated atmospheric conditions: formation of nitrosamines, nitramines, amides, and photochemical oxidant. *Environmental Science & Technology* **1978**, *12*, 946–953.

(38) Nielsen, C. J.; Herrmann, H.; Weller, C. Atmospheric chemistry and environmental impact of the use of amines in carbon capture and storage (CCS). *Chemical Society Reviews* **2012**, *41*, 6684–6704.

(39) Lijinsky, W.; Epstein, S. S. Nitrosamines as Environmental Carcinogens. *Nature* **1970**, *225*, 21–23.

(40) Ravnum, S.; Rundén-Pran, E.; Fjellsbø, L.; Dusinska, M. Human health risk assessment of nitrosamines and nitramines for potential application in CO_2 capture. *Regulatory Toxicology and Pharmacology* **2014**, *69*, 250–255.

(41) Shapley, D. Nitrosamines: scientists on the trail of prime suspect in urban cancer. *Science* **1976**, *191*, 268–270.

(42) Kamkeng, A. D.; Wang, M.; Hu, J.; Du, W.; Qian, F. Transformation technologies for CO_2 utilisation: Current status, challenges and future prospects. *Chemical Engineering Journal* **2021**, *409*, 128138.

(43) Meng, F.; Meng, Y.; Ju, T.; Han, S.; Lin, L.; Jiang, J. Research progress of aqueous amine solution for CO_2 capture: A review. *Renewable and Sustainable Energy Reviews* **2022**, *168*, 112902.

(44) Wang, T.; Hovland, J.; Jens, K. J. Amine reclaiming technologies in post-combustion carbon dioxide capture. *Journal of Environmental Sciences* **2015**, *27*, 276–289.

(45) Veltman, K.; Singh, B.; Hertwich, E. G. Human and environmental impact assessment of postcombustion CO_2 capture focusing on emissions from amine-based scrubbing solvents to air. *Environmental Science & Technology* **2010**, *44*, 1496–1502.

(46) Zhu, L.; Schade, G. W.; Nielsen, C. J. Real-time monitoring of emissions from monoethanolamine-based industrial scale carbon capture facilities. *Environmental Science & Technology* **2013**, *47*, 14306–14314.

(47) Onel, L.; Dryden, M.; Blitz, M. A.; Seakins, P. W. Atmospheric oxidation of piperazine by OH has a low potential to form carcinogenic compounds. *Environmental Science & Technology Letters* **2014**, *1*, 367–371.

(48) Ren, Z.; da Silva, G. Atmospheric oxidation of piperazine initiated by OH: A theoretical kinetics investigation. *ACS Earth and Space Chemistry* **2019**, *3*, 2510–2516.

(49) Tan, W.; Zhu, L.; Mikoviny, T.; Nielsen, C. J.; Wisthaler, A.; D'anna, B.; Antonsen, S.; Stenstrøm, Y.; Farren, N. J.; Hamilton, J. F., et al. Experimental and theoretical study of the OH-initiated degradation of piperazine under simulated atmospheric conditions. *The Journal of Physical Chemistry A* **2020**, *125*, 411–422.

(50) Rochelle, G.; Chen, E.; Freeman, S.; Van Wagener, D.; Xu, Q.; Voice, A. Aqueous piperazine as the new standard for CO_2 capture technology. *Chemical Engineering Journal* **2011**, *171*, 725–733.

(51) Teich, M.; van Pinxteren, D.; Kecorius, S.; Wang, Z.; Herrmann, H. First quantification of imidazoles in ambient aerosol particles: potential photosensitizers, brown carbon constituents, and hazardous components. *Environmental Science & Technology* **2016**, *50*, 1166–1173.

(52) Takao, Y.; Atarashi, T.; Kubo, T.; Nagae, M.; Nakayama, T. Quantification of imidazole compounds in ambient aerosols at suburban and forest sites in Western Japan. *Asian Journal of Atmospheric Environment* **2019**, *13*, 259–265.

(53) Teich, M.; Schmidtpott, M.; van Pinxteren, D.; Chen, J.; Herrmann, H. Separation and quantification of imidazoles in atmospheric particles using LC–Orbitrap-MS. *Journal of Separation Science* **2020**, *43*, 577–589.

(54) Moise, T.; Flores, J. M.; Rudich, Y. Optical properties of secondary organic aerosols and their changes by chemical processes. *Chemical Reviews* **2015**, *115*, 4400–4439.

(55) Lin, G.; Penner, J. E.; Flanner, M. G.; Sillman, S.; Xu, L.; Zhou, C. Radiative forcing of organic aerosol in the atmosphere and on snow: Effects of SOA and brown carbon. *Journal of Geophysical Research: Atmospheres* **2014**, *119*, 7453–7476.

(56) Laskin, A.; Laskin, J.; Nizkorodov, S. A. Chemistry of atmospheric brown carbon. *Chemical reviews* **2015**, *115*, 4335–4382.

(57) Drugé, T.; Nabat, P.; Mallet, M.; Michou, M.; Rémy, S.; Dubovik, O. Modeling radiative and climatic effects of brown carbon aerosols with the ARPEGE-Climat global climate model. *Atmospheric Chemistry and Physics* **2022**, *22*, 12167–12205.

(58) Kurtén, T.; Møller, K. H.; Nguyen, T. B.; Schwantes, R. H.; Misztal, P. K.; Su, L.; Wennberg, P. O.; Fry, J. L.; Kjaergaard, H. G. Alkoxy radical bond scissions explain the anomalously low secondary organic aerosol and organonitrate yields from α-pinene + NO_3. *The Journal of Physical Chemistry Letters* **2017**, *8*, 2826–2834.

(59) Draper, D. C.; Myllys, N.; Hyttinen, N.; Møller, K. H.; Kjaergaard, H. G.; Fry, J. L.; Smith, J. N.; Kurtén, T. Formation of Highly Oxidized Molecules from NO_3 Radical Initiated Oxidation of Δ-3-Carene: A Mechanistic Study. *ACS Earth and Space Chemistry* **2019**, *3*, 1460–1470.

(60) Fry, J. L.; Draper, D. C.; Barsanti, K. C.; Smith, J. N.; Ortega, J.; Winkler, P. M.; Lawler, M. J.; Brown, S. S.; Edwards, P. M.; Cohen, R. C., et al. Secondary organic aerosol formation and organic nitrate yield from NO_3 oxidation of biogenic hydrocarbons. *Environmental Science & Technology* **2014**, *48*, 11944–11953.

(61) Vereecken, L.; Peeters, J. Theoretical study of the formation of acetone in the OH-initiated atmospheric oxidation of α-pinene. *The Journal of Physical Chemistry A* **2000**, *104*, 11140–11146.

(62) Atkinson, R. Atmospheric chemistry of VOCs and NO_x. *Atmospheric environment* **2000**, *34*, 2063–2101.

(63) Vereecken, L.; Francisco, J. S. Theoretical studies of atmospheric reaction mechanisms in the troposphere. *Chemical Society Reviews* **2012**, *41*, 6259–6293.

(64) Tsang, W.; Hampson, R. Chemical kinetic data base for combustion chemistry. Part I. Methane and related compounds. *Journal of Physical and Chemical Reference Data* **1986**, *15*, 1087–1279.

(65) Baulch, D.; Cobos, C.; Cox, R.; Esser, C.; Frank, P.; Just, T.; Kerr, J.; Pilling, M.; Troe, J.; Walker, R., et al. Evaluated kinetic data for combus-

tion modelling. *Journal of Physical and Chemical Reference Data* **1992**, *21*, 411–734.

(66) Atkinson, R. Kinetics and mechanisms of the gas-phase reactions of the hydroxyl radical with organic compounds under atmospheric conditions. *Chemical Reviews* **1986**, *86*, 69–201.

(67) Stone, D.; Whalley, L. K.; Heard, D. E. Tropospheric OH and HO_2 radicals: field measurements and model comparisons. *Chemical Society Reviews* **2012**, *41*, 6348–6404.

(68) Prinn, R.; Weiss, R.; Miller, B.; Huang, J.; Alyea, F.; Cunnold, D. M.; Fraser, P.; Hartley, D.; Simmonds, P. Atmospheric trends and lifetime of CH_3CCl_3 and global OH concentrations. *Science* **1995**, *269*, 187–192.

(69) Bey, I.; Aumont, B.; Toupance, G. The nighttime production of OH radicals in the continental troposphere. *Geophysical Research Letters* **1997**, *24*, 1067–1070.

(70) Stark, H.; Lerner, B.; Schmitt, R.; Jakoubek, R.; Williams, E.; Ryerson, T.; Sueper, D.; Parrish, D.; Fehsenfeld, F. Atmospheric in situ measurement of nitrate radical (NO_3) and other photolysis rates using spectroradiometry and filter radiometry. *Journal of Geophysical Research: Atmospheres* **2007**, *112*.

(71) Geyer, A.; Alicke, B.; Ackermann, R.; Martinez, M.; Harder, H.; Brune, W.; Di Carlo, P.; Williams, E.; Jobson, T.; Hall, S., et al. Direct observations of daytime NO_3: Implications for urban boundary layer chemistry. *Journal of Geophysical Research: Atmospheres* **2003**, *108*.

(72) Vereecken, L.; Peeters, J. H-atom abstraction by OH-radicals from (biogenic)(poly)alkenes: C–H bond strengths and abstraction rates. *Chemical Physics Letters* **2001**, *333*, 162–168.

(73) Criegee, R. Mechanism of ozonolysis. *Angewandte Chemie International Edition in English* **1975**, *14*, 745–752.

(74) Johnson, D.; Marston, G. The gas-phase ozonolysis of unsaturated volatile organic compounds in the troposphere. *Chemical Society Reviews* **2008**, *37*, 699–716.

(75) Onel, L.; Blitz, M.; Dryden, M.; Thonger, L.; Seakins, P. Branching ratios in reactions of OH radicals with methylamine, dimethylamine, and ethylamine. *Environmental Science & Technology* **2014**, *48*, 9935–9942.

(76) Atkinson, R.; Perry, R.; Pitts Jr, J. Rate constants for the reactions of the OH radical with $(CH_3)_2NH$, $(CH_3)_3N$, and $C_2H_5NH_2$ over the tem-

perature range 298–426 K. *The Journal of Chemical Physics* **1978**, *68*, 1850–1853.

(77) Borduas, N.; Abbatt, J. P.; Murphy, J. G.; So, S.; da Silva, G. Gas-phase mechanisms of the reactions of reduced organic nitrogen compounds with OH radicals. *Environmental Science & Technology* **2016**, *50*, 11723–11734.

(78) Galano, A.; Alvarez-Idaboy, J. R. Branching ratios of aliphatic amines+ OH gas-phase reactions: A variational transition-state theory study. *Journal of Chemical Theory and Computation* **2008**, *4*, 322–327.

(79) Lindley, C. R.; Calvert, J. G.; Shaw, J. H. Rate studies of the reactions of the $(CH_3)_2N$ radical with O_2, NO, and NO_2. *Chemical Physics Letters* **1979**, *67*, 57–62.

(80) Liu, C.; Ma, F.; Elm, J.; Fu, Z.; Tang, W.; Chen, J.; Xie, H.-B. Mechanism and predictive model development of reaction rate constants for N-center radicals with O_2. *Chemosphere* **2019**, *237*, 124411.

(81) Tang, Y.; Nielsen, C. J. A systematic theoretical study of imines formation from the atmospheric reactions of R_nNH_{2-n} with O_2 and NO_2 (R= CH_3 and CH_3CH_2; n= 1 and 2). *Atmospheric Environment* **2012**, *55*, 185–189.

(82) Bunkan, A. J. C.; Tang, Y.; Sellevåg, S. R.; Nielsen, C. J. Atmospheric Gas Phase Chemistry of CH_2=NH and HNC. A First-Principles Approach. *The Journal of Physical Chemistry A* **2014**, *118*, 5279–5288.

(83) Kalinowski, J.; Heinonen, P.; Kilpeläinen, I.; Räsänen, M.; Gerber, R. B. Stability of Criegee intermediates formed by ozonolysis of different double bonds. *The Journal of Physical Chemistry A* **2015**, *119*, 2318–2325.

(84) Lazarou, Y. G.; Papagiannakopoulos, P. Kinetic studies of the reactions of atomic chlorine with N-methylmethylenimine and 1,3,5-trimethylhexahydro-1,3,5-triazine. *The Journal of Physical Chemistry* **1993**, *97*, 4468–4472.

(85) Akbar Ali, M.; Barker, J. R. Comparison of three isoelectronic multiple-well reaction systems: OH + CH_2O, OH + CH_2CH_2, and OH + CH_2NH. *The Journal of Physical Chemistry A* **2015**, *119*, 7578–7592.

(86) Bunkan, A. J. C.; Reijrink, N. G.; Mikoviny, T.; Müller, M.; Nielsen, C. J.; Zhu, L.; Wisthaler, A. Atmospheric Chemistry of N-Methylmethanimine (CH_3N): A Theoretical and Experimental Study. *The Journal of Physical Chemistry A* **2022**, *126*, 3247–3264.

(87) Atkinson, R. Gas-phase tropospheric chemistry of organic compounds: a review. *Atmospheric Environment. Part A. General Topics* **1990**, *24*, 1–41.

(88) Lazarou, Y. G.; Kambanis, K. G.; Papagiannakopoulos, P. Gas-phase reactions of $(CH_3)_2N$ radicals with NO and NO_2. *The Journal of Physical Chemistry* **1994**, *98*, 2110–2115.

(89) Orlando, J. J.; Tyndall, G. S. Laboratory studies of organic peroxy radical chemistry: an overview with emphasis on recent issues of atmospheric significance. *Chemical Society Reviews* **2012**, *41*, 6294–6317.

(90) Glowacki, D. R.; Pilling, M. J. Unimolecular reactions of peroxy radicals in atmospheric chemistry and combustion. *ChemPhysChem* **2010**, *11*, 3836–3843.

(91) Jenkin, M. E.; Valorso, R.; Aumont, B.; Rickard, A. R.; Wallington, T. J. Estimation of rate coefficients and branching ratios for gas-phase reactions of OH with aliphatic organic compounds for use in automated mechanism construction. *Atmospheric Chemistry and Physics* **2018**, *18*, 9297–9328.

(92) Bernardi, F.; Epiotis, N. D.; Cherry, W.; Schlegel, H. B.; Whangbo, M.-H.; Wolfe, S. A molecular orbital interpretation of the static, dynamic, and chemical properties of CH_2X radicals. *Journal of the American Chemical Society* **1976**, *98*, 469–478.

(93) Fleming, I., *Molecular Orbitals and Organic Chemical Reactions*; John Wiley & Sons: 2011.

(94) Clayden, J.; Greeves, N.; Warren, S., *Organic Chemistry*, 2nd ed.; Oxford University Press, USA: 2012.

(95) Anslyn, E. V.; Dougherty, D. A., *Modern Physical Organic Chemistry*; University science books: 2006.

(96) Alabugin, I. V.; dos Passos Gomes, G.; Abdo, M. A. Hyperconjugation. *Wiley Interdisciplinary Reviews: Computational Molecular Science* **2019**, *9*, e1389.

(97) Yin, G.; Hu, E.; Yang, F.; Ku, J.; Huang, Z. Kinetics of H abstraction and addition reactions of 2,4,4-trimethyl-1-pentene by OH radical. *Fuel* **2017**, *210*, 646–658.

(98) Yang, F.; Deng, F.; Pan, Y.; Zhang, Y.; Tang, C.; Huang, Z. Kinetics of hydrogen abstraction and addition reactions of 3-hexene by OH radicals. *The Journal of Physical Chemistry A* **2017**, *121*, 1877–1889.

(99) Chen, L.; Huang, Y.; Xue, Y.; Jia, Z.; Wang, W. Atmospheric oxidation of 1-butene initiated by OH radical: Implications for ozone and nitrous acid formations. *Atmospheric Environment* **2021**, *244*, 118010.

(100) Du, B.; Zhang, W. Theoretical mechanistic study of OH-initiated atmospheric oxidation reaction of allyl alcohol in the presence of O_2 and NO. *Computational and Theoretical Chemistry* **2011**, *977*, 111–122.

(101) Rio, C.; Flaud, P.-M.; Loison, J.-C.; Villenave, E. Experimental revaluation of the importance of the abstraction channel in the reactions of monoterpenes with OH radicals. *ChemPhysChem* **2010**, *11*, 3962–3970.

(102) De Vleeschouwer, F.; Van Speybroeck, V.; Waroquier, M.; Geerlings, P.; De Proft, F. Electrophilicity and nucleophilicity index for radicals. *Organic Letters* **2007**, *9*, 2721–2724.

(103) Bertrand, M. P.; Surzur, J.-M. Reactivite des radicaux alkoxy vis a vis des olefines une interpretation basee sur les effets orbitalaires. *Tetrahedron Letters* **1976**, *17*, 3451–3454.

(104) Amador-Balderas, J. A.; Ramírez, R. E.; Méndez, F.; Meléndez, F. J.; Richaud, A. Hyperconjugation enhances electrophilic addition to monocyclic monoterpenes: a Fukui function perspective. *Journal of Molecular Modeling* **2018**, *24*, 1–6.

(105) Spittler, M.; Barnes, I.; Bejan, I.; Brockmann, K.; Benter, T.; Wirtz, K. Reactions of NO_3 radicals with limonene and α-pinene: Product and SOA formation. *Atmospheric Environment* **2006**, *40*, 116–127.

(106) Ramírez-Ramírez, V. M.; Nebot-Gil, I. Theoretical study of the OH addition to the endocyclic and exocyclic double bonds of the d-limonene. *Chemical Physics Letters* **2005**, *409*, 23–28.

(107) Richters, S.; Pfeifle, M.; Olzmann, M.; Berndt, T. endo-Cyclization of unsaturated RO_2 radicals from the gas-phase ozonolysis of cyclohexadienes. *Chemical Communications* **2017**, *53*, 4132–4135.

(108) Berndt, T.; Richters, S.; Kaethner, R.; Voigtländer, J.; Stratmann, F.; Sipilä, M.; Kulmala, M.; Herrmann, H. Gas-phase ozonolysis of cycloalkenes: formation of highly oxidized RO_2 radicals and their reactions with NO, NO_2, SO_2, and other RO_2 radicals. *The Journal of Physical Chemistry A* **2015**, *119*, 10336–10348.

(109) Orlando, J. J.; Tyndall, G. S.; Wallington, T. J. The atmospheric chemistry of alkoxy radicals. *Chemical Reviews* **2003**, *103*, 4657–4690.

(110) Otkjær, R. V.; Jakobsen, H. H.; Tram, C. M.; Kjaergaard, H. G. Calculated hydrogen shift rate constants in substituted alkyl peroxy radicals. *The Journal of Physical Chemistry A* **2018**, *122*, 8665–8673.

(111) Vereecken, L.; Vu, G.; Wahner, A.; Kiendler-Scharr, A.; Nguyen, H. A structure activity relationship for ring closure reactions in unsaturated alkylperoxy radicals. *Physical Chemistry Chemical Physics* **2021**, *23*, 16564–16576.

(112) Jenkin, M. E.; Valorso, R.; Aumont, B.; Rickard, A. R. Estimation of rate coefficients and branching ratios for reactions of organic peroxy radicals for use in automated mechanism construction. *Atmospheric Chemistry and Physics* **2019**, *19*, 7691–7717.

(113) Vereecken, L.; Nozière, B. H migration in peroxy radicals under atmospheric conditions. *Atmospheric Chemistry and Physics* **2020**, *20*, 7429–7458.

(114) Møller, K. H.; Otkjær, R. V.; Chen, J.; Kjaergaard, H. G. Double bonds are key to fast unimolecular reactivity in first-generation monoterpene hydroxy peroxy radicals. *The Journal of Physical Chemistry A* **2020**, *124*, 2885–2896.

(115) Hyttinen, N.; Knap, H. C.; Rissanen, M. P.; Jørgensen, S.; Kjaergaard, H. G.; Kurtén, T. Unimolecular HO_2 loss from peroxy radicals formed in autoxidation is unlikely under atmospheric conditions. *The Journal of Physical Chemistry A* **2016**, *120*, 3588–3595.

(116) Da Silva, G.; Kirk, B. B.; Lloyd, C.; Trevitt, A. J.; Blanksby, S. J. Concerted HO_2 elimination from α-aminoalkylperoxyl free radicals: Experimental and theoretical evidence from the gas-phase $NH_2CHCO_2^- + O_2$ reaction. *The Journal of Physical Chemistry Letters* **2012**, *3*, 805–811.

(117) Rissanen, M. P.; Eskola, A. J.; Nguyen, T. L.; Barker, J. R.; Liu, J.; Liu, J.; Halme, E.; Timonen, R. S. $CH_2NH_2 + O_2$ and $CH_3CHNH_2 + O_2$ reaction kinetics: photoionization mass spectrometry experiments and master equation calculations. *The Journal of Physical Chemistry A* **2014**, *118*, 2176–2186.

(118) Møller, K. H.; Berndt, T.; Kjaergaard, H. G. Atmospheric autoxidation of amines. *Environmental Science & Technology* **2020**, *54*, 11087–11099.

(119) Da Silva, G. Atmospheric chemistry of 2-aminoethanol (MEA): Reaction of the NH_2CHCH_2OH radical with O_2. *The Journal of Physical Chemistry A* **2012**, *116*, 10980–10986.

(120) Cheng, C. T.; Chan, M. N.; Wilson, K. R. Importance of unimolecular HO_2 elimination in the heterogeneous OH reaction of highly oxygenated

tartaric acid aerosol. *The Journal of Physical Chemistry A* **2016**, *120*, 5887–5896.

(121) Tan, W.; Zhu, L.; Mikoviny, T.; Nielsen, C. J.; Wisthaler, A.; D'anna, B.; Antonsen, S.; Stenstrøm, Y.; Farren, N. J.; Hamilton, J. F., et al. Experimental and Theoretical Study of the OH-Initiated Degradation of Piperidine under Simulated Atmospheric Conditions. *The Journal of Physical Chemistry A* **2024**, *128*, 2789–2814.

(122) Zádor, J.; Martí, C.; Van de Vijver, R.; Johansen, S. L.; Yang, Y.; Michelsen, H. A.; Najm, H. N. Automated reaction kinetics of gas-phase organic species over multiwell potential energy surfaces. *The Journal of Physical Chemistry A* **2023**, *127*, 565–588.

(123) Atkinson, R.; Carter, W. P. Reactions of alkoxy radicals under atmospheric conditions: The relative importance of decomposition versus reaction with O_2. *Journal of Atmospheric Chemistry* **1991**, *13*, 195–210.

(124) Atkinson, R. Atmospheric reactions of alkoxy and β-hydroxyalkoxy radicals. *International Journal of Chemical Kinetics* **1997**, *29*, 99–111.

(125) Atkinson, R. Rate constants for the atmospheric reactions of alkoxy radicals: An updated estimation method. *Atmospheric Environment* **2007**, *41*, 8468–8485.

(126) Vereecken, L.; Peeters, J. Decomposition of substituted alkoxy radicals—part I: a generalized structure–activity relationship for reaction barrier heights. *Physical Chemistry Chemical Physics* **2009**, *11*, 9062–9074.

(127) Carter, W. P.; Darnall, K. R.; Lloyd, A. C.; Winer, A. M.; Pitts Jr, J. N. Evidence for alkoxy radical isomerization in photooxidations of C_4–C_6 alkanes under simulated atmospheric conditions. *Chemical Physics Letters* **1976**, *42*, 22–27.

(128) Vereecken, L.; Peeters, J. The 1, 5-H-shift in 1-butoxy: A case study in the rigorous implementation of transition state theory for a multirotamer system. *The Journal of Chemical Physics* **2003**, *119*, 5159–5170.

(129) Vereecken, L.; Nguyen, T.; Hermans, I.; Peeters, J. Computational study of the stability of α-hydroperoxyl-or α-alkylperoxyl substituted alkyl radicals. *Chemical Physics Letters* **2004**, *393*, 432–436.

(130) Vereecken, L. Computational study of the stability of α-nitroxy-substituted alkyl radicals. *Chemical Physics Letters* **2008**, *466*, 127–130.

(131) Wang, L.; Wang, L. Atmospheric oxidation mechanism of sabinene initiated by the hydroxyl radicals. *The Journal of Physical Chemistry A* **2018**, *122*, 8783–8793.

(132) Atkins, P. W.; Friedman, R. S., *Molecular Quantum Mechanics*, 5th ed.; Oxford University Press: 2011.

(133) Clark, T.; Chandrasekhar, J.; Spitznagel, G. W.; Schleyer, P. V. R. Efficient diffuse function-augmented basis sets for anion calculations. III. The 3-21+G basis set for first-row elements, Li–F. *Journal of Computational Chemistry* **1983**, *4*, 294–301.

(134) Ditchfield, R.; Hehre, W. J.; Pople, J. A. Self-consistent molecular-orbital methods. IX. An extended Gaussian-type basis for molecular-orbital studies of organic molecules. *The Journal of Chemical Physics* **1971**, *54*, 724–728.

(135) Hariharan, P. C.; Pople, J. A. The influence of polarization functions on molecular orbital hydrogenation energies. *Theoretica Chimica Acta* **1973**, *28*, 213–222.

(136) Hehre, W. J.; Ditchfield, R.; Pople, J. A. Self-consistent molecular orbital methods. XII. Further extensions of Gaussian-type basis sets for use in molecular orbital studies of organic molecules. *The Journal of Chemical Physics* **1972**, *56*, 2257–2261.

(137) Knizia, G.; Adler, T. B.; Werner, H.-J. Simplified CCSD(T)-F12 methods: Theory and benchmarks. *The Journal of Chemical Physics* **2009**, *130*, 054104.

(138) Kong, L.; Bischoff, F. A.; Valeev, E. F. Explicitly correlated R12/F12 methods for electronic structure. *Chemical Reviews* **2012**, *112*, 75–107.

(139) Jensen, F., *Introduction to Computational Chemistry*, 2nd ed.; John wiley & sons: 2007.

(140) Becke, A. D. A new mixing of Hartree–Fock and local density-functional theories. *The Journal of Chemical Physics* **1993**, *98*, 1372–1377.

(141) Lee, C.; Yang, W.; Parr, R. G. Development of the Colle-Salvetti correlation-energy formula into a functional of the electron density. *Physical Review B* **1988**, *37*, 785.

(142) Chai, J.-D.; Head-Gordon, M. Long-range corrected hybrid density functionals with damped atom–atom dispersion corrections. *Physical Chemistry Chemical Physics* **2008**, *10*, 6615–6620.

(143) Grimme, S. Semiempirical GGA-type density functional constructed with a long-range dispersion correction. *Journal of Computational Chemistry* **2006**, *27*, 1787–1799.

(144) Baer, T.; Hase, W. L., *Unimolecular Reaction Dynamics: Theory and Experiments*; Oxford university press: 1996; Vol. 31.

(145) Atkins, P.; De Paula, J.; Friedman, R., *Quanta, Matter, and Change: A molecular approach to physical chemistry*; Oxford University Press, USA: 2009.

(146) Atkins, P. W.; De Paula, J., *Atkins' Physical Chemistry*, 10th ed.; Oxford university press: 2014.

(147) Eyring, H. The activated complex in chemical reactions. *The Journal of Chemical Physics* **1935**, *3*, 107–115.

(148) Pilling, M. J.; Seakins, P. W., *Reaction Kinetics*; Oxford university press: 1995.

(149) Greer, E. M.; Kwon, K.; Greer, A.; Doubleday, C. Thermally activated tunneling in organic reactions. *Tetrahedron* **2016**, *72*, 7357–7373.

(150) Qiu, G.; Schreiner, P. R. The Intrinsic Barrier Width and Its Role in Chemical Reactivity. *ACS Central Science* **2023**, *9*, 2129–2137.

(151) Johnston, H. S.; Heicklen, J. Tunnelling corrections for unsymmetrical Eckart potential energy barriers. *The Journal of Physical Chemistry* **1962**, *66*, 532–533.

(152) Eckart, C. The penetration of a potential barrier by electrons. *Physical Review* **1930**, *35*, 1303.

(153) Lindemann, F. A.; Arrhenius, S.; Langmuir, I.; Dhar, N.; Perrin, J.; Lewis, W. M. Discussion on "the radiation theory of chemical action". *Transactions of the Faraday Society* **1922**, *17*, 598–606.

(154) Rice, O. K.; Ramsperger, H. C. Theories of unimolecular gas reactions at low pressures. *Journal of the American Chemical Society* **1927**, *49*, 1617–1629.

(155) Kassel, L. S. Studies in homogeneous gas reactions. I. *The Journal of Physical Chemistry* **1928**, *32*, 225–242.

(156) Marcus, R. A. Unimolecular dissociations and free radical recombination reactions. *The Journal of Chemical Physics* **1952**, *20*, 359–364.

(157) Miller, J. A.; Klippenstein, S. J. Master equation methods in gas phase chemical kinetics. *The Journal of Physical Chemistry A* **2006**, *110*, 10528–10544.

(158) Fernández-Ramos, A.; Ellingson, B. A.; Meana-Pañeda, R.; Marques, J. M.; Truhlar, D. G. Symmetry numbers and chemical reaction rates. *Theoretical Chemistry Accounts* **2007**, *118*, 813–826.

(159) Beyer, T.; Swinehart, D. Algorithm 448: number of multiply-restricted partitions. *Communications of the ACM* **1973**, *16*, 379.

(160) Glowacki, D. R.; Liang, C.-H.; Morley, C.; Pilling, M. J.; Robertson, S. H. MESMER: an open-source master equation solver for multi-energy well reactions. *The Journal of Physical Chemistry A* **2012**, *116*, 9545–9560.

(161) Forst, W. Unimolecular rate theory test in thermal reactions. *The Journal of Physical Chemistry* **1972**, *76*, 342–348.

(162) Forst, W. Test of Laplace transform inversion of unimolecular rate constant. *The Journal of Physical Chemistry* **1982**, *86*, 1771–1775.

(163) Robertson, S.; Pilling, M.; Baulch, D.; Green, N. Fitting of pressure-dependent kinetic rate data by master equation/inverse Laplace transform analysis. *The Journal of Physical Chemistry* **1995**, *99*, 13452–13460.

(164) Davies, J. W.; Green, N. J.; Pilling, M. J. The testing of models for unimolecular decomposition via inverse Laplace transformation of experimental recombination rate data. *Chemical Physics Letters* **1986**, *126*, 373–379.

(165) Barker, J. R. Energy transfer in master equation simulations: A new approach. *International Journal of Chemical Kinetics* **2009**, *41*, 748–763.

(166) Golden, D. M.; Barker, J. R. Pressure-and temperature-dependent combustion reactions. *Combustion and Flame* **2011**, *158*, 602–617.

(167) Tardy, D. C.; Rabinovitch, B. Collisional energy transfer. Thermal unimolecular systems in the low-pressure region. *The Journal of Chemical Physics* **1966**, *45*, 3720–3730.

(168) Pilling, M. J.; Robertson, S. H. Master equation models for chemical reactions of importance in combustion. *Annual Review of Physical Chemistry* **2003**, *54*, 245–275.

(169) Shannon, R.; Glowacki, D. R. A simple "boxed molecular kinetics" approach to accelerate rare events in the stochastic kinetic master equation. *The Journal of Physical Chemistry A* **2018**, *122*, 1531–1541.

(170) Robertson, S. H.; Pilling, M. J.; Jitariu, L. C.; Hillier, I. H. Master equation methods for multiple well systems: application to the 1-,2-pentyl system. *Physical Chemistry Chemical Physics* **2007**, *9*, 4085–4097.

(171) Miller, J. A.; Klippenstein, S. J.; Robertson, S. H.; Pilling, M. J.; Green, N. J. Detailed balance in multiple-well chemical reactions. *Physical Chemistry Chemical Physics* **2009**, *11*, 1128–1137.

(172) Dunning Jr, T. H. Gaussian basis sets for use in correlated molecular calculations. I. The atoms boron through neon and hydrogen. *The Journal of Chemical Physics* **1989**, *90*, 1007–1023.

(173) Kendall, R. A.; Dunning Jr, T. H.; Harrison, R. J. Electron affinities of the first-row atoms revisited. Systematic basis sets and wave functions. *The Journal of Chemical Physics* **1992**, *96*, 6796–6806.

(174) Zhao, Y.; Truhlar, D. G. The M06 suite of density functionals for main group thermochemistry, thermochemical kinetics, noncovalent interactions, excited states, and transition elements: two new functionals and systematic testing of four M06-class functionals and 12 other functionals. *Theoretical Chemistry Accounts* **2008**, *120*, 215–241.

(175) Peterson, K. A.; Adler, T. B.; Werner, H.-J. Systematically convergent basis sets for explicitly correlated wavefunctions: The atoms H, He, B–Ne, and Al–Ar. *The Journal of Chemical Physics* **2008**, *128*, 084102.

(176) Frisch, M. J. et al. Gaussian'16 Revision C.01, Gaussian, Inc., Wallingford, CT, 2016.

(177) Werner, H.-J.; Knowles, P. J., et al. MOLPRO, version 2022.2 , a package of ab initio programs.

(178) Werner, H.-J.; Knowles, P. J.; Manby, F. R.; Black, J. A.; Doll, K.; Heßelmann, A.; Kats, D.; Köhn, A.; Korona, T.; Kreplin, D. A., et al. The Molpro quantum chemistry package. *The Journal of Chemical Physics* **2020**, *152*, 144107.

(179) Werner, H.-J.; Knowles, P. J.; Knizia, G.; Manby, F. R.; Schütz, M. Molpro: a general-purpose quantum chemistry program package. *Wiley Interdisciplinary Reviews: Computational Molecular Science* **2012**, *2*, 242–253.

(180) Pawlak, M.; Pobłocki, K.; Drzeżdżon, J.; Gawdzik, B.; Jacewicz, D. Isocyanates and isocyanides – Life-threatening toxins or essential compounds? *Science of The Total Environment* **2024**, 173250.

(181) Samunl, A.; Neta, P. Electron spin resonance study of the reaction of hydroxyl radicals with pyrrole, imidazole, and related compounds. *The Journal of Physical Chemistry* **1973**, *77*, 1629–1635.

(182) Llano, J.; Eriksson, L. A. Mechanism of hydroxyl radical addition to imidazole and subsequent water elimination. *The Journal of Physical Chemistry B* **1999**, *103*, 5598–5607.

(183) Bansal, K.; Sellers, R. Polarographic and optical pulse radiolysis study of the radicals formed by hydroxyl radical attack on imidazole and re-

lated compounds in aqueous solutions. *The Journal of Physical Chemistry* **1975**, *79*, 1775–1780.

(184) Safaei, Z.; Shiroudi, A.; Zahedi, E.; Sillanpää, M. Atmospheric oxidation reactions of imidazole initiated by hydroxyl radicals: kinetics and mechanism of reactions and atmospheric implications. *Physical Chemistry Chemical Physics* **2019**, *21*, 8445–8456.

(185) Mai, T. V.-T.; Huynh, L. K. Comment on "Atmospheric oxidation reactions of imidazole initiated by hydroxyl radicals: kinetics and mechanism of reactions and atmospheric implications" by Safaei et al., Phys. Chem. Chem. Phys., 2019, 21, 8445. *Physical Chemistry Chemical Physics* **2019**, *21*, 21162–21165.

(186) Pekkanen, T. T.; Lendvay, G.; Döntgen, M.; Timonen, R. S.; Eskola, A. J. An experimental and computational investigation of the reaction between pent-1-en-3-yl radicals and oxygen molecules under autoignition conditions. *Proceedings of the Combustion Institute* **2023**, *39*, 189–197.

(187) Zádor, J.; Van de Vijver, R.; Dewyer, A.; Martí, C. KinBot, `https://github.com/zadorlab/KinBot.git`, version 2.2.1, 2023.

(188) Van de Vijver, R.; Zádor, J. KinBot: Automated stationary point search on potential energy surfaces. *Computer Physics Communications* **2020**, *248*, 106947.

(189) Kumar, A.; Neese, F.; Valeev, E. F. Explicitly correlated coupled cluster method for accurate treatment of open-shell molecules with hundreds of atoms. *The Journal of Chemical Physics* **2020**, *153*, 094105.

(190) Saitow, M.; Becker, U.; Riplinger, C.; Valeev, E. F.; Neese, F. A new near-linear scaling, efficient and accurate, open-shell domain-based local pair natural orbital coupled cluster singles and doubles theory. *The Journal of Chemical Physics* **2017**, *146*, 164105.

(191) Hansen, A.; Liakos, D. G.; Neese, F. Efficient and accurate local single reference correlation methods for high-spin open-shell molecules using pair natural orbitals. *The Journal of Chemical Physics* **2011**, *135*, 214102.

(192) Neese, F. The ORCA Program System. *Wiley Interdisciplinary Reviews: Computational Molecular Science* **2012**, *2*, 73–78.

(193) Neese, F. Software update: the ORCA program system, version 4.0. *Wiley Interdisciplinary Reviews: Computational Molecular Science* **2018**, *8*, e1327.

(194) Ng, N. L.; Brown, S. S.; Archibald, A. T.; Atlas, E.; Cohen, R. C.; Crowley, J. N.; Day, D. A.; Donahue, N. M.; Fry, J. L.; Fuchs, H., et al. Nitrate

radicals and biogenic volatile organic compounds: oxidation, mechanisms, and organic aerosol. *Atmospheric Chemistry and Physics* **2017**, *17*, 2103–2162.

(195) Nielsen, C. J.; Bossi, R.; Bunkan, A. J. C.; Dithmer, L.; Glasius, M.; Hallquist, M.; Hansen, A. M. K.; Lutz, A.; Salo, K.; Maguta, M. M., et al. Atmospheric Degradation of Amines (ADA): summary report from atmospheric chemistry studies of amines, nitrosamines, nitramines and amides. **2012**.